Multi-scale Models of Tumor Growth and Invasion

by

Boglarka Soos

A thesis
presented to the University of Waterloo
in fulfillment of the
thesis requirement for the degree of
Master of Mathematics
in
Applied Mathematics

Waterloo, Ontario, Canada, 2012

I hereby declare that I am the sole author of this thesis. This is a true copy of the thesis, including any required final revisions, as accepted by my examiners.

I understand that my thesis may be made electronically available to the public.

Abstract

Cancer is a complex, multi-scale disease marked by unchecked cellular growth and proliferation. As a tumor grows, it is known to lose its capacity to maintain a compact structure. This stage of development, known as invasion, is marked by the disaggregation and dispersion of peripheral cells, and the formation of finger-like margins. This thesis provides an overview of three multi-scale models of tumor growth and invasion. The hybrid discrete-continuum (HDC) model couples a cellular automaton approach, which is used to direct the behavior and interactions of individual cells, with a system of reaction-diffusion-chemotaxis equations that describe the micro-environment. The evolutionary hybrid cellular automaton (EHCA) model maintains the core of the HDC approach, but employs an artificial response network to describe cellular dynamics. In contrast to these two, the immersed boundary (IBCell) model describes cells as fully deformable, viscoelastic entities that interact with each other using membrane bound receptors.

As part of this thesis, the HDC model has been modified to examine the role of the ECM as a barrier to cellular expansion. The results of these simulations will be presented and discussed in the context of tumor progression.

Acknowledgements

I would like to thank my supervisor Dr. Siv Sivaloganathan for his wisdom, valuable comments, and positive attitude. I would also like to thank Dr. Mohammad Kohandel, Dr. Guiseppe Tenti, and Dr. Hamid Molavian for providing me with keen insight into cancer biology and mathematical modelling.

There are many people in the department whose friendship and intellect have inspired me. A special acknowledgement goes out to Dale Connor, Zhao Jin, Wilten Nicola, Ian Payne, and Jared Penney.

I want to thank all of my friends in Calgary, especially Anna Ordog, for their encouragement and support.

Most of all, I would like to thank my family for their guidance and love. I want to thank my mom for her edits, my dad for the LaTeXhelp, my sister for the amazing diagrams, and my brother for keeping me in touch with my inner child.

Table of Contents

List of Figures

Chapter 1

Introduction

1.1 Cancer

Cancer is a complex, multi-scale disease [1]. Its prevalence has attracted broad resources and the interest of scientists from varying disciplines [2]. Despite decades of research and advancements in experimental techniques, the dynamics of tumor growth and invasion are still poorly understood and the ability to predict and treat this disease is limited [3–5]. Regardless, a general optimism remains, in part due to the recent success of mathematical modelling of cancer progression and tumor growth.

The goal of this thesis is twofold: 1) to present an overview of multi-scale mathematical models of avascular tumor growth and invasion; and 2) to modify the hybrid discrete-continuum model in order to examine the role of the ECM as a barrier to cellular expansion.

A variety of different mathematical models are examined; however, all adhere to the hypothesis that invasion is a property derived from the adaption[1] of cancer cells to selective pressures from their microenvironment [6]. In these models, changes in the overall morphology of the tumor are traced [7], with special attention given to the emergence of fingering morphology and the fragmentation of the boundary [8] since these are among the diagnostic and prognostic criteria used by pathologists [9] in qualitative evaluations of tumor patterns.

[1]The cells in these models have varying properties and are subject to mutation. Those that are most likely survive in a given environment are labelled as the best adapted.

1.1.1 An Overview of Malignant Tumor Formation

The general motivation behind this research is to gain a better understanding of the early stages of cancer invasion since early detection of neoplastic changes in healthy tissue is the crucial step in the prevention and the successful treatment of cancer patients [10]. For a contextual understanding, it is important to have an idea of the progression of this disease. To begin with, it is essential to differentiate between malignant and benign tumors [5, 11]. Benign tumors are characterized by low rates of cell migration and proliferation, are self-limited in growth and are unable to escape beyond well-defined tumor boundaries. Malignant tumors on the other hand are composed of abnormal cells which have a limitless capacity for proliferation, lack contact inhibition, and are able to survive in hostile environments [5]. These cells are known to migrate into healthy tissue, either through active penetration, matrix degradation, or entry into the circulatory system. Furthermore, they tend to form tumors with poorly defined margins.

The formation of a malignant tumor is driven by the accumulation of genetic and epigenetic mutations in a single cell line[2] [12]. These mutations may be attributed to hereditary effects, DNA damage during cell division, and the influence of mutagenic compounds or external factors which set awry the cell cycle [13, 14]. In certain scenarios, a mutated cell can gain a competitive advantage in its ability to reproduce and invade the surrounding tissue [12]. Over successive divisions, its progeny will form a small cluster and eventually develop into an avascular tumor [15]. However, such events are extremely rare when considering the fact that humans can undergo up to 10^{16} mitoses during their lifetime, each of which confers the risk of a genetic disaster from the miscopying of DNA and the breakage or segregation of chromosomes [16]. This suggests that various anticancer defenses have co-evolved against DNA damage and are wired into intracellular signalling circuits where they work in collaboration with the immune system. Weinberg [16] suggests that at least five or six such mechanisms must be breached before a full-blown tumor can form.

Currently, there are two prominent points of view on the pathogenesis and evolution of malignant cancers [17]. The cell-centric approach postulates that tumor formation is a consequence of an aggressive form of differentiation that is induced by either internal (e.g. an abnormal state of development) or external (e.g. the microenvironment) factors. The gene-centric approach associates tumor development with the mutation of genes. It is the latter that will be used in the models presented in this overview. In particular, it will be assumed that it is the loss of function of tumor suppressor genes that promotes

[2] A cell line is a population of cells with a genetic mutation that enables them to replicative indefinitely.

genome instability and permits mutated cells with a selective advantage to thrive [18]. It is well known that mutation of the $p53$ gene[3], commonly known as the Guardian of the Genome [19], is linked with the accumulation of variability and heterogeneity at the genetic level [20, 21]. In its un-mutated form, this gene controls cell proliferation, death, and DNA repair, and regulates cellular response to environmental pressure, such as hypoxia and osmotic stress [22]. Furthermore, it is known to elicit cell cycle arrest to repair DNA damage and apoptosis in events where the damage is irreparable [18]. Its loss of function permits the propagation of damaged DNA to daughter cells and inhibits apoptosis during hypoxia [21, 23, 24]. Based on experimental data, mutation of the $p53$ gene is estimated to occur in approximately 50% of tumors, with the incidence rate increasing with disease progression for certain forms of cancer [21].

1.1.2 Properties of Malignant Tumors

Although cancers vary widely in and amongst themselves, they are known to consistently display certain properties. These traits, acquired through tumor-producing inflammation and genome instability and mutation [25], drive tumor progression toward malignancy and enable cancers to overcome intrinsic and extrinsic barriers that would otherwise thwart their development and dissemination. Hanahan and Weinberg [18, 25] claim that resisting cell death, sustaining proliferative signalling, evading growth suppressors, activating invasion and metastasis, enabling replicative immortality, and inducing angiogenesis are the hallmarks of cancer. In addition, reprogramming energy metabolism and evading immune destruction are listed as emerging hallmarks and believed to be involved in the pathogenesis of some if not all cancers. However, these have yet to be generalized and fully validated (i.e., cancer biologists must show their inhibition would impair tumor growth and progression). A chart depicting the hallmarks of cancer is presented in Figure 1.1, while Figure 1.2 highlights the emerging hallmarks and enabling characteristics

Scientists hypothesize that it is sufficient for some of the traits to be acquired by a reduced part of the tumor for the benefits to be shared by the tumor as a whole [26]. The basic postulate behind this theory is that cancer is not one but many diseases that must be de-convolved and treated independently [6].

[3]The $p53$ gene is a tumor suppressor gene that plays an active role in the arrest of cells with damaged DNA. Inactivating mutations of this gene are commonly found in many human cancers.

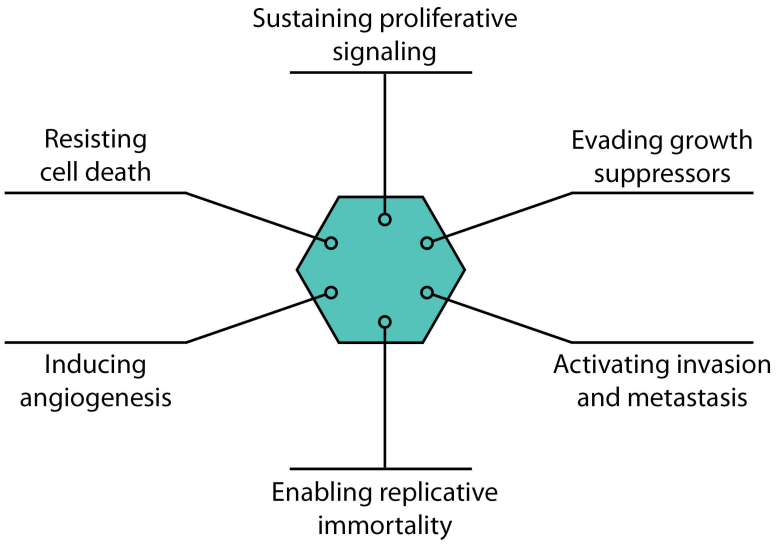

Figure 1.1: The hallmarks of cancer
Adapted from Hanahan and Weinberg [25].

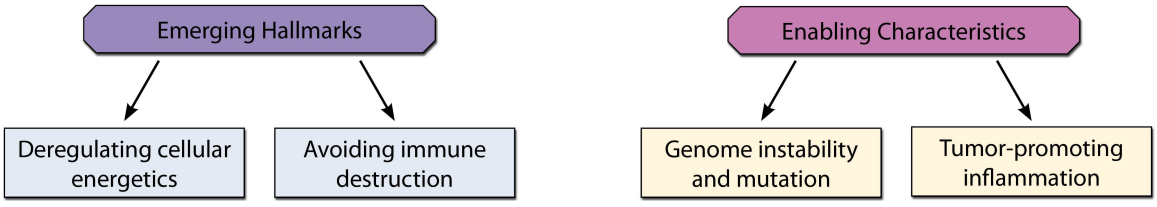

Figure 1.2: The emerging hallmarks and enabling characteristics of cancer
Adapted from Hanahan and Weinberg [25].

The growth advantage, sustained by the acquisition of these hallmarks, results in the breakdown of homeostatic mechanisms [21]. This upsets the balance of proliferation, differentiation, and death, disrupts tissue architecture and function, and makes coexistence between normal and abnormal clones impossible [26, 27]. Above all, it allows the rapidly proliferating cells to aggregate, and form avascular tumors. These tumors rely on diffusion to provide nutrients and remove waste products and, hence, are limited in size to about $1 - 2mm$, or approximately 10^6 cells [2]. In general, they cause little to no damage to the patient, who is unlikely to exhibit any of the symptoms of cancer at this stage [28].

Unable to fulfill their own metabolic needs, these tumors are characterized by a large necrotic core [3], which is surrounded by a ring of quiescent cells and a rim of proliferating cells [7]. However, they are able to overcome the constraints of diffusion-limited growth by releasing chemicals that trigger the formation of new blood vessels. This process, known as neoangiogenesis, is believed to be caused by the mutation of key genes and the exposure of cells to stressful conditions such as hypoxia [29]. The newly formed neovascular networks tend to be leaky, inefficient, and composed primarily of immature and tortuous vessels [30]. Regardless, they are still able to supply growing tumors with oxygen, glucose, blood, and growth factors [3], albeit without proficiency.

As tumors progress, they are known to lose their capacity to maintain a compact structure [13, 27]. This stage of development, known as invasion, is marked by changes in the balance of protease and antiprotease [31], a hypoxia-induced transition from collective motion to individual driven movement [30], and the formation of an uncontrolled feedback loop, whereby cells are continuously stimulated to produce matrix degrading enzymes and growth factors [32]. Concurrently, the tumor undergoes a series of morphological changes. In particular, the disaggregation and dispersion of the peripheral cells [32], the formation of finger-like margins [33], and the detachment of branch-like structures from the core of the tumor [33] can be expected. Some of the cancer cells that escape from the primary tumor are able to enter into the lymphatic or circulatory system [34]. These cells are then able to circulate throughout the body and to transmigrate through vessel walls to establish new colonies in distant organs [5, 35]. It is at this stage that cancer is categorized as lethal, and cure by surgery alone becomes impossible [36].

The quest for a general understanding of cancer and its inherent complexity highlights the need for novel tools and techniques that provoke new insight into tumor progression and potential therapies. Various mathematical techniques that can be applied to cancer modelling described next.

1.2 Mathematical Models and Techniques

A wide variety of approaches and techniques are used to study tumor growth. The most commonly used are the so called in vivo, in vitro, and in silico studies [37]. In vivo methods alter certain aspects or properties of a cell or tumor environment implanted in a living organism. Although this approach is the most realistic, it is difficult to control and interpret since induced changes are typically compensated for by other (sometimes multiple) factors. In vitro models fail to reconstruct the complexity of the in vivo environment but allow for better control of individual factors and provide exceptional test systems with which the effects of certain variables can be assessed [38].

Finally, in silico methods use computer simulations to systematically analyze the behavior of individual cells and tumors. This approach attempts to reconstruct various aspects of the in vivo environment using experimental measurements and must be properly parameterized and fine-tuned to accurately represent the biological processes being studied. Since the parameters are often collected from various tumors grown under different environmental conditions (e.g., different cell lines implanted in various animal breeds), the results may not correspond to a single real tumor. However, these models are cheap, accurate, quick to provide results, and allow for the systematic analysis of variables under a spectrum of different environmental conditions.

In this thesis we propose that an in silico mathematical model, which incorporates data from multiple scales, may well provide the much needed rational approach and guidance that is necessary to unravel the mysteries of cancer and to accurately predict tumor development and control. In the next section, we will explore the different forms and features that this model may take.

1.2.1 An Introduction to Multi-scale Models

Multi-scale mathematical models represent novel approaches that can be used to study how genetic mutations are manifested as functional and morphological changes at the cellular and tissue scales [17]. These models consist of a set of equations which focus on cellular processes believed to be crucial to cancer development. In general, they consider how cells grow, divide, move, and interact with their neighboring cells and microenvironment. Figure 1.3 illustrates two different ways in which the construction of a mathematical model

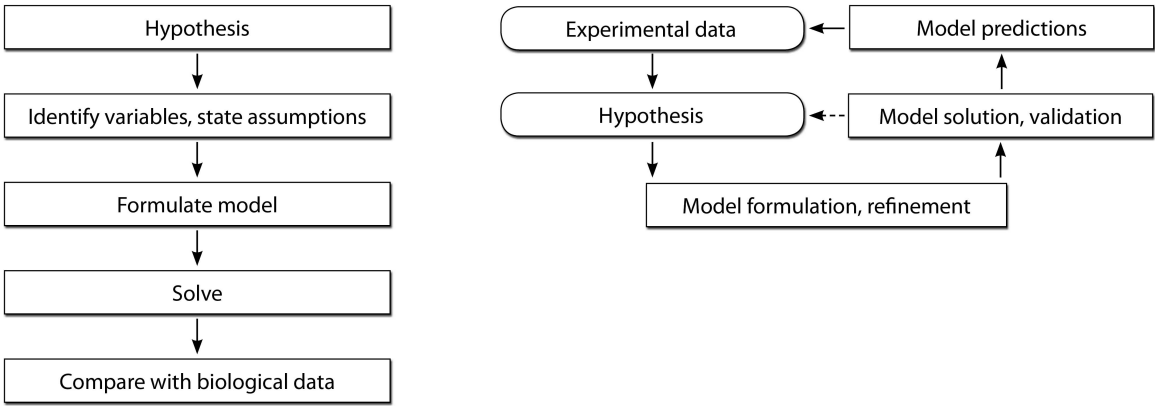

Figure 1.3: Building a mathematical model of cancer
Adapted from Byrne [39].

can be approached.

Ideally, a computational model of cancer should respect the structural and functional complexity of cellular behavior. In order to accomplish this, one approach is to bridge models that explore tumor progression on distinct spatial or temporal scales. Figure 1.4 highlights three scales that are often associated with tumor invasion. The microscale refers to the ensemble of activities that take place within a cell or along its membrane and includes DNA synthesis, gene expression, as well as the regulation of membrane receptors [40]. The mesoscale (or cellular level) refers to the cell cycle and individual interactions among tumor cells and the stroma. Lastly, the tissue scale encompasses the activity of the cell cluster as a whole, and examines its interactions with the environment.

With regards to cancer, there are two broad categories of computational models [8]: descriptive and mechanistic models. Descriptive models attempt to reproduce the dynamics of a tumor without emphasizing the biological details. Mechanistic models address the underlying biology in great detail and tend to focus on a specific aspect of tumor progression. Of course, these are just the extreme ends of the spectrum and most models fall somewhere in between these two. To be truly useful to a biologist, a model must be mechanistic to a significant extent and must relate multiple components of the system in order to capture the underlying behavior of the cells. To accomplish this, mathematicians use continuous, discrete, and hybrid methods.

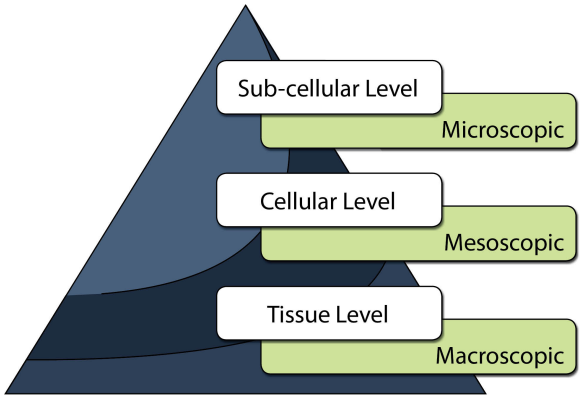

Figure 1.4: The multiscale nature of cancer
Adapted from Preziosi [40].

Continuum Models

The continuum approach describes the relationship between the cell density and one or more chemical species that influence the cell cycle or serve as nutrients [13]. Relying on reaction-diffusion-convection equations, integro-differential equations, or continuum mechanics, such models are applicable in studies involving the tissue scale and high density aggregations of tumors cells. They are often used to model mechanical and spatio-temporal interactions, such as stress, strain, pressure, and changes in the network expansion rate. The main advantages of using continuum models are that they require few parameters and are typically amenable to mathematical analysis. However, the validity of the implicit space averaging over cells is questionable and there are inherent challenges in incorporating the active nature of cells into these models, which assume gradual changes. Instead, it seems more appropriate to use a discrete model when examining cell-cell interactions and activity on the single cell scale.

Discrete Models

The cellular automaton (CA) model is a prime example of an individual-based model that can be used to simulate the behavior of cells in response to their local environment [41].

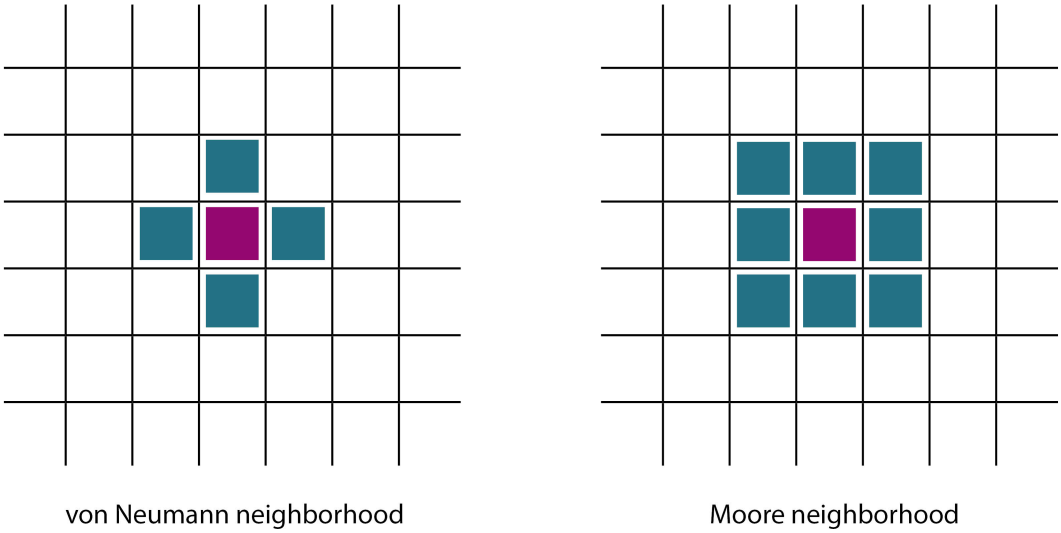

Figure 1.5: The von Neumann and Moore neighborhoods
Adapted from Moreira and Deutsch [41].

Although they serve as simplified caricatures of the systems they represent, these models are still capable of capturing the underlying dynamics [42]. CA models use a regular lattice to define the placement of cells with each site taking on one of a finite number of states. All sites are considered equal and are subject to the same transition rules, which may be deterministic (i.e., based on a series of thresholds) or probabilistic. These rules, which regulate state dynamics, are dependent on the site's current state and that of its neighboring sites. As shown in Figure 1.5, a cell's interactions may be restricted to either its von Neumann neighborhood or its Moore neighborhood.

Another fundamental characteristic of these models is that they consider time to be a discrete variable, with all of the sites updated simultaneously at each time step. Unlike numerical schemes, which take great care to overcome spurious behavior that can be attributed to discretization, CA models make no attempt to disguise such features [43].

There are a few commonly used variants of CA models. A coupled-map lattice approach has a continuous state space while an asynchronous cellular automaton updates only a randomly chosen subset of the cells at each time step. In addition, a nonhomogeneous cellular automaton allows transition rules to vary from site to site and/or in time. Some models

may have non-homogeneous, non-local transition rules that vary with the population size while others have non-local transition rates that are dependent on the position of the site. Moreira and Deutsch [41] also give examples of cellular automaton models where each lattice site can represent a different number of cells, where a cell occupies multiple adjacent sites, and where the state of a lattice site is determined by a stochastic energy minimization technique.

In the context of this study, discrete models function as an abstraction of tumor dynamics, with simple rules that form a caricature of local interactions and serve as a gross simplification of the biological system [26]. Nonetheless, these rules are able to incorporate cell-based data and describe the life cycle of the cells, signal transduction pathways, and biophysical laws [13, 41]. By incorporating statistical methods, differences and idiosyncrasies in the behavior of the cells can be modeled. Randomness is particularly relevant when considering long-range dispersion or the migration of a population that is small in size [13]. In these situations, the behavior of the population is predominantly statistical and randomness may indeed play a larger role in the outcome than the average behavior of the cell cluster [36].

Discrete models are easy to implement, allow cell tracking, and can provide visual feedback that replicates, or at least resembles, experimentally observed patterns [44]. In addition, it becomes feasible to describe the cells as individual entities with their own arbitrary shape and location (albeit not in the context of a cellular automaton). However, discrete models often require a large number of parameters, many of which have yet to be determined experimentally [13]. Without these parameters, assumptions must be made. This then calls into question the realism of these models, which provide qualitative insights rather than detailed quantitative predictions. Furthermore, discrete models can be computationally expensive and rigorous mathematical analysis of the results is difficult, if not impossible [2].

Multi-scale models

By their very nature, multiscale models are the ideal tool to capture biophysical interactions across spatial and temporal scales and to connect the chemical and physical details of an invasive tumor [8]. One class of multi-scale models is the hybrid model. These models blend continuum, discrete, and stochastic techniques in order to form a comprehensive model which describes both chemical reactions and the tissue landscape [8, 29]. The hybrid

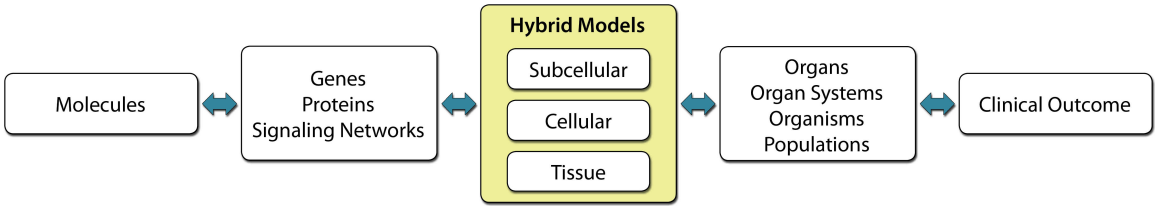

Figure 1.6: Modelling scales
Adapted from Rejniak and Anderson [46].

models discussed here treat individual cells as discrete entities that interact with various continuum fields. Another option is to use differential equations to describe high density regions and discrete algorithms to regulate cell behaviour along the low density rim of the tumor.

Hybrid models link the interactions of individual cells to the overall population dynamics. By doing so, they bridge activity on the genetic, sub-cellular, cellular, and tissue scales [45]. Some models focus on large populations of cells with a simplified geometry while others consider small colonies of fully deformable cells. The former class of models can consider thousands to millions of individual cells and provides an overview of the interactions between immediate neighbors [7]. On the other hand, the latter allows for a more realistic portrayal of cellular processes and early stage tumor development. A schematic diagram of modeling scales is presented in Figure 1.6.

The focus of hybrid models can include cell cycle dynamics, the impact of mutations on growth and division, phenotype survival, and cooperative and competitive behaviors amongst cells. Signaling and metabolic pathways, the mechanical and molecular details of cellular processes, and interactions amongst cells and their environment are among the biological phenomena that are well suited to be described in this way. In addition, the use of these models makes it possible to investigate the space and time dependent growth of the cells, the orientation of cell division (i.e., the axis of cell division), and migration [46].

When developing a model, there are many intricacies that must be carefully considered. One example is the evolution of cellular phenotypes. Some researchers choose to undertake a deterministic approach, using a flow chart that compares the current state of a cell with predetermined thresholds. For instance, the age of the cell, the nutrient levels, the number

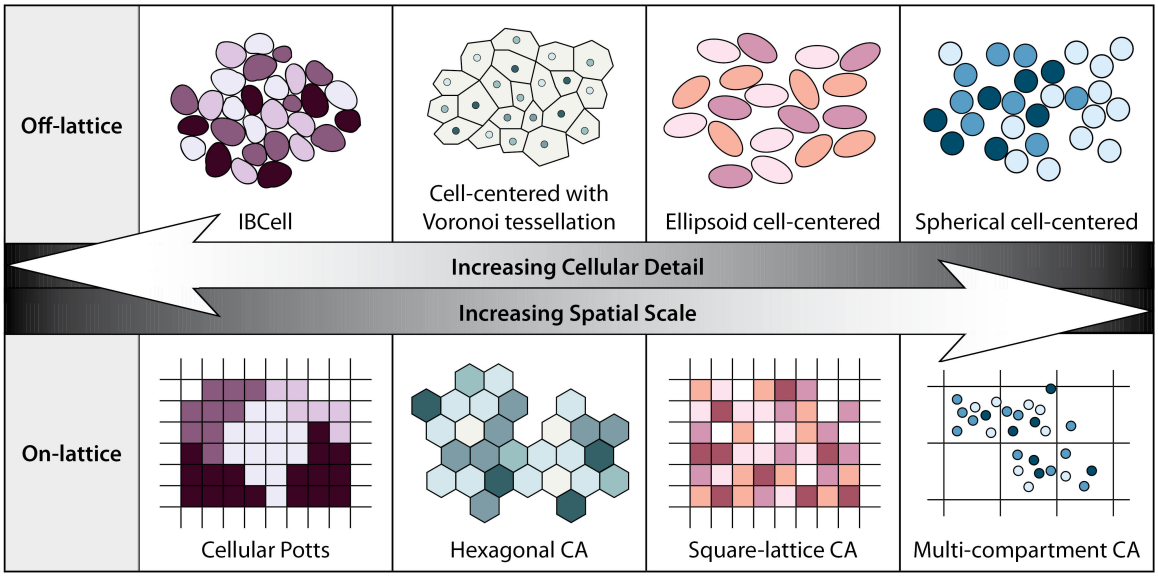

Figure 1.7: Examples of on-lattice and off-lattice models
Adapted from Rejniak and Anderson [46].

of neighbors, and the configuration of the cell membrane receptors can be examined to determine whether the cell grows, divides, moves, dies, or stays as is. Another possibility is to adopt a probabilistic approach with the cell's phenotype altered via random mutations acquired during cell division which modify the cell's speed, doubling time, life span, and oxygen consumption rate. Lastly, an artificial neural network can be implemented to determine cellular activity.

Another important issue to consider is the partitioning of the lattice. As shown in Figure 1.7, the lattice may be fixed in time or may vary as the elements move. "On-lattice" models constrain the cells to grid points and assume that the interactions between cells and their surrounding are localized to small neighborhoods [13]. Although this simplifies the task of reading cues from the cells' microenvironment, it limits the directions of movement and the number of neighboring cells. Among these models, there is variation in the dimension of the grid and the number of neighbours surrounding a single point. Furthermore, some models allow multiple cells to co-exist at each site. Examples of on-lattice models include multi-compartment cellular automata, square-lattice cellular automata, hexagonal-lattice cellular automata, and the Potts or Glazier-Granier-Hogeweg (GGH) model. GGH

models allow a cell to occupy several 2D square or 3D cubic lattice sites that, as an ensemble, define its surface area or volume. The defining characteristic of these models is their use of energy minimization and Monte Carlo simulations to determine the shape of the cells and their interactions with one another and their microenvironment. Tumor invasion is explored using the GGH approach in [33].

"Off-lattice" models do not require the spatial location of cells to be uniformly distributed on a fixed grid. This allows for a more realistic representation in which cells have the freedom to move in any direction and to take on either spherical, elliptical, or polygonal forms. The disadvantages of this approach are the inherent risk that an inappropriately chosen discrete-time step will result in cell collision and the necessity of developing an algorithm that can efficiently manage the interactions of cells with their immediate vicinity. Examples of off-lattice models include spherical cell-centered, ellipsoidal cell-centered, voronnoi tesselation, and fluid-based elastic cell models. Regardless of the approach taken to model cell position and movement, chemical and physical fields are generally defined on a regular (on-lattice) square or rectangular grid.

Most mathematical models are simulated in one or two spatial dimensions. Although they display numerous features of interest, they provide an incomplete representation of tumor invasion [27], particularly when the data is spatially heterogeneous [44]. Three dimensional models, which are often studied by examining two orthogonal slices of the simulated image [19], make it possible to analyze quantitative information and to examine the network architecture and expansion rate, as well as properties of growth and invasion in greater detail [47]. Enderling and his colleagues [44] suggest applying the marching cube volume rendering technique to aid in the study of solid tumor growth in irregular, heterogeneous, three-dimensional domains. They describe the implementation of this method and outline how it can aid in the visualisation of either Boolean information or the density or concentration of variables in their publication.

1.2.2 Mathematical Models

We will consider the hybrid discrete-continuum (HDC), the evolutionary hybrid cellular automaton (EHCA) and the immersed boundary (IBCell) models. These hybrid models focus on the interactions between cells and their micro-environment. Each model is agent-based and the cells are considered to be distinct units whose behavior is determined by intrinsic

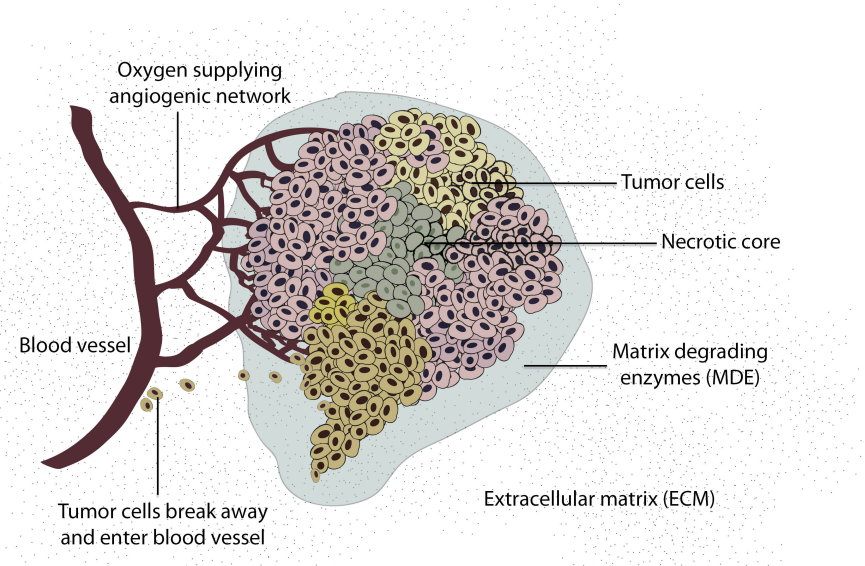

Figure 1.8: The key variables involved in solid tumor gowth
Adapted from Anderson [19].

cellular kinetic and the surrounding medium [48]. During tumorigenesis and cancer progression, these cells must overcome a variety of micro-environmental barriers triggered by the surrounding tissue [22]. To take this into account, the density of the extracellular matrix (ECM) and the respective concentrations of oxygen and matrix degradative enzymes (MDEs) are included in the models. These variables form a non-exclusive field that can have non-zero values at any point on the lattice and can co-occupy the same space as a cell [33]. Although an attempt is made to describe cell-microenvironmental interactions in a manner that reflects physiochemical laws and biological knowledge [6], these models are essentially gross simplifications that neglect precise biological details. However, their intent is to provide a qualitative framework, rather than mimic a biological system, and they are able to successfully fulfill this objective [6]. A schematic diagram labelling the key variables that are considered in this thesis is presented in Figure 1.8.

Each cell is anchored into its position by the ECM and the connective tissue [27]. The ECM is a heterogeneous melange of macromolecules that vary in their respective roles and

functions. Some are vital to maintain the structural integrity of the cells whereas others contribute to cellular adhesion, motility, and growth [45]. At times, the role played by the ECM may seem contradictory. For instance, although this nondiffusive substance is a barrier that must be physically removed to allow normal cellular motility, it also acts as a substratum to which cells may adhere in order to move [49]. Furthermore, it can sequester cell growth factors that speed up mitosis [26], and is known to do so when degraded [15]. It is a highly dynamic substance that, at any time, is actively secreted and degraded by cells [28] and that co-evolves with cancer cells [26]. However, in these models, it will be represented in a very generalized manner, without consideration of elastic forces or the molecular structure of the tissue [22].

To degrade the ECM, tumor cells secrete MDEs, also referred to as proteases, which diffuse slowly and locally degrade the ECM upon contact, creating gradients of bound cell-adhesion molecules [21, 45]. MDEs are often secreted by cells as inactive precursors and must be partially degraded to reach full activity [28]. They quickly bind to the matrix and remain localized near the interface between the invading tumor and the receding connective tissue [1, 50]. When the balance between proteases and anti-proteases is disrupted, excessive matrix degradation may be observed in the vicinity of the tumor [31]. This promotes motility and growth by providing the tumor cells with new space into which they can move by a process analogous to diffusion [21]. However, the excessive production of proteases is believed to incite a chemotactic pull that annihilates ECM gradients and prevents tumor expansion [31].

The production and consumption of nutrients is at the heart of cell survival and maintenance. Although various chemicals are required for tumor growth and development, the models that will be discussed typically focus on oxygen for the sake of simplicity. The models make the assumption that the concentration of oxygen is sufficiently high to allow successful application of partial differential equations and that its rate of diffusion occurs at a much shorter time scale than cellular dynamics (e.g., cell division) [17]. Physically, this means that the oxygen field is in a quasi-stationary state and hence satisfies the equation $\nabla^2 c(\mathbf{x}, t) = 0$ outside of the tumor. This implies that a linear function can be used to approximate the nutrient prolife in the vicinity of the tumor [51].

The oxygen is supplied to the system via capillary blood vessels [18] and is consumed by the cells at different rates, depending on their life cycle state [14]. The local concentration of oxygen plays a significant role in determining cellular behavior. If it is above the growth threshold, then proliferation may be observed. On the other hand, at a distance exceeding

$100 - 150\mu m$ from a blood vessel [52], the oxygen concentration falls below the hypoxic threshold and cell death occurs due to nutrient deprivation. Above the hypoxic threshold but below the growth threshold, quiescence is typically observed [6].

Cellular motion and proliferation are the crucial factors that determine tumor growth and invasion [9]. Since both require space, they are heavily influenced by surface stresses, which are often represented by cell crowding in mathematical models [43]. In some models, the cells must have access to a free lattice site in order to move; in other models, an empty place is created as the surrounding cells are shifted outwards [53]. Proliferation is typically most concentrated at the tumor's border where the flux of oxygen is high, the pressure is low, and the pH is normal [53]. In fact, the radius of the living region, which surrounds the necrotic core, has a velocity of propagation which is proportional to the rate of growth [43] and the growth rate is proportional to the gradient of the oxygen field [54]. On the other hand, motion is strongly influenced by adhesion [55]. Homotypic (cell-cell) adhesion results in a decreased tendency to invade the surrounding tissue. Conversely, heterotypic adhesion, whereby cells adhere to the connective tissue or different cell types, will enhance invasion.

The heterogeneous nature of the tumor is a central factor underlying cancer progression, with variability among cells nurturing competitive and invasive behaviors. There are three forms of variability that are believed to be important to tumor growth: phenotypic variability, phenotypic plasticity, and intrinsic noise [17].

Phenotypic variability encompasses genetic mutations and epigenetic gene regulation, while discrepancies between phenotypic traits are considered when examining phenotypic plasticity. Finally, there is the inherent noise within biological systems which should not be neglected when developing a model and analyzing simulation results.

In this thesis, three different single cell based multi-scale models will be used to investigate how various intrinsic and extrinsic factors influence the development of avascular tumors. In all of these models, the cells are driven by their genetic makeup and cues from their microenvironment.In addition, information from varying spatial scales are integrated in order to create a cohesive view of tumor dynamics [1, 21]. However, many cellular mechanisms have been either neglected or grossly simplified [1]. Although this greatly reduces the scope of the models, it does not detract from their ability to provide a surface description of how changes in the properties of the cells are manifested at the tissue scale [1].

There are fundamental similarities in all three models [6,17]. First, the cells are treated individually and their respective cell cycles dictate their proliferation, mutation, displacement, and death. Second, three types of cells are considered. Proliferating and quiescent cells compete for limited space and nutrients, while dead cells are labelled as necrotic. As they compete for resources, the proliferating and quiescent cells are able to sense the presence of, and interact with, other cells and their micro-environment. Proliferating cells are highly competitive as they engage in cell division and hence require exposure to high concentrations of oxygen. If the oxygen level remains above the hypoxic threshold but the cell lacks the space or nutrients necessary for it to undergo mitosis, it will become quiescent. A quiescent cell can revert back to a proliferative state if exposed to sufficient space and nutrients.

The hybrid discrete-continuum (HDC) model couples a cellular automaton approach, which is used to direct the behaviour and the interactions of the individual cells, with a system of reaction-diffusion-chemotaxis equations that describe the tissue. The value of this model is the novel insight it provides into cancer progression through the coupling of activity on various spatial scales [23]. Certain HDC models assign a predefined phenotype to each cell and examine how the different phenotypes respond under diverse environmental conditions [6]. Such models explore aspects of cellular activity such as motility and adhesion.

The evolutionary hybrid cellular automaton (EHCA) model uses an artificial response network to describe tumor growth and invasion and employs a feed-forward decision mechanism to determine the behavior of each cell. Every time a cell undergoes mitosis, the response network of the parent is copied to the daughter cells with a small probability of error to take into account mutations and noise. Each time an error occurs, it modifies the processing of the input layer and, hence, the generated output. In this way, it alters the ability of the cell and its progeny to compete for space and nutrients. Since the focus of this model is connecting a cell's genotype with its phenotype [23], the MDEs and the ECM are neglected.

In contrast to those aforementioned, the immersed boundary (IBCell) model rejects the notion of lattice sites and, instead, describes cells as fully deformable entities that interact with each other using membrane bound receptors [23]. These receptors, which sense free space, growth factors, nutrients, and other chemical concentrations [37], function as

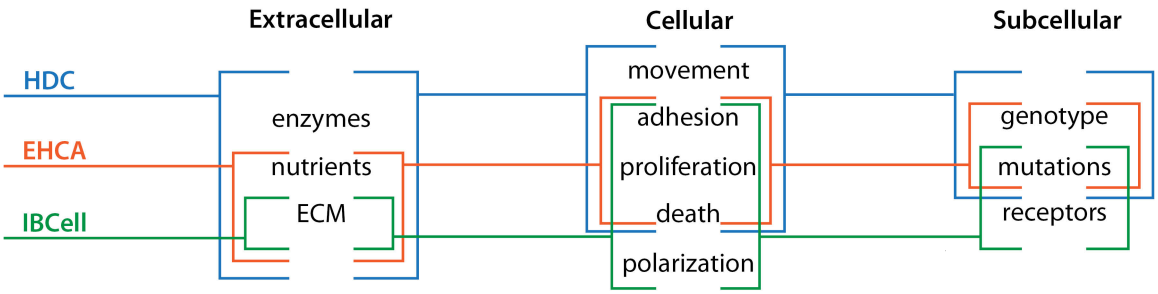

Figure 1.9: A comparison of the HDC, EHCA, and IBCell models
Adapted from Anderson et al. [23].

decision mechanisms and determine the state of each cell [56]. Although cellular receptors transduce all forms of mechanochemical information in a living cell, the simulated receptors here are abstractions which are grouped into broad categories based on their function (e.g., basal receptors and lateral receptors). A cell's receptors are connected by fully deformable elastics. These springs define the cell's shape and enclose its nuceleus as well as the viscous incompressible fluid which represents the cytoplasm and provides cell mass. The cells' microenvironment is also modelled as an incompressible viscous Newtonian fluid. Focusing on the cellular level, this approach links the physical mechanisms of elastic cells with the kinetics of nutrient distribution [17] and attempts to discover how cells form invasive tumors [6].

When working with different models it is important to compare and contrast their defining properties. Here, the HDC and EHCA models are phenotype/genotype driven and consider cells at lattice sites, while the IBCell model is receptor driven and represents cells as fluid filled elastic entities. In addition, the EHCA and HDC models are initiated with a cluster of cells, among which some have undergone mutations, while the cells in the IBCell model are considered normal cells and the tumor can progress without ever undergoing mutations [6]. Tumor expansion in the EHCA and IBCell models is proliferation driven, but is influenced by both proliferation and migration (i.e., haptotaxis and chemotaxis) in the HDC model. In all three models, oxygen acts as a nutrient. However, its production and consumption differs from one model to the next. The source of oxygen may be the boundary (i.e., the surrounding blood vessels), the ECM, or a combination of both. A summary of the similarities and differences amongst the models is presented in Figure 1.9.

There are many advantages to building different types of models and juxtaposing their respective results. When outcomes are comparable, the models pinpoint common assumptions and link them to the underlying biological mechanism. Thus, they provide experimentalists with new possible mechanisms on which they can focus. Alternatively, if outcomes vary, the variables and the core mechanisms must be re-evaluated and the source of the discrepancy uncovered. In this way, further insight can arise.

Although many aspects of these models can be manipulated and a variety of biological phenomena can be incorporated, models tend to be phenomenological and predictions are typically heuristic. Furthermore, rather than being cancer-specific, they tend to be general, in part due to a paucity of experimental data available to parameterize and validate overly detailed models. Nevertheless, mathematical models possess good predictive potential and provide an efficient method by which the interplay between intracellular and extracellular factors can be synthesized [1]. In addition, they have the capacity to integrate diverse experimental measurements in order to generate testable predictions and to provide experimentalists with new subject matter. The last decade has seen increasing interaction and collaborations between experimentalists and mathematicians. This synergy where theory guides experiment and, conversely, where experimental data leads to developments in theory, may well lead to dramatic advances in the future.

1.3 Outline of the Thesis

This thesis presents an overview of multi-scale mathematical models of tumor growth and invasion. In Chapter 2, we consider Anderson's hybrid discrete-continuum model of tumor invasion. We present both the original "anaerobic model and the later "aerobic variants, which include oxygen as one of the key variables and describe the life cycle of the individual cells in greater depth. In addition, we perform simulations which study the role of the ECM as a barrier to cellular expansion. We end the chapter by discussing our recommendations for future work.

Chapter 3 describes the evolutionary hybrid cellular automaton model. In this chapter, we explore the theory behind artificial networks and discuss how they can be applied to our study of tumor progression. In particular, we explore how Gerlee and colleagues use this approach to try to understand how the genotype, cell motility, and metabolism affect the phenotype of a cell.

An immersed boundary model is presented in Chapter 4. In contrast to the previous methods, cell behavior in this model is receptor driven. Furthermore, the cells take on varying shapes and change their configuration in response to environmental cues.

In Chapter 5, we summarize the salient results that are reiterated in all three models. We also explore the advantages and disadvantages of mathematical modelling and conclude by suggesting improvements and future directions in research.

Chapter 2

Hybrid Discrete-Continuum Models

2.1 Anaeorbic Hybrid Discrete-Continuum Model of Tumor Growth

In 2000, Anderson and Chaplain [45] published a model describing the invasion of host tissue by cancerous cells. In this model, reaction-diffusion equations are used to express the time evolution of the tumor cell density, the production and activation of matrix degradative enzymes, and the resulting disintegration of the matrix. To account for the multi-scale nature of tumor growth, the authors couple this continuous system with a discrete one, which aims to capture the small scale and stochastic interactions between individual cells.

2.1.1 Continuous model of anaerobic tumor growth

According to this model, a tumor undergoes changes in its density as it evolves through time. Since the tumor is being mapped onto a regular 2-dimensional grid, this may seem incongruous with our understanding of cancer cells as discrete entities. However, rather than being construed in the literal sense, the density is meant to be interpreted as the probability that there is a tumor cell at a given point in space and is modulated to take on a value between 0 and 1.

Anderson and Chaplain [45] claim that the tumor cell density n is determined by the random and haptotactic migration of the cells. The unbiased motion of the cells is com-

parable to the phenomenon of Brownian motion [3] and is considered to be analogous to molecular diffusion [47]. However, experimental data indicates an "overwhelming dominance" of directed movement in invasive tumors [55]. Here, this behavior is attributed to haptotaxis. Haptotaxis is defined as the directional migration of cells up gradients of cellular adhesion sites or substrate-bound chemoattractants [4]. It is commonly described as the motile response of cells to gradients of bound, insoluble, and non-diffusive stimuli [57].

Under this framework, the conservation of matter dictates that the tumor cell density must satisfy

$$\frac{\partial n}{\partial t} + \nabla \cdot (\mathbf{J}_{rand} + \mathbf{J}_{hapto}) = 0.$$

Here, $\mathbf{J}_{hapto} = \chi n \nabla f$, $\chi > 0$ describes the haptotactic flux that drives cells up gradients of the ECM, where f is the density of the ECM, and $\mathbf{J}_{rand} = -D_n \nabla n$ describes the flux attributed to random motion. Hence,

$$\frac{\partial n}{\partial t} = \nabla \cdot D_n \nabla n - \chi \nabla \cdot (n \nabla f), \tag{2.1}$$

where D_n is the random motility coefficient and $\chi > 0$ is the haptotactic coefficient. These coefficients quantify the strength of the cellular response, with augmented values indicating faster migration.

The tumor cells produce matrix degradation enzymes m (MDEs), which decay as they diffuse through the tissue and degrade the extracellular matrix (ECM) . Expressed mathematically,

$$\frac{\partial m}{\partial t} = D_m \nabla^2 m + g(n, m) - h(n, m, f), \tag{2.2}$$

where D_m is the diffusion coefficient, $g(n, m)$ is the rate at which tumor cells produce MDEs, and $h(n, m, f)$ is the rate of decay. Anderson and Chaplain [45] explore a variety of different ways to model the decay rate before selecting the one that best describes the interactions between MDEs and heterogeneous ECM. In particular, they considered:

$$h(n, m, f) = \lambda m, \tag{2.3}$$

$$h(n, m, f) = \lambda m f, \text{ and} \tag{2.4}$$

$$h(n, m, f) = \lambda m (1 - f), \tag{2.5}$$

where equation 2.3 corresponds to natural decay and equations 2.4 and 2.5 are consistent

with scenarios where the rate of decay is proportional and inversely proportional to the density of the ECM, respectively. From a biological perspective, equation 2.4 asserts that the production of MDE inhibitors is directly proportional to the density of the ECM. In contrast, equation 2.5 describes a scenario where the MDEs bind to and degrade the tissue in a more aggressive manner in regions with higher densities of ECM.

In order to select the appropriate decay pattern, simulations were performed and the impact on the ECM was assessed. When the $h(n, m, f)$ was proprotional to the density of the ECM (equation 2.4), comparatively less decay was observed and the leading edge of the tumor was not as well defined. However, the aforementioned differences were only minimal. In fact, the presence of MDEs was deemed to be more significant than the precise functional form of $h(m, n, f)$ [45]. Ultimately, the decision was made to assume a linear production of MDEs and natural decay with:

$$\frac{\partial m}{\partial t} = D_m \nabla^2 m + \mu n - \lambda m, \tag{2.6}$$

for some positive constants μ and λ.

The ECM f is assumed to be an insoluble matrix of macromolecules that are degraded immediately upon contact with the MDEs. Since the macromolecules are much larger than the cells, their motility is considered to be negligible [55]. This means that

$$\frac{\partial f}{\partial t} = -\delta m f, \tag{2.7}$$

where δ is a positive constant.

Anderson and Chaplain [45] non-dimensionalize their model [58]. Thus, the variables are independent of units of measurement and are compared to intrinsic reference values instead. Non-dimensionalization reduces the number of parameters and simplifies the analysis and simulation of the model [3]. However, this step necessitates knowledge of the main features of the solution in order to make accurate order of magnitude and scaling estimates. Moreover, spatial heterogeneity in the parameter range must also be considered [58].

Anderson and Chaplain [45] rescale distance using the length scale L, which corresponds to the maximum invasive distance of the cancer cells at this stage of tumor progression. In addition, they let $\tau = \frac{L^2}{D}$ to rescale time, where D is referred to as the "chemical diffusion

coefficient". Furthermore, the tumor cell density is rescaled with n_0, the ECM density with f_0, and the MDE concentration with m_0, where n_0, m_0, and f_0 are the appropriate reference variables, and

$$\tilde{n} = \frac{n}{n_0}, \qquad \tilde{f} = \frac{f}{f_0}, \qquad \tilde{m} = \frac{m}{m_0}, \qquad \tilde{x} = \frac{x}{L}, \quad \text{and} \quad \tilde{t} = \frac{t}{\tau}. \tag{2.8}$$

Substituting into the equations above and dropping the tildes, the following system of equations is obtained:

$$\frac{\partial n}{\partial t} = d_n \nabla^2 n - \gamma \nabla \cdot (n \nabla f) \tag{2.9}$$

$$\frac{\partial f}{\partial t} = -\eta m f \tag{2.10}$$

$$\frac{\partial m}{\partial t} = d_m \nabla^2 m + \alpha n - \beta m, \tag{2.11}$$

where $d_n = \frac{D_n}{D}, \gamma = \frac{\chi f_0}{D}, \eta = \tau m_0 \delta, d_m = \frac{D_m}{D}, \alpha = \frac{\tau \mu n_0}{m_0}$, and $\beta = \tau \lambda$.

Since the total number of cells is conserved and the system is closed, it is reasonable to impose zero flux boundary conditions. The boundary conditions imposed are then:

$$\underline{\zeta} \cdot (-d_n \nabla n + \gamma n \nabla f) = 0 \tag{2.12}$$

for the cells and

$$\underline{\zeta} \cdot (-d_m \nabla m) = 0 \tag{2.13}$$

for the MDEs, where $\underline{\zeta}$ is the appropriate outward unit normal

2.1.2 Discrete model of anaerobic tumor growth

Although a continuous approach can successfully capture cell-matrix interactions and other forms of activity on the tissue scale, a cellular automaton model is better suited to capture activity at the cellular and subcellular scales. The main advantage of using a discrete model is that it allows for quantitative comparisons to be made between in vivo and in silico results. Furthermore, the behavior of individual tumor cells can be monitored and rules for cell proliferation and motion can be explicitly expressed.

This model assumes that cells must be mature and have sufficient space in order to proliferate. By definition, maturity is reached 500 time steps after birth and a cell has sufficient space to undergo mitosis if at least one of its orthogonal neighbors is empty. If more than one empty site is available, one daughter cell will occupy the position of the parent cell and the position of the other one will be randomly[1] selected.

For these simulations, the capacity of the grid is limited to 3000 cells. This restriction implies that the structures which evolve will be a product of migration rather than proliferation. To describe the motion of the cells, a discrete quasi-stochastic scheme is derived using the principles of a biased random walk. In this scheme, the tumor cell density n at the grid point (i, j) at time q is denoted $n^q_{i,j}$. The cell density at $(i, j, q + 1)$ is calculated by collecting the relevant data at the point (i, j) and at its four orthogonal neighbors at time q and then averaging according to the equation

$$n^{q+1}_{i,j} = P_0 n^q_{i,j} + P_1 n^q_{i+1,j} + P_2 n^q_{i-1,j} + P_3 n^q_{i,j+1} + P_4 n^q_{i,j-1} \tag{2.14}$$

where P_0 is proportional to the probability of staying stationary and P_1, P_2, P_3, and P_4 are proportional to the probabilities of moving left, right, down, and up, respectively. Each of these probability terms can be broken down into two mechanisms: random motion and a directed response toward an external stimulus,

$$P_n = \text{random motion} + \text{haptotaxis}. \tag{2.15}$$

When determining the direction of motion, the first step is to calculate

$$P_0 = 1 - \frac{4d_n\Delta t}{\Delta x^2} - \frac{\gamma\Delta t}{\Delta x^2}(f^q_{i+1,j} + f^q_{i-1,j} - 4f^q_{i,j} + f^q_{i,j+1} + f^q_{i,j-1}) \tag{2.16}$$

$$P_1 = \frac{d_n\Delta t}{\Delta x^2} - \frac{\gamma\Delta t}{4\Delta x^2}(f^q_{i+1,j} - f^q_{i-1,j}) \tag{2.17}$$

$$P_2 = \frac{d_n\Delta t}{\Delta x^2} + \frac{\gamma\Delta t}{4\Delta x^2}(f^q_{i+1,j} - f^q_{i-1,j}) \tag{2.18}$$

$$P_3 = \frac{d_n\Delta t}{\Delta x^2} - \frac{\gamma\Delta t}{4\Delta x^2}(f^q_{i,j+1} - f^q_{i,j-1}) \tag{2.19}$$

$$P_4 = \frac{d_n\Delta t}{\Delta x^2} + \frac{\gamma\Delta t}{4\Delta x^2}(f^q_{i,j+1} - f^q_{i,j-1}). \tag{2.20}$$

[1]The position of this cell will be determined using a computer algorithm that selects one of the empty neighboring sites, without bias.

These cofficients are obtained using a 5-point finite difference discretization[2] of the partial differential equation 2.9.

Once obtained, these values are normalized with $P_i^{norm} = \frac{P_i}{\sum_{j=0}^{4} P_j}$ for $i = 0, 1, 2, 3, 4$. Next, the probability ranges R_i are computed. Anderson and Chaplain let $R_0 = 0$ to P_0^{norm} and $R_i = \sum_{j=0}^{i-1} P_j^{norm}$ to $\sum_{j=0}^{i} P_j^{norm}$ for $i = 1, 2, 3, 4$. They then generate a random number $0 \leq g_{rand} \leq 1$ which determines the direction of motion based on the range into which it falls.

According to this model, the geometry of the tumor, the concentrations of the nutrients and the MDEs, the cell life cycle, and the interactions among neighboring cells are some of the factors that impact cell migration [15, 34, 59]. However, it is assumed that the motion of the cells is most strongly influenced by their interactions with the macromolecules in their immediate vicinity, with tumor cells moving up gradients toward higher densities of the ECM. In the event that there is no ECM present, the values of P_j for $j = 1, 2, 3, 4$ are all equivalent; thus, there is no bias and the random walk scheme dictates the direction of motion.

One salient concern is that the probability coefficients can take on negative values. According to Anderson [19, 59], this problem should be addressed by making the grid size and the time step sufficiently small to ensure that $\frac{4\Delta t d_n}{\Delta x^2} < 1$ is satisfied. However, it is important to keep in mind that the grid size is fixed by the scale of the organism, that a small time step might reduce the computational speed, and that the haptotaxis and diffusion coefficients must remain within a reasonable range.

Anderson [59] lists various reasons why it makes sense to derive the discrete model from the tumor cell density equation in this scenario. First, he claims that it is easier to begin by establishing the continuum model when considering the migration of an organism that is influenced by stimuli on various scales. Second, he declares that this approach guarantees that the space and time step for the "biased random walk"[3] will match that of the continuous scheme. Ergo, it will be easier to interpret the interplay of the interactions on the different scales. However, from a mathematical standpoint, it makes more sense to

[2] Although the application of a nine-point stencil may seem more favorable, the increased computational time does not yield a corresponding increase in insight due to the sizeable impact of random motility [21].

[3] In the context of the model being considered, the "biased random walk" is more of an analogy than a true definition [59].

examine the motion of the individual cells and then derive a continuous equation describing the motion of the tumor cluster, in the limit of a large cellular population size.

In order to confirm the validity of a related model, Othmer and Stevens [12] demonstrate how discrete transitional probabilities can be used to derive a partial differential equation in the continuous limit. Anderson [59] adopts this approach and implements it in one dimension. Here, we will take it one step further and consider two dimensions. We begin our analysis by considering the central difference semi-discretization of equation 2.9:

$$\frac{\partial n_i}{\partial t} = p_1 n^q_{i+1,j} + p_2 n^q_{i-1,j} + p_3 n^q_{i,j+1} + p_4 n^q_{i,j-1} - p_0 n^q_{i,j} \tag{2.21}$$

where

$$\begin{aligned} p_1 &= \varpi - \Upsilon(f_{i+1,j} - f_{i-1,j}) \\ p_2 &= \varpi + \Upsilon(f_{i+1,j} - f_{i-1,j}) \\ p_3 &= \varpi - \Upsilon(f_{i,j+1} - f_{i,j-1}) \\ p_4 &= \varpi + \Upsilon(f_{i,j+1} - f_{i,j-1}) \\ p_0 &= 4\varpi + 4\Upsilon(f_{i+1,j} + f_{i-1,j} - 4f_{i,j} + f_{i,j+1} + f_{i,j-1}) \end{aligned} \tag{2.22}$$

and $x = ih, y = jh, \varpi = \frac{d_n}{h^2}$, and $\Upsilon = \frac{\gamma}{4h^2}$.

To validate the assumption that the values P_1, P_2, P_3, and P_4 represent the probabilities of motion and P_0 is the probability of remaining stationary, we shall use equations 2.21 and 2.22 and attempt to recover equation 2.9. Upon substituting equation 2.22 into equation 2.21, we obtain:

$$\begin{aligned} \frac{\partial n_i}{\partial t} &= n^q_{i+1,j}(\varpi - \Upsilon(f_{i+1,j} - f_{i-1,j})) + n^q_{i-1,j}(\varpi + \Upsilon(f_{i+1,j} - f_{i-1,j})) \\ &+ n^q_{i,j+1}(\varpi - \Upsilon(f_{i,j+1} - f_{i,j-1})) + n^q_{i,j-1}(\varpi + \Upsilon(f_{i,j+1} - f_{i,j-1})) \\ &- n^q_{i,j}(4\varpi + 4\Upsilon(f_{i+1,j} + f_{i-1,j} - 4f_{i,j} + f_{i,j+1} + f_{i,j-1})) \end{aligned}$$

which can be rearranged as

$$\begin{aligned} \frac{\partial n_i}{\partial t} &= \varpi(n_{i+1,j} + n_{i-1,j} - 4n_{i,j} + n_{i,j-1} + n_{i,j+1}) - \Upsilon n_{i+1,j}(f_{i+1,j} - f_{i-1,j}) \\ &+ \Upsilon n_{i-1,j}(f_{i+1,j} - f_{i-1,j}) - \Upsilon n_{i,j+1}(f_{i,j+1} - f_{i,j-1}) \\ &+ \Upsilon n_{i,j-1}(f_{i,j+1} - f_{i,j-1}) - 4\Upsilon n_{i,j}(f_{i+1,j} + f_{i-1,j} - 4f_{i,j} + f_{i,j-1} + f_{i,j+1}). \end{aligned} \tag{2.23}$$

Since the domain is a regular two-dimensional lattice with mesh size h (i.e., $x = ih, y = jh$), we can expand the right hand side of equation 2.23 as a Taylor series to second order in h, to obtain,

$$\begin{aligned}\frac{\partial n_i}{\partial t} &= \varpi h^2 \nabla^2 n - 2\Upsilon h f_x \left(n + h n_x + \frac{h^2}{2} n_{xx} \right) + 2\Upsilon h f_x \left(n - h n_x + \frac{h^2}{2} n_{xx} \right) \\ &- 2\Upsilon h f_y \left(n + h n_y + \frac{h^2}{2} n_{yy} \right) + 2\Upsilon h f_y \left(n - h n_y + \frac{h^2}{2} n_{yy} \right) - 4\Upsilon h^2 n \nabla^2 f + O(h^4).\end{aligned}$$

which simplifies to

$$\frac{\partial n_i}{\partial t} = \varpi h^2 \nabla^2 n - 4\Upsilon h^2 \left(f_x n_x + f_y n_y \right) - 4\Upsilon h^2 n \nabla^2 f + O(h^4). \tag{2.24}$$

Assuming that a scaling of transition rates $f = \vartheta \bar{f}$ and $\varpi = \vartheta \bar{\varpi}$ exists, such that

$$lim_{h \to 0, \vartheta \to \infty} \vartheta h^2 = D$$

for some positive constant D, we let $d_n = D\bar{\varpi}$ and $\gamma = 4D\Upsilon$. Substituting back into equation 2.24 we determine that the diffusion limit is

$$\frac{\partial n}{\partial t} = d_n \nabla^2 n - \gamma \nabla \cdot (n \nabla f),$$

which is as desired.

By acknowledging this intricate link between the discrete and the continuous models, we are able to appreciate how this approach ties together the micro-scale with the macro-scale and creates a cohesive model that links individual level and population level dynamics. However, this method is only valid if we assume that the individual cells do not interact with one another, a biologically infeasible constraint [19]. Furthermore, a biological explanation behind the probability coefficients in the master equation is lacking. Expressing the migration of the cells using stochastic differential equations would have been a more appropriate approach.

2.1.3 Simulation results

In their paper, Anderson and Chaplain [45] compare the results obtained from the discrete and continuous models[4]. Their simulations are initiated with 500 tumor cells and run for a duration of 4000 time steps.

To validate their model, Anderson and Chaplain [45] systematically vary the parameters. They establish that increasing the value of the haptotaxis coefficient[5] increases the invasive behavior of the cells. On the other hand, invasion is more localized and the degradation of the matrix is more prominent when the MDE diffusion coefficient[6] is increased. When both coefficients are increased simultaneously, there is a sizable augmentation in the fraction of the cells that separate from the tumor mass. These cells invade the host tissue at a faster rate and are driven primarily by haptotaxis.

In the litterature, the diffusion coefficient and its impact on tumor morphology are also explored. When the diffusion rate is constant, haptotaxis-induced migration results in the formation of small clusters of cells at the leading edge. With time, these clusters move further away from the tumor core as they slowly but continually invade the extracellular matrix. Anderson acknowledges that, with sufficient time, these cells will eventually aggregate beyond the boundary of the domain. To prevent this biologically infeasible solution from manifesting, Anderson and Chaplain present diffusion as a nonlinear chemokinetic response, and let the rate of the random motility be directly proportional to the concentration of the MDEs (i.e., $d_n = d_{nn}m$ where d_{nn} is a positive constant). Under this assumption, there is a pronounced build up of cells at the leading edge of the tumor within a relatively short period of time. Furthermore, the cells are more likely to break away from the main tumor mass and the speed of invasion is reduced. As this system begins to stabilize, two distinct clusters form, with the cells driven by haptotaxis segregating from the tumor body, migrating faster and further into the ECM.

Besides these parameters, Anderson and Chaplain [45] also study the relationship between the tissue environment and tumor growth. As shown in Figure 2.1, the leading edge is the region of highest cell density, and will ultimately detach to form multiple separate rings of invasive cells in the continuous model with homogeneous ECM. These findings are

[4]They use the same parameter values for both models.

[5]in 2.9

[6]in equation 2.11

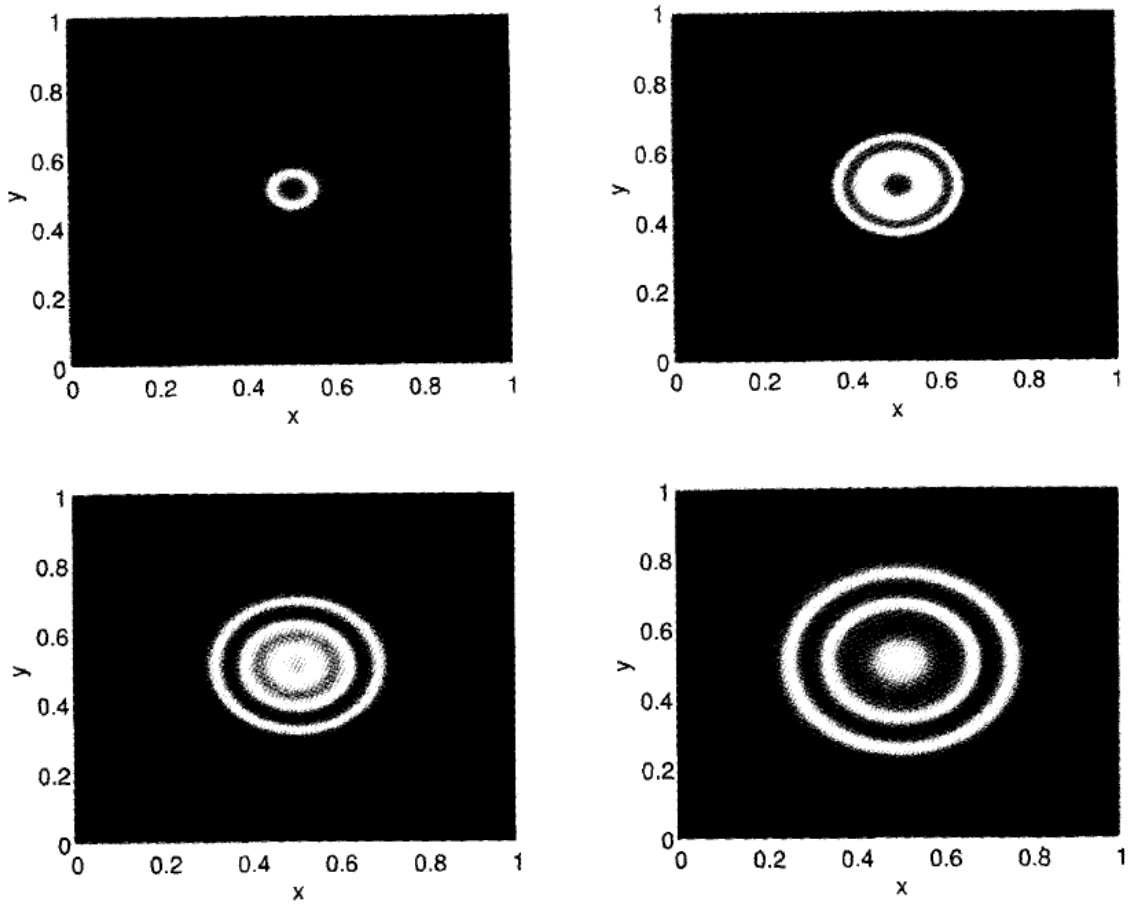

Figure 2.1: The spatio-temporal evolution of the tumor cell density in homogeneous ECM *The tumor is observed to break into concentric rings of cells that invade into the ECM. These results are derived from the continuous model, under the assumption of a constant diffusion coefficient. Reprinted from Journal of Theoretical Medicine, 2, A.R.A. Anderson, M.A.J. Chaplain, E.L. Newman, R.J.C. Steele, and A.M. Thompson, Mathematical modelling of tumor invasion and metastasis, 129-154, Copyright (2000). [45]*

recognized as being blatantly unrealistic; fortunately, the authors have been able to obtain more reasonable results when considering heterogeneous ECM. Figure 2.2 illustrates how the symmetry in the cellular density is broken and how small regions with higher cell density form under this assumption. Similar results are obtained when the focus moves to the discrete model, although there are some notable differences with regards to tumor progression in the heterogeneous environment. In particular, greater dispersion is seen, followed by the emergence of numerous high density clusters, as illustrated in Figure 2.3.

Anderson and Pitcairn [15] combine the discrete and continuous systems into a single hybrid model and use this framework to further investigate the relationship between the distribution of the ECM and tumor morphology. In particular, they consider homogenous, heterogeneous and random distributions of macromolecules in the ECM. Their simulations indicate that large, symmetric tumors, that can rapidly invade the surrounding matrix, form under the constraint of a homogeneous environment. In contrast, small tumors with ragged boundaries are observed given a random distribution of MM and a heterogeneous environment is seen to yield tumors which lack symmetry and compactness.

2.1.4 Conclusions

Comparing the continuous and the discrete models, more aggressive behavior is observed in the latter where the cells invade further into the ECM and are more likely to separate from the tumor body. Clinically, this corresponds to an increased risk of metastasis. Furthermore, these results indicate an abatement of surgical efficiency since the small clusters of detached tumor cells are likely to go unnoticed by a doctor who is trying to excise the tumor.

Based on their simulations, Anderson and Chaplain [45] also conclude that ECM heterogeneity and haptotaxis are two key factors that shape tumor morphology. Furthermore, they assert that parallels between these simulations and histological observations make their results applicable in vivo [15]. Spurred on by these results, they decided to extend this model to include phenotypic variation in cells and oxygen limited growth. Their extensions will be discussed in the next section. Additional suggestions regarding areas of modification as well as potential extensions will be summarized in Section 2.4.

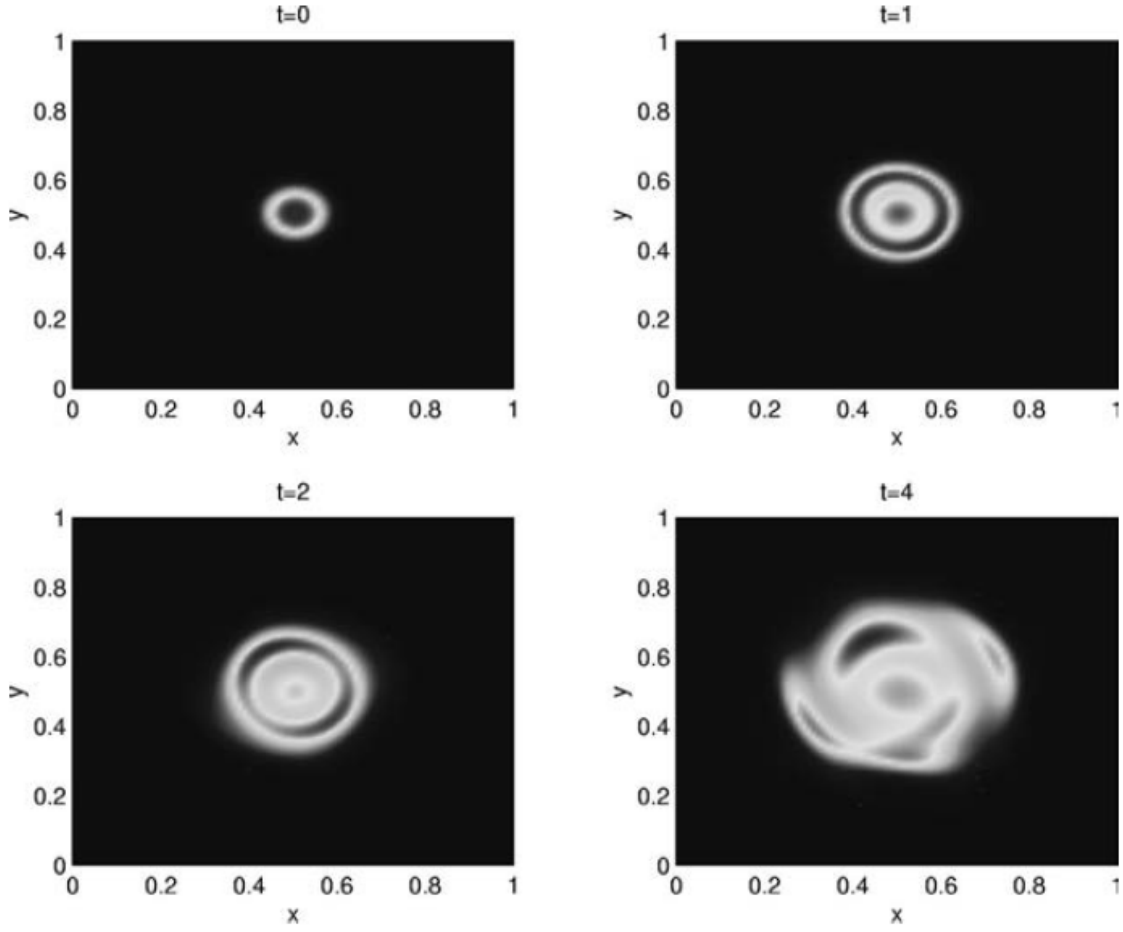

Figure 2.2: The spatio-temporal evolution of the tumor cell density in heterogeneous ECM *The effect of the heterogeneous ECM becomes apparent for larger values of t. As above, these results are also derived from the continuous model under the assumption of a constant diffusion coefficient. Reprinted from Journal of Theoretical Medicine, 2, A.R.A. Anderson, M.A.J. Chaplain, E.L. Newman, R.J.C. Steele, and A.M. Thompson, Mathematical modelling of tumor invasion and metastasis, 129-154, Copyright (2000). [45]*

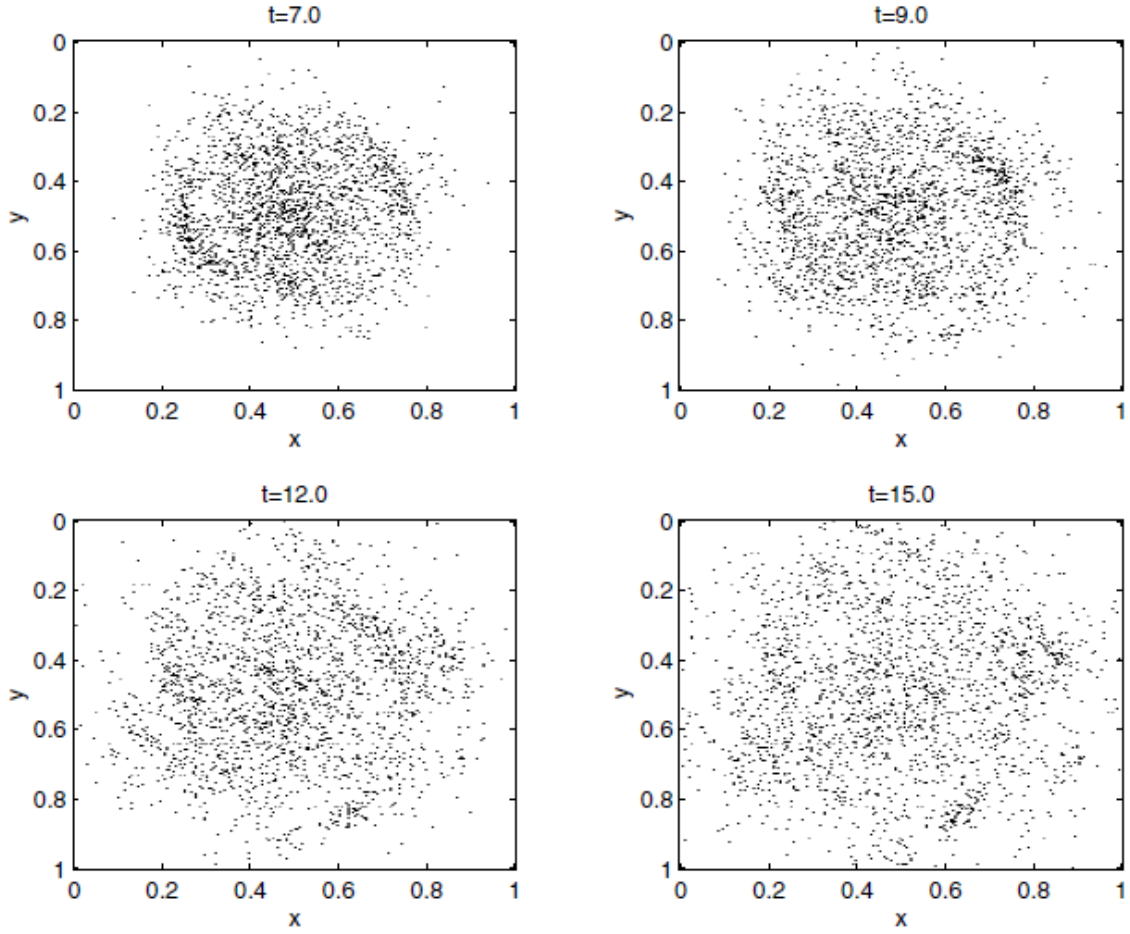

Figure 2.3: The spatio-temporal evolution of discrete cells in a heterogeneous environment *The migration of the tumor cells into the heterogeneous ECM is illustrated. Anderson and Chaplain claim there are similarities between the distribution of the cells and the density of the ECM. Reprinted from Journal of Theoretical Medicine, 2, A.R.A. Anderson, M.A.J. Chaplain, E.L. Newman, R.J.C. Steele, and A.M. Thompson, Mathematical modelling of tumor invasion and metastasis, 129-154, Copyright (2000). [45]*

2.2 Aerobic Hybrid Discrete-Continuum Model

2.2.1 Continuous model of aerobic tumor growth

This section describes the modifications made by Anderson and colleagues [1,8,17,19–21,23, 35] to the hybrid model presented in Chapter 2. In particular, we discuss how they attempt to capture tumor growth immediately following vascularization by modelling the tumor as a cluster of cells enclosed by blood vessels which supply oxygen at a constant rate [23]. To describe the macroscopic events, the authors supplement the reaction-diffusion-chemotaxis equations presented by Anderson and Chaplain in [45] with an equation which describes the time dependent evolution of the oxygen field. This nutrient is assumed to diffuse and decay and is produced at a rate proportional to the density of the ECM at each lattice site. This representation implies that haptotaxis drives cells toward the oxygen rich regions and that tumors disrupt their oxygen supply as they grow [17].

The system of equations which describes activity at the tissue scale is

$$\begin{aligned} \frac{\partial n}{\partial t} &= d_n \nabla^2 n - \gamma \nabla \cdot (n \nabla f) \\ \frac{\partial f}{\partial t} &= -\eta m f \\ \frac{\partial m}{\partial t} &= d_m \nabla^2 m + \alpha n - \beta m \\ \frac{\partial c}{\partial t} &= d_c \nabla^2 c + \lambda f - \kappa n - \mu c \end{aligned} \tag{2.25}$$

where n is the density of the tumor cells and f, m, and c are the concentrations of the ECM, the MDEs, and oxygen, respectively. In addition, d_n, d_m, and d_c are the diffusion coefficients for the tumor cell density, the MDEs, and the oxygen, γ is the haptotaxis coefficient, and $\eta, \alpha, \beta, \lambda, \kappa$, and μ are positive constants.

There have been a few variants of this model published over the years. For instance, Anderson refers to f as the concentration of macromolecules (MM) rather than the concentration of ECM in [21]. In another article, he proposes that oxygen diffuses at a slower rate at grid points that are occupied by cells and lets the diffusion coefficient be $d_{cell} < d_c$ at these points [19]. Finally, in [1], he and his colleagues consider discrete cells instead of the tumor cell density and formulate the following system of reaction-diffusion-chemotaxis

equations

$$\begin{aligned}
\frac{\partial f}{\partial t} &= -\eta m f \\
\frac{\partial m}{\partial t} &= d_m \nabla^2 m + \alpha N_{i,j} - \beta m \\
\frac{\partial c}{\partial t} &= d_c \nabla^2 c - \mu c - \kappa N_{i,j} c + \lambda f
\end{aligned}$$

where $N_{i,j}$ is used to denote the tumor cell located at lattice site (i, j).

For all variants of the HDC model, the behavior of the cells is mapped onto a 2-dimensional lattice and the simulations are initialized with a predefined number of tumor cells, aged 0 to 16 hours, positioned at the center of the grid. In terms of the initial conditions, the concentration of the MDEs is set to 0, the oxygen concentration is set to 1, and the concentration of the ECM falls within the range $0 \leq f \leq 1$ [21]. In addition, zero-flux boundary conditions are imposed on the system.

2.2.2 Discrete model of aerobic tumor growth

As the simulation proceeds, changes in the life cycle of the cells are obtained. To differentiate between the cells, each one is assigned an identification number which determines the order in which it will be updated during each time step. Since this may give preference to certain cells and visibly bias the results, the identification numbers are distributed randomly [19].

When a cell is being updated, its ability to move is assessed and its age is examined. If the cell has reached maturity, Figure 2.4 outlines how it will respond based on the distribution of its neighbors and its access to nutrients. A careful analysis of the life cell cycle is presented in the sections below, with an emphasis on how the different constrain1ts on the cell impact its behavior.

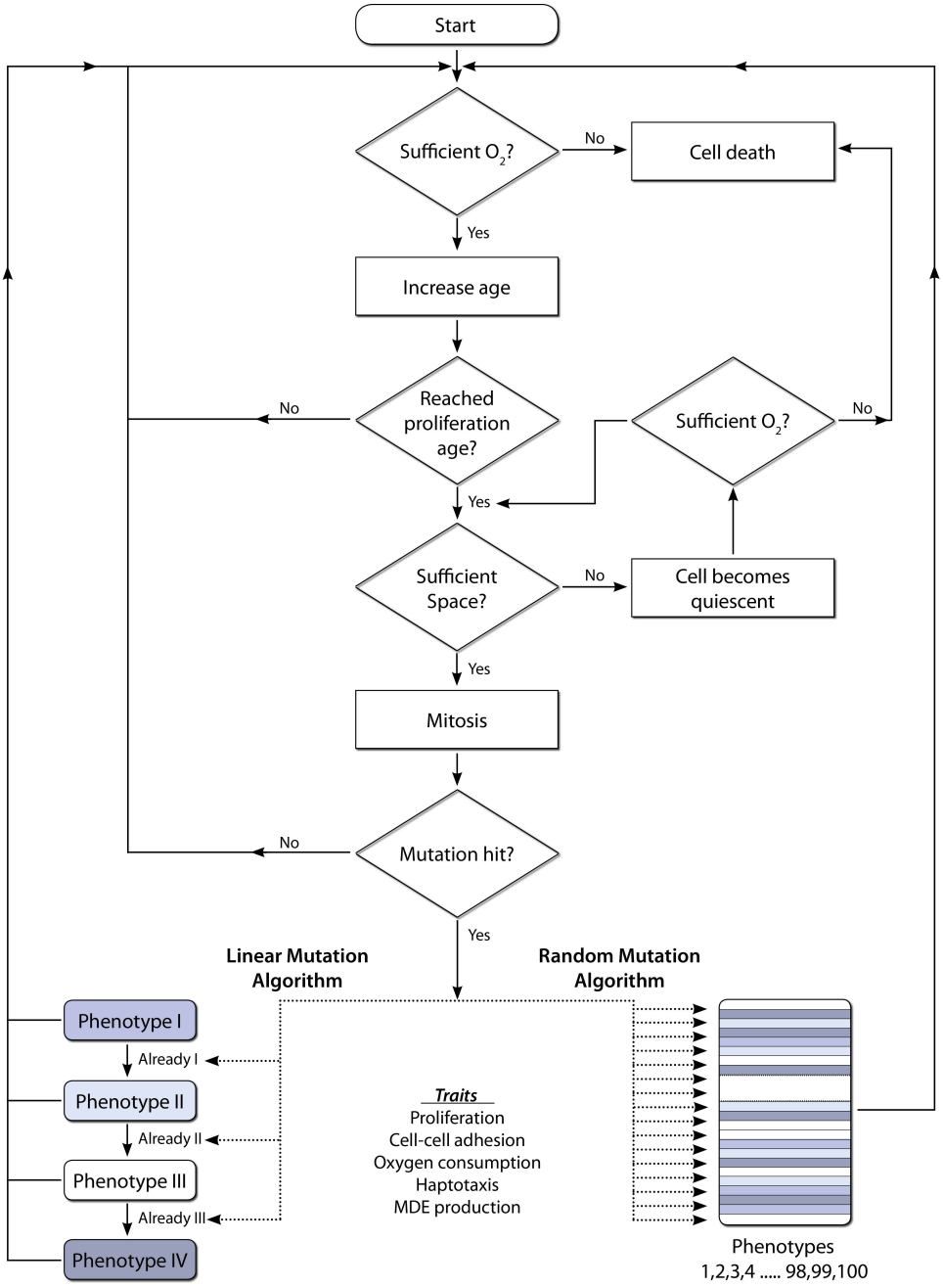

Figure 2.4: The life cycle of a cell

Flowchart describing the life cycle of a cell subject to either linear or random mutations. Adapted from Anderson [19].

Motility

Since it cannot push its neighbors to create space, a cell will remain stationary if there are no vacant sites in its von Neumann neighborhood[7]. However, if space is available and the restriction on cell-cell adhesion is met, a combination of unbiased motility and haptotaxis will drive its movements.

As with the anaerobic HDC model, the tumor cell density at grid point (i, j) at time t is

$$n_{i,j}^{q+1} = P_0 n_{i,j}^q + P_1 n_{i+1,j}^q + P_2 n_{i1,j}^q + P_3 n_{i,j+1}^q + P_4 n_{i,j-1}^q. \tag{2.26}$$

where

$$P_0 = 1 - \frac{4d_n\Delta t}{\Delta x^2} - \frac{\gamma\Delta t}{\Delta x^2}(f_{i+1,j}^q + f_{i-1,j}^q - 4f_{i,j}^q + f_{i,j+1}^q + f_{i,j-1}^q) \tag{2.27}$$

$$P_1 = \frac{d_n\Delta t}{\Delta x^2} - \frac{\gamma\Delta t}{4\Delta x^2}(f_{i+1,j}^q - f_{i-1,j}^q) \tag{2.28}$$

$$P_2 = \frac{d_n\Delta t}{\Delta x^2} + \frac{\gamma\Delta t}{4\Delta x^2}(f_{i+1,j}^q - f_{i-1,j}^q) \tag{2.29}$$

$$P_3 = \frac{d_n\Delta t}{\Delta x^2} - \frac{\gamma\Delta t}{4\Delta x^2}(f_{i,j+1}^q - f_{i,j-1}^q) \tag{2.30}$$

$$P_4 = \frac{d_n\Delta t}{\Delta x^2} + \frac{\gamma\Delta t}{4\Delta x^2}(f_{i,j+1}^q - f_{i,j-1}^q). \tag{2.31}$$

Figure 2.5 illustrates the movement probabilities and the layout of the tumor. For a detailed examination of how cellular motion is implemented, see Section 2.1.2.

Quiescence and cell death

Once motility has been considered, the cell's properties and its environment are revised to reflect the passage of time. The age of the cell is increased and the oxygen concentration is reduced to account for cellular consumption [21]. The cell is then categorized as proliferating, quiescent, or dead.

[7]The von Neumann neighborhood of a cell on a two-dimensional square lattice is comprised of its its four orthogonal neighbours (see Figure 1.5).

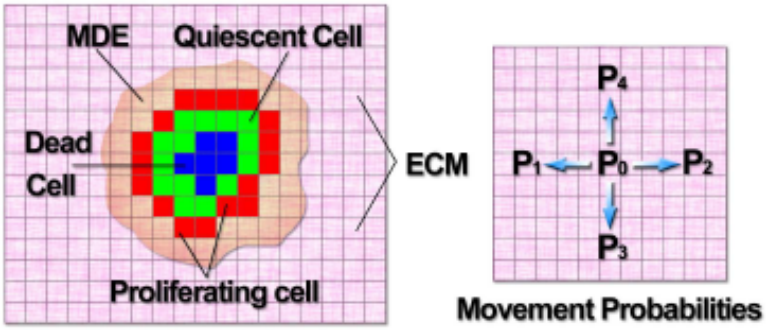

Figure 2.5: The key variables and the movement probabilites
A schematic diagram of cell subpopulations, the MDEs, and the ECM (left). The movement probabilities (right) are also shown. Springer and the Journal of Mathematical Biology, 58, 2009, 579-624, Microenvironment driven invasion: a multiscale multimodel investigation, Alexander R.A. Anderson, Katarzyna A. Rejniak, Philip Gerlee, and Vito Quaranta, Fig. 8; with kind permission from Springer Science and Business Media. [17]

At birth, each cell is assigned a maturation age, chosen randomly from a normal distribution $N(\tau, \sigma)$, where τ is the mean age and $\sigma = \tau/2$ is the variance [19]. After a cell has reached maturity, it can proliferate as long as it has access to sufficient space (i.e., one of its orthogonal neighbors is empty). However, if this condition is not satisfied, the cell will become quiescent and proliferation will be delayed until the necessary space becomes available. Since they are in a resting state, quiescent cells are assumed to require half as much oxygen as normal cells. However, this value is much debated in the literature and some sources claim that a normal cell may consume up to 5 times more oxygen than a quiescent cell [21].

There are two forms of cell death that are often included in mathematical models. Apoptosis is programmed cell death in response to DNA mutation or physiological stress [18]. It is characterized by the systematic breakdown of the cell into small components which are then engulfed by phagocytic cells. On the other hand, starved cells undergo necrosis, a process whereby they become bloated and explode, releasing cytokines which stimulate the proliferation of viable cells [25] and act as chemotactic signals that pull outer cells toward the tumor's core [36, 38, 41].

A lattice site occupied by an apoptotic cell becomes vacant at the next time step. In

contrast, the necrotic cells are assumed to remain present but will cease to produce MDEs and to consume oxygen. Necrosis occurs when the oxygen concentration drops below a threshold level h. The value of this threshold is difficult to determine experimentally, in part due to its dependency on the extent to which the tissue has been vascularized [21]. According to Anderson and colleagues [17], the oxygen concentration in the necrotic core is estimated to be anywhere between $0.5-30\%$ of the concentration in the surrounding tissue.

Cellular heterogeneity

Since tumors tend to have a large necrotic core, the viable cells are often isolated from one another and subject to diverse environmental conditions and evolutionary pressures. However, genetic and phenotypic heterogeneity can be detected even within the same lesion of the tumor tissue [29]. To incorporate this into his model, Anderson introduces the concept of inheritable variation and assigns each cell a set of phenotypic traits (i.e., a set of numbers which describe its response to the environment) [59]. The cell's phenotype identifies its affinity for cell-cell adhesion and its rates of proliferation, migration, and nutrient consumption, respectively.

During mitosis, the phenotypic traits are inherited by the daughter cells. However, there is a small chance P_{mutat} that at least one of its daughter cells will mutate. When determining the value of the mutation rate, a balance must be drawn between having a high enough value which allows selection pressures to act within a realistic timescale, while ensuring the rate is not so high that the effects of selection disappear among the stochastic noise [11]. Another important decision to make is how the mutations will transpire. In their work, Anderson and colleagues have described the application of both a linear and a random mutation scheme.

The linear approach considers four distinct phenotypes and assumes that subsequent mutations result in the manifestation of increasingly aggressive traits [1, 19, 21, 35]. Phenotype I corresponds to the first p53 mutation. Whenever a type I cell undergoes mitosis, there is a small probability that a mutation will cause at least one of the daughter cells to adopt the properties of the slightly more aggressive Phenotype II. Similarly, Phenotype II cells can mutate to become Phenotype III and so on. The most aggressive cells are those labeled Phenotype IV. These have a low maturation age, high rates of oxygen consumption and MDE production, large haptotaxis coefficients, and prefer not to adhere to other cells. Although this approach may appear to be extreme or greatly simplified, mutations are

Phenotype	Proliferation Age (hrs)	O_2 Uptake	MDE Production	Internal Adhesion Value	Haptotaxis
Phenotype I	16	κ	α	3	γ
Phenotype II	14	4/3κ	4/3α	2	4/3γ
Phenotype III	12	2κ	2α	1	2γ
Phenotype IV	8	4κ	4α	0	4γ
Random	[8 , 16]	[κ , 4κ]	[α , 4α]	[0 , 3]	[γ , 4γ]

Figure 2.6: The parameter values for the phenotypes in the linear and random mutation schemes.
Adapted from Anderson [19].

known to provoke radical behavior when there are strong selective pressures which favor such a change [60].

The random mutation scheme offers a simple yet astute representation of genetic instability [1,17]. According to this approach, the cells are already mutated when the simulation is initialized, with each one adopting the properties of one of 100 randomly predefined phenotypes. When a mutation occurs, the affected cell assumes the characteristics of a different phenotype, which is selected randomly and without bias.

The phenotypic traits

Figure 2.6 lists the phenotypic traits. The interpretation and implementation of these traits is straight forward, with the exception of cell-cell adhesion which is described using a very crude set of rules. According to the adhesion algorithm, each cell is given an internal adhesion value A_i which designates the number of neighbors to which the cell preferentially adheres. If the number of external neighbors A_e is such that $A_e \geq A_i$, the cell is allowed to migrate; otherwise, it must remain stationary. In this way, cell-cell adhesion serves to mediate contact inhibition with the motion of the cells restricted for larger internal adhesion values [22, 35].

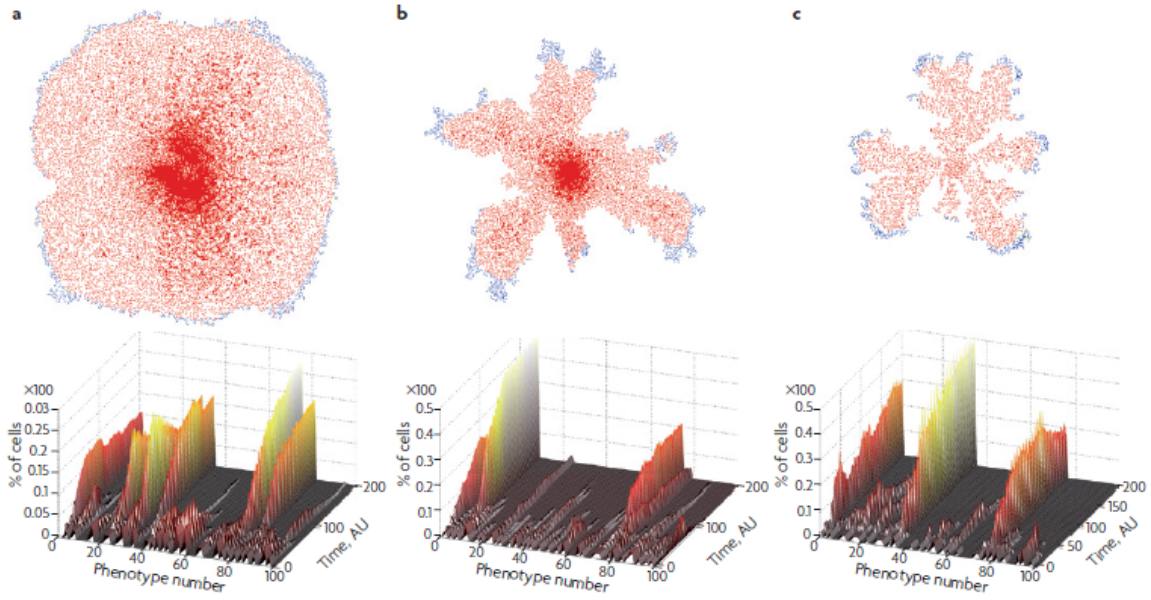

Figure 2.7: Tumor growth in (a) homogeneous, (b) random, and (c) hypoxic environments *This diagram presents a comparison of the tumor morphologies (top) and the phenotype distributions (bottom). Reprinted by permission from Macmillan Publishers Ltd: Nature Reviews Cancer ([8]), copyright (2008).* http://www.nature.com/nrc/

2.2.3 Simulation results

Anderson and colleagues place 50 tumor cells around the centre of a 400x400 grid and run their simulations for 2000 time steps. They scale their variables such that $0 \leq c, m, f \leq 1$ and set the initial conditions $m_0 = 0$ and $c_0 = f_0 = 1$. To compare and contrast the morphologies produced, they use morphocharts [61]. These mapping allow them to juxtapose tumor growth in environments with homogeneous (i.e., $f_0(x, y) = 1$), heterogenenous (or "bumpy"), and random (or "grainy") distributions of the ECM and to assess the impact of low oxygen availability (i.e., $c_0(x, y) = 0.25$).

Tumor progression is characterized by the depletion of resources and the development of a large necrotic core. Figure 2.7 compares the growth of tumors in homogneous, hypoxic, and random environments, respectively. Examining the plots, a large, compact, circular tumor is seen to form in the homogeneous ECM [21, 35]. In contrast, a small tumor with

a jagged rim is seen in the environment with scant oxygen[8]. However, the most significant finding is the correlation between branched fingering morphology and randomly distributed ECM [1, 21]. In terms of the phenotype distribution, the tumor population is seen to be dominated by six, two, and three phenotypes, respectively, in the homogeneous, random, and low oxygen environments. In all three scenarios, the dominant phenotypes favor zero cell-cell adhesion, and have short proliferation cycles and high haptotaxis coefficients. In addition, the most aggressive phenotype is always expressed by the largest fraction of the population. In Anderson [21], tumor growth is also simulated in a heterogeneous environment, which is generated from a combination of sine and cosine functions. As expected, these tumors display invasive features, although to a lesser extent than those in the random environment, and favor the propagation of aggressive clones [6].

The formation of a smooth tumor in a homogeneous environment is labeled an "artificial" result and is described as "unsurprising" given the unrealistic nature of this assumption [21]. In contrast, the tumor in the random environment is deemed to be the most realistic representation of invasive growth since the cells receive conflicting migration signals and are subject to selective pressures which favor the proliferation of aggressive clones [19].

Oxygen availability

Various environmental stress factors are known to favor the selection of aggressive clones and to promote the emergence of morphologically invasive features [1]. They include hypoxia, low nutrient availability, ECM densities that are difficult to navigate, a low level of growth factors, and a lack of vascularity [8]. Antithetically, low competition in normoxic and homogeneous tissue allows cells with various phenotypes to peacefully coexist as a large conglomerate with a smooth, noninvasive margin [8].

These findings seem to suggest that a potential treatment could involve suppressing the selective influence of the micro-environment while simultaneously starving the malignant cells [19]. To test this hypothesis, the oxygen available to a group of cells in a homogeneous environment is alternated between high and low levels. Initially, oxygen is readily available to the cells and a large, circular tumor forms. This tumor is composed of various phenotypes that peacefully co-exist and there is a low incidence of necrosis. When the

[8]The ECM is assumed to be homogeneous in this environment.

oxygen concentration is lowered, wide-scale cell death and a steep decline in tumor size are observed. Within a short timeframe, the tumor core becomes necrotic and thin, finger-like extensions protrude from its boundary. During this phase, the quiescent cells become extinct and, among the few proliferating cells that survive, a single aggressive clone thrives. Once the cellular response has stabilized, the oxygen concentration is modelled to increase. This causes the space between the finger-like structures to fill up and merge into a smooth boundary. Quiescent cells become populous once more and a slight increase in phenotype diversity is observed. When the oxygen concentration is lowered a second time, cellular activity analogous to that seen during the previous hypoxic phase is observed. The changes in morphology described above can be seen in Figure 2.8, while the evolution of the tumor population and the phenotype abundance are mapped in Figures 2.9 and 2.10, respectively.

Population dynamics are also examined for the oxygen switching experiment. Although aggressive and nonaggressive cells are seen to co-exist during the first period of hypoxia, phenotypes with different adhesive properties later segregate, forming distinct lobes at the edge of the tumor [1]. During both the hypoxic and subsequent normoxic periods, the same two phenotypes dominate the population. In fact, this pair is also selected in the follow-up trials where the ECM is assumed to be heterogeneous. Their common feature is that they favor cell-matrix adhesion in lieu of forming cell-cell bonds.

Oxygen consumption and the necrotic threshold

In Anderson [17], the HDC model is used to study how the tumor's morphology changes as the oxygen consumption rate and the apoptotic threshold are altered. As shown in Figure 2.11, increasing either the consumption rate or the apoptotic threshold instigates the emergence of finger-like patterns and yields an overall decrease in tumor size. In contrast, low oxygen consumption rates and apoptotic thresholds can be seen to foster symmetric growth.

Mutations

In numerous publications, the authors examine how the phenotype distribution changes as the tumor grows. To describe the evolution of the mutations, a linear and a random scheme are used. Both are deemed to portray realistic representations of cellular dynamics and are observed to elicit a trend toward increasingly aggressive behavior [1]. Figure 2.12 compares the results obtained by Anderson and his colleagues when they examined the

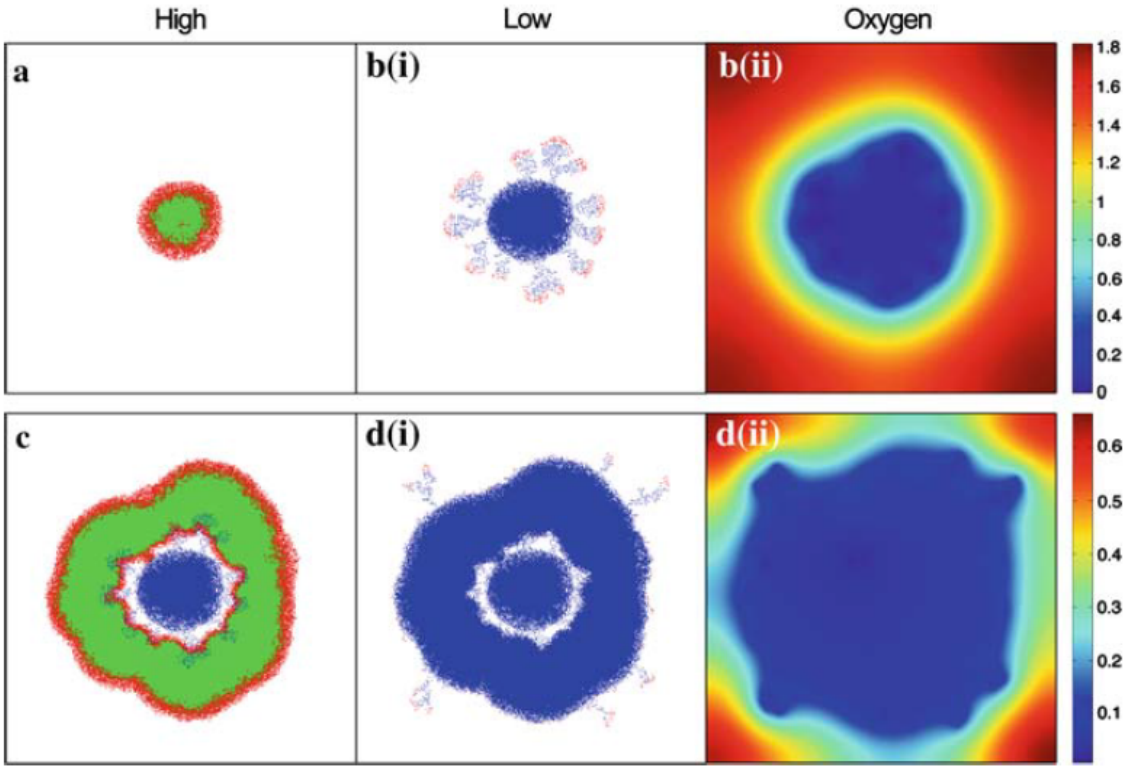

Figure 2.8: The tumor cell distribution for the oxygen switching experiment *Springer and the Journal of Mathematical Biology, 58, 2009, 579-624, Microenvironment driven invasion: a multiscale multimodel investigation, Alexander R.A. Anderson, Katarzyna A. Rejniak, Philip Gerlee, and Vito Quaranta, Fig. 8; with kind permission from Springer Science and Business Media. [17]*

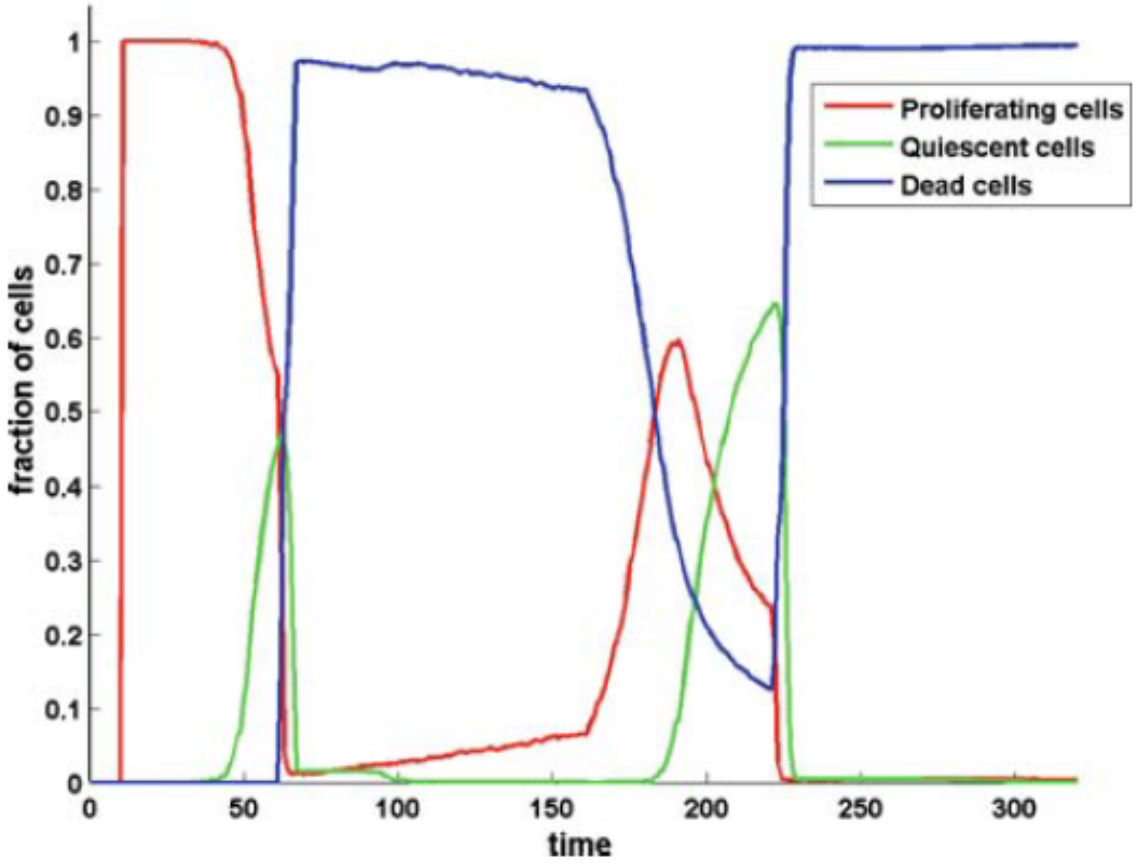

Figure 2.9: The time evolution of the fraction of proliferating, quiescent, and dead cells in the oxygen switching experiment
Springer and the Journal of Mathematical Biology, 58, 2009, 579-624, Microenvironment driven invasion: a multiscale multimodel investigation, Alexander R.A. Anderson, Katarzyna A. Rejniak, Philip Gerlee, and Vito Quaranta, Fig. 9; with kind permission from Springer Science and Business Media. [17]

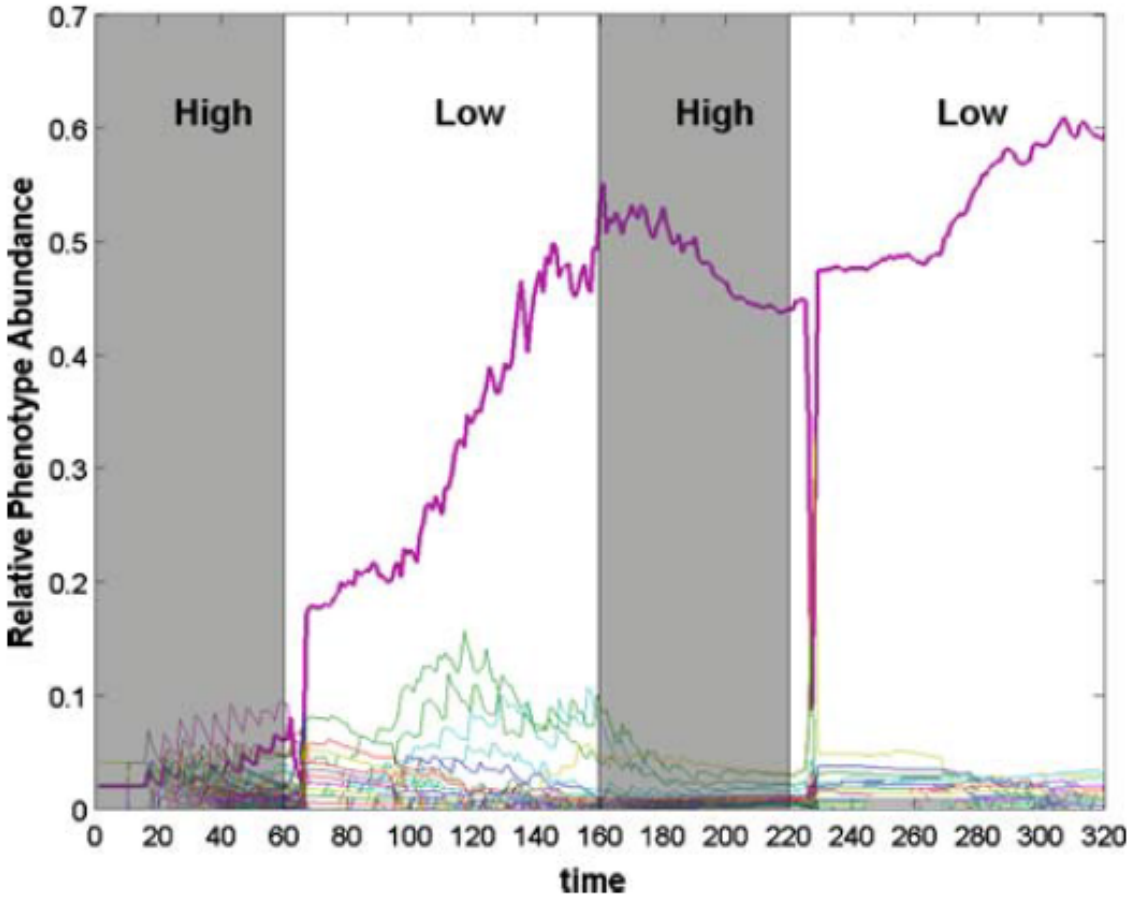

Figure 2.10: The time evolution of the relative phenotype abundance for the oxygen switching experiment with random mutations
Springer and the Journal of Mathematical Biology, 58, 2009, 579-624, Microenvironment driven invasion: a multiscale multimodel investigation, Alexander R.A. Anderson, Katarzyna A. Rejniak, Philip Gerlee, and Vito Quaranta, Fig. 10; with kind permission from Springer Science and Business Media. [17]

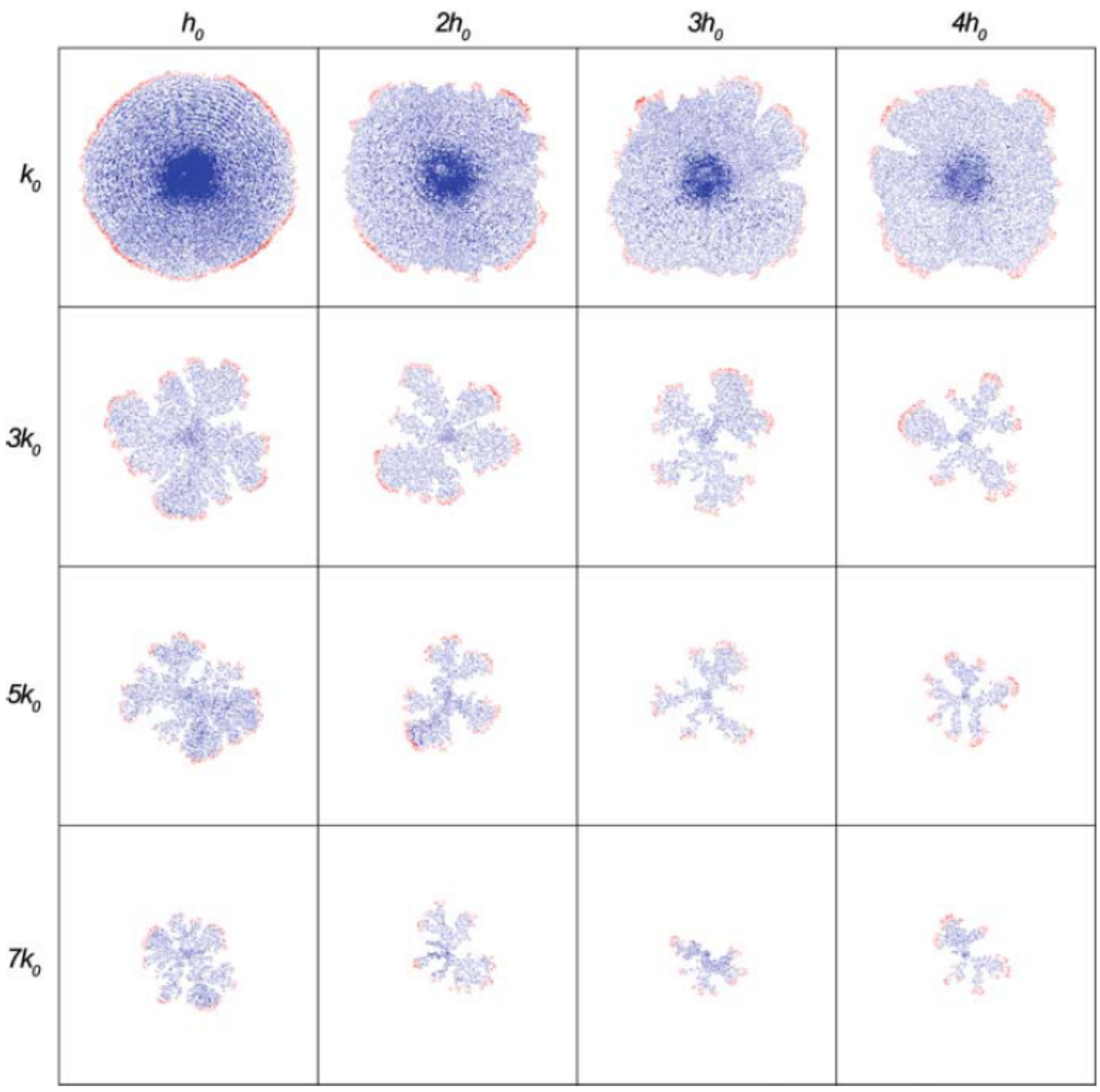

Figure 2.11: Tumor morphologies for various combinations of the apoptotic threshold (h) and the nutrient consumption rate (k)
Springer and the Journal of Mathematical Biology, 58, 2009, 579-624, Microenvironment driven invasion: a multiscale multimodel investigation, Alexander R.A. Anderson, Katarzyna A. Rejniak, Philip Gerlee, and Vito Quaranta, Fig. 4; with kind permission from Springer Science and Business Media. [17]

impact of these schemes on growth in environments with homogeneous, heterogeneous, and random distributions of the ECM, respectively.

Linear mutation scheme

During the early stages of its development, a tumor subject to linear mutations evolves as a growing disk in which the four phenotypes coexist. However, with passing time, a necrotic core develops and type IV cells prevail. In the figure above, the tumor in the homogeneous ECM is the only one which maintains its smooth boundary. In both the heterogeneous and random ECM, the living cells emanate from the necrotic core in the form of finger-like structures [1, 21].

Random mutation scheme

Differences in morphology are also observed under the assumption of a random mutation scheme. In the simulations involving heterogeneous and random ECM, the tumor develops invasive features [1]. In contrast, a thin, smooth rim of proliferating cells encloses the necrotic core in the trials involving homogeneous ECM [1]. In all three environments, the tumor population is composed primarily of aggressive clones which are driven to migrate via haptotaxis [1, 21]. These cells have internal adhesion values of zero, short proliferation cycles, high haptotaxis coefficients, and, in antithesis to the linear mutation scheme, low oxygen consumption rates [21].

2.2.4 Conclusions

According to the literature, a harsh environment can induce genetic and biomechanical changes that yield the development of finger-like margins [17, 23]. Anderson and colleagues emphasize hypoxia and heterogeneous ECM as prime examples of hostile environments; however, similar results are expected in tissue with elevated levels of interstitial pressure, substrate stiffness, or oxygen tension. Unfortunately, there is no formal definition of invasion which means that theories regarding the formation of malignant tumors remain unverified. In addition, gaps in the current understanding of cancer suggest that it is possible that some unquantifiable features, which drive tumor progression, may exist.

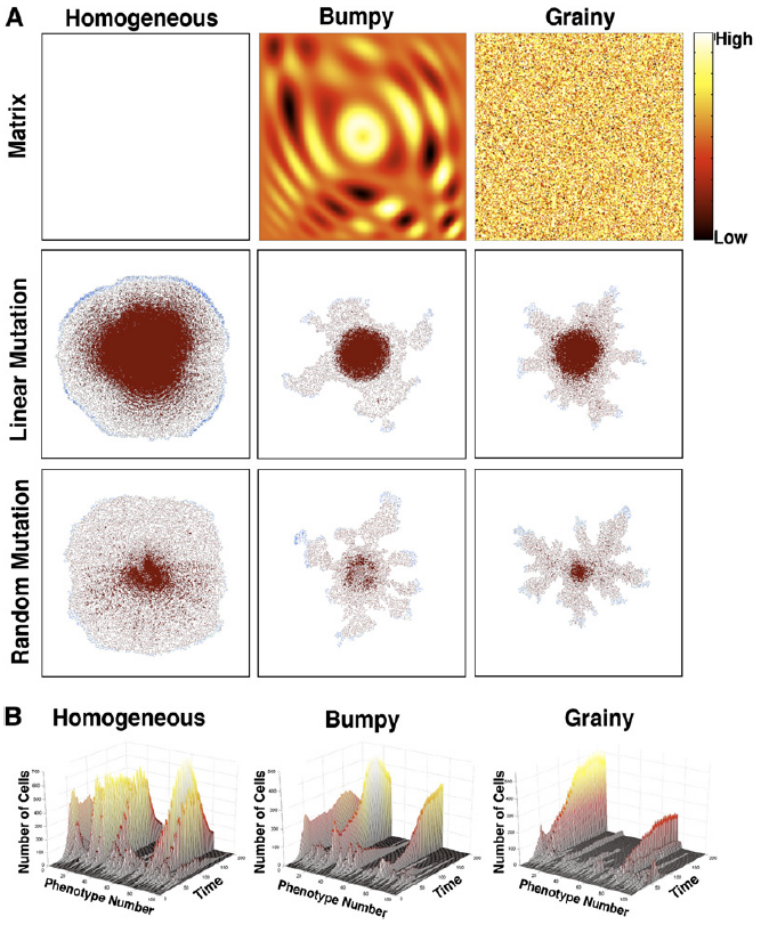

Figure 2.12: Comparing linear and random mutations schemes
(A) A comparison of the tumor morphologies in (left) homogeneous, (middle) heterogeneous, and (right) random distributions of the ECM is presented, as well as a (B) chart depicting the phenotype abundance for the random mutation scheme. Reprinted from Cell, 127, Alexander R.A Anderson, Alissa M. Weaver, Peter T. Cummings, and Vito Quaranta, Tumor Morphology and Phenotypic Evolution Driven by Selective Pressure from the Microenvironment, 905-915, Copyright (2006), with permission from Elsevier. http://www.sciencedirect.com/science/journal/00928674 [1]

In the next section, we will describe how we expand the aerobic HDC model to examine the impact of the ECM on tumor growth.

2.3 Examining the Role of the ECM as a Barrier to Cellular Expansion

There is always some way to improve or to expand an existing model. For example, one can obtain more accurate parameters, incorporate a new variable, or apply the model to a new problem. This section describes how the aerobic hybrid discrete-continuum model, presented in section 2.2, has been modified as part of this thesis work,to study the role of the ECM in cellular expansion.

Consider the equations

$$\frac{\partial n}{\partial t} = d_n \nabla^2 n - \gamma \nabla \cdot (n \nabla f) \tag{2.32}$$

$$\frac{\partial m}{\partial t} = d_m \nabla^2 m + \alpha n - \beta m \tag{2.33}$$

$$\frac{\partial f}{\partial t} = -\eta m f \tag{2.34}$$

$$\frac{\partial c}{\partial t} = d_c \nabla^2 c + \lambda f - \kappa n - \mu c, \tag{2.35}$$

where $m, f, c \geq 0$ represent the concentrations of the MDEs, the ECM, and oxygen, respectively. The diffusion coefficients of the cells, the MDEs, and the oxygen are d_n, d_m, and d_c, respectively, and γ denotes the haptotactic coefficient. α and β are the respective rates at which the MDEs are produced and naturally degraded, and η is the rate at which the MDEs degrade the ECM. Finally, oxygen is produced by the ECM at a rate λ, consumed by cells at a rate κ, and degraded at a rate μ.

Following Anderson's lead, the equation which describes the time evolution of the cellular density n is discretized to obtain

$$n_{i,j}^{q+1} = P_0 n_{i,j}^q + P_1 n_{i+1,j}^q + P_2 n_{i1,j}^q + P_3 n_{i,j+1}^q + P_4 n_{i,j-1}^q. \tag{2.36}$$

where

$$P_0 = 1 - \frac{4d_n\Delta t}{\Delta x^2} - \frac{\gamma\Delta t}{\Delta x^2}(f^q_{i+1,j} + f^q_{i-1,j} - 4f^q_{i,j} + f^q_{i,j+1} + f^q_{i,j-1}) \quad (2.37)$$

$$P_1 = \frac{d_n\Delta t}{\Delta x^2} - \frac{\gamma\Delta t}{4\Delta x^2}(f^q_{i+1,j} - f^q_{i-1,j}) \quad (2.38)$$

$$P_2 = \frac{d_n\Delta t}{\Delta x^2} + \frac{\gamma\Delta t}{4\Delta x^2}(f^q_{i+1,j} - f^q_{i-1,j}) \quad (2.39)$$

$$P_3 = \frac{d_n\Delta t}{\Delta x^2} - \frac{\gamma\Delta t}{4\Delta x^2}(f^q_{i,j+1} - f^q_{i,j-1}) \quad (2.40)$$

$$P_4 = \frac{d_n\Delta t}{\Delta x^2} + \frac{\gamma\Delta t}{4\Delta x^2}(f^q_{i,j+1} - f^q_{i,j-1}). \quad (2.41)$$

In Anderson et al. [23], $d_n = 0.0005, \gamma = 0.01, d_m = 0.0005, \alpha = 1, \beta = 0, \eta = 50, d_c = 0.5, \lambda = 0.5, \kappa = 0.57$, and $\mu = 0.025$ are cited as the values of the parameter upon non-dimensionalization. In this thesis, the same parameters are used with the exception of γ, which we set to 0.

Examining the parameters, it is evident that the diffusion of oxygen occurs at a significantly higher rate than MDE diffusion and cellular motion. In fact, Gerlee and Anderson [51] state that the oxygen field can be assumed to be in a quasi-stationary state. Accordingly, we replace equation 2.35 with the time-independent equation

$$0 = d_c\nabla^2 c + \lambda f - \kappa n - \mu c, \quad (2.42)$$

and isolate for c,

$$c = \left(d_c\nabla^2 - \mu\right)^{-1}(\kappa n - \lambda f). \quad (2.43)$$

A finite difference discretization is used to determine the solution to these equations and zero flux boundary conditions are applied to confine the cells, MDEs, and oxygen to the grid. It is difficult to ensure that the laplaican will have an inverse if we think of it as an operator that acts on a space of functions. However, in this thesis, we consider it in a numerial sense. Based on our boundary conditions, the inverse for the laplacian exists so long as $\mu \neq 0$.

One of the challenges of performing these calculations is that the matrix of the laplacian is n^2xn^2 when discretized, where n^2 is the number of lattice sites on the grid. Even though we can build a sparse matrix $d_c\nabla^2 - \mu$, we cannot guarantee that its inverse will also be

sparse . To account for the increased computation cost, it is necessary to downgrade from the 400 by 400 grid, used by Anderson and colleagues, to one which is 100 by 100. Despite changing the dimensions of the grid, we continue to scale the mesh spacing so that each grid point corresponds to the size of a single cell (i.e., $\Delta x = 1$ since we are considering activity on the cellular scale). With respect to the time step, we let $\Delta t = \frac{1}{2000}$ and we run the simulations for 200 time steps. The simulations are initialized by setting an optimal concentration of oxygen, $c(\mathbf{x}, 0) = 1$, and it is assumed that there are no MDEs, $m(\mathbf{x}, t) = 0$. Furthermore, we assume a random distribution of the ECM, with $0 \leq f(\mathbf{x}, 0) \leq 1$, and set $f(\mathbf{x}, t) = 0$ at any point occupied by a cell.

We begin by placing 81 proliferating cells at the centre of the grid (i.e., forming a circle of radius 5). Each cell is given an identification number and a mutation number between $1 - 100$. In addition, each is also randomly assigned an age $0 \leq age \leq 15$, a maturation age $5 \leq age_{proliferation} \leq 15$, and an internal adhesion value A_i. The value A_i specifies the number of external neighbors A_e to which the cell preferentially adheres. If $A_i \leq A_e$, the cell will attempt to migrate. In this way, an overcrowded cell will be given the opportunity to move toward a less dense region, provided that it has access to empty space.

To determine the effects of the ECM, we impose the condition that a cell is allowed to move into a grid space only if the concentration of the ECM at that point is below a threshold value f_t. One argument is that the lower bound of this interval should be greater than 0 to account for the fact that the ECM acts as a scaffold on which the cell moves. However, since the ECM is randomly distributed, we argue that it is the length of this interval, rather than its endpoints, that matters. Furthermore, selecting 0 as the lower bound seems appropriate since Anderson and colleagues set $f(\mathbf{x}, t) = 0$ at lattice sites occupied by a cell.

At each time step, we randomize the identification numbers of the cells is randomized to ensure that this numbering system will not bias the final configuration of the tumor. Then each cell is updated, one at a time. When considering a cell, we begin by examining the oxygen concentration at the lattice site where it is positioned. If the input value is below 0.05 or the consumption rate of the cell exceeds the amount available, the cell is declared necrotic. Although these cells continue to occupy space, they ceases to produces MDEs and to consume oxygen. On the contrary, if sufficient oxygen is available to a cell, its age is increased and the focus shifts to its neighbors. The concentration of ECM at each of the lattice sites which lie orthogonal to the cell is then analyzed, and information is retained regarding the presence of other cells.

If a cell has access to a sufficiently degraded, empty lattice site and has not yet reached maturity, it is given the opportunity to migrate. If more than one lattice site is available, the new position of the cell is selected at random. However, if the cell has reached maturity but does not have access to empty space, it will enter quiescence. It will remain in this resting state until one of its orthogonal neighbors becomes vacant, at which point it will become proliferative once more. Any mature cell that has access to a sufficiently degraded, empty lattice site will choose to proliferate rather than migrate. Of the two daughter cells which result from the mitosis, one will remain at the same location as the parent cell while the position of the other cell will be randomly selected among the available sites. The age of the newly formed daughter cells is set to 0 and these cells are categorized as proliferative. Each time a cell is placed into an empty grid point $\mathbf{x}_{new}$, whether by proliferation or migration, the concentration of the ECM is reduced[9] to $f(\mathbf{x}_{new}) = 0$.

With each cell division, comes the potential for mutation, $P_{mut} = 0.01$, which we model by overwriting the properties of the cell. Specifically, we randomly select 1 of the 100 predefined phenotypes, each of which has an equal chance of being selected, and alter the cell's properties accordingly. During this process, the daughter cells' proliferative age, oxygen uptake, MDE production rate, and internal adhesion value may change.

Using this framework, we simulate how cellular dynamics unfold. In particular, changes in the behavior and the properties of the cells are monitored. Close attention is also given to the concentrations of oxygen, MDEs, and the ECM. The findings from our simulations will be summarized next.

2.3.1 Results

Since oxygen is assumed to be in a steady state, it is not surprising that it is only the cells around the leading edge which survive past the first time step. Even though the rate of oxygen diffusion is high, it is not enough to offset the fact that the inner cells must share it amongst themselves. Throughout the simulations, it is a combination of the consumption rate, the oxygen diffusion rate, and the vicinity of the ECM which determines whether a given cell survives.

[9]This indicates that oxygen is no longer produced at these points.

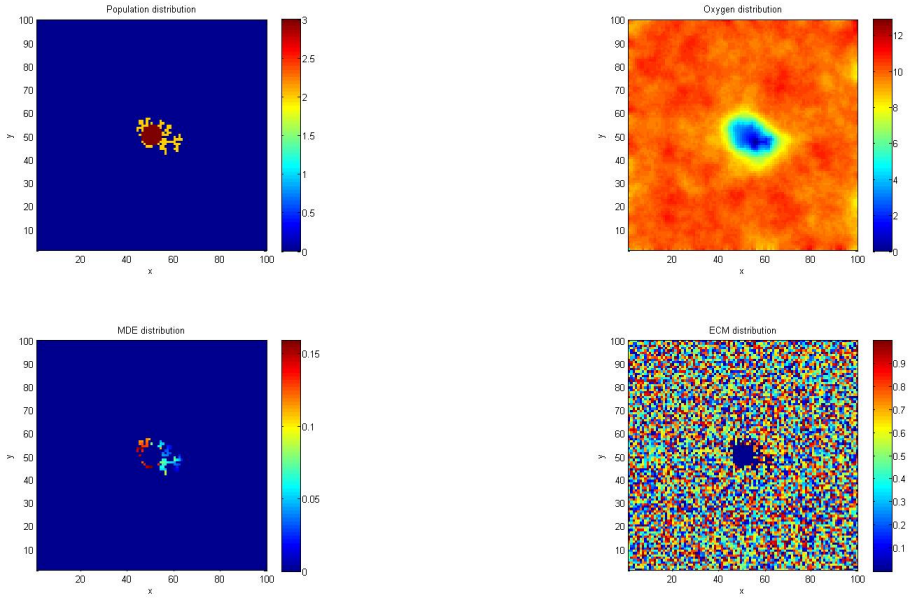

Figure 2.13: An example of the distribution of the cells, the oxygen, the MDEs, and the ECM after 200 time steps when $f_t = 0.4$

.

An example of the final configuration of a tumor when $f_t = 0.4$ is presented in Figure 2.13. One observation is the high concentration of oxygen surrounding the tumor[10]. This is a consequence of the fact that oxygen is produced at each empty lattice site at a rate proportional to the concentration of the ECM at that point. However, when the magnitude of the oxygen production term is reduced, the entire tumor dies during the first time step. This suggests that this method may not be the best to accurately study the effects of oxygen. Nevertheless, the spatial distribution of the subpopulations and the gradients in the oxygen concentration suggest that we are still able to capture important properties of oxygen-limited growth.

Figure 2.14 presents the final configuration of the cells for various values of the threshold f_t. Based on these results, we conclude that the ECM plays a significant role in restricting

[10]This result is consistent throughout all of the simulations for all values f_t.

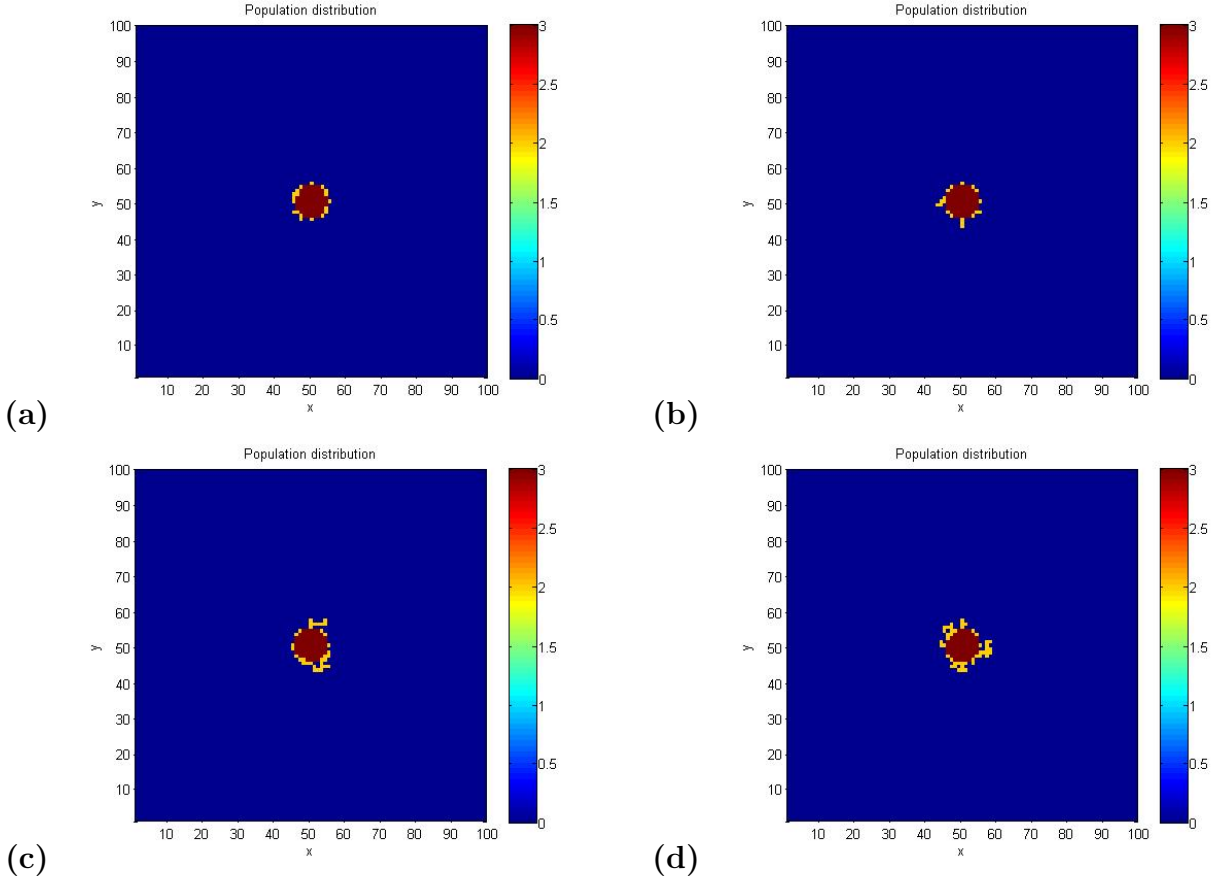

tumor growth for $f_t \leq 0.5$. In support of this conclusion, we note that there are no proliferating cells and that the quiescent cells form a thin ring around the necrotic core for $f_t \leq 0.3$. The tumors maintain their small, compact structure and there does not appear to be any sort of phenotype selection or preference. However, even if there was any, it would be difficult to detect due to the low growth rate. The invasive distance of the tumor and the population size slowly climb as the value of f_t increases. When $f_t = 0.4, 0.5$, the tumor begins to exhibit branch- and finger-like margins, with proliferating cells located at the very tip of these invasive extensions.

When we let $f_t = 0.6$, the tumor's size burgeons, with the cells growing around the high density regions of the ECM. Moreover, a surge in the population of proliferating and quiescent cells is observed. Some of the rapidly proliferating cells have a low maturation

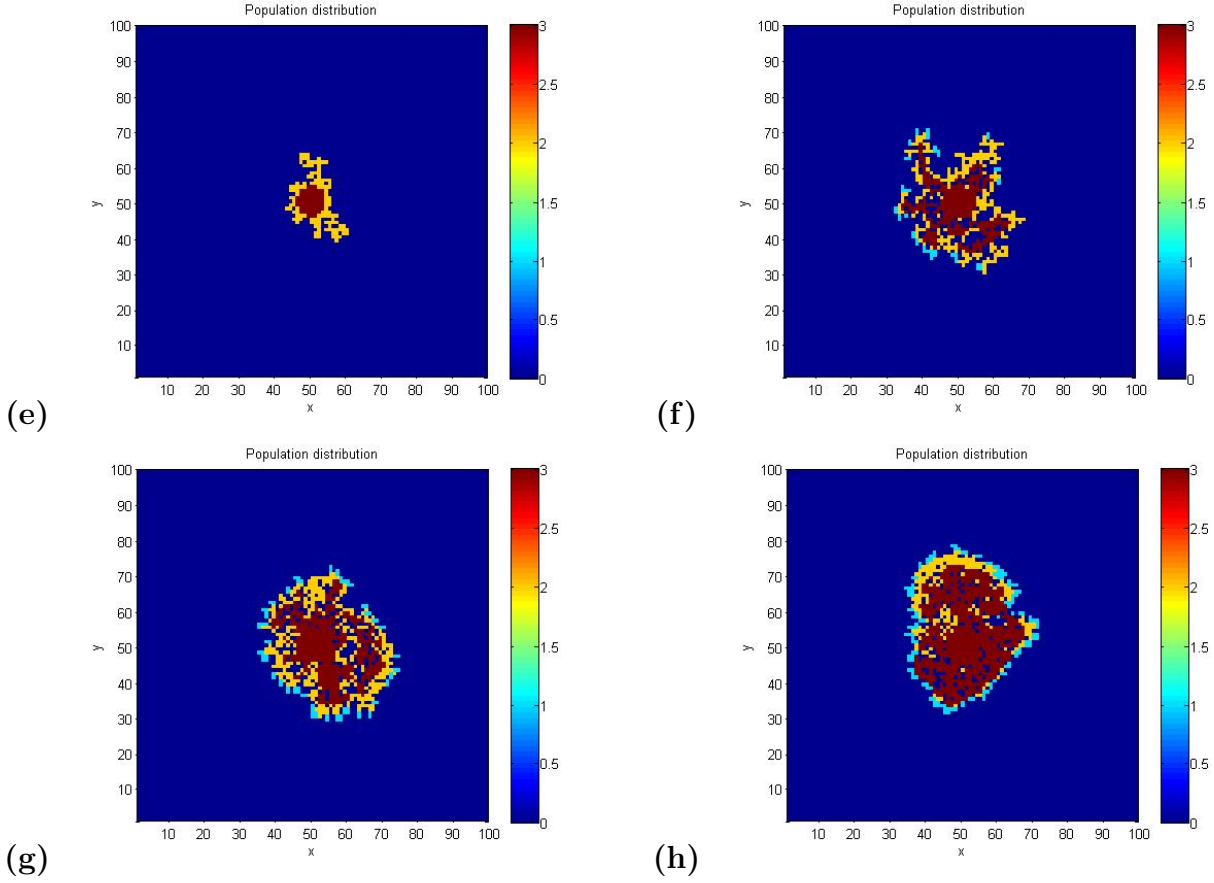

age or a low oxygen consumption rate, while others produce high quantities of MDEs.

When $f_t \geq 0.7$, a ring of proliferating cells encircles the quiescent cells which surround the necrotic core. Within the tumor, the cells that border the impenetrable, high density regions of the ECM have access to oxygen and are more likely to remain quiescent, regardless of their distance from the leading edge. For larger values of f_t, there are fewer lattice sites with impenetrable ECM densities and phenotypes with a low proliferative age dominate the tumor population. Thus, the size of the tumor increases and the number of quiescent cells declines.

During these simulations, the migration of the cells could not be detected. This is attributed to the fact that the migration probabilities $\frac{d_n \Delta t}{\Delta x^2}$ are of the order 10^{-7}.

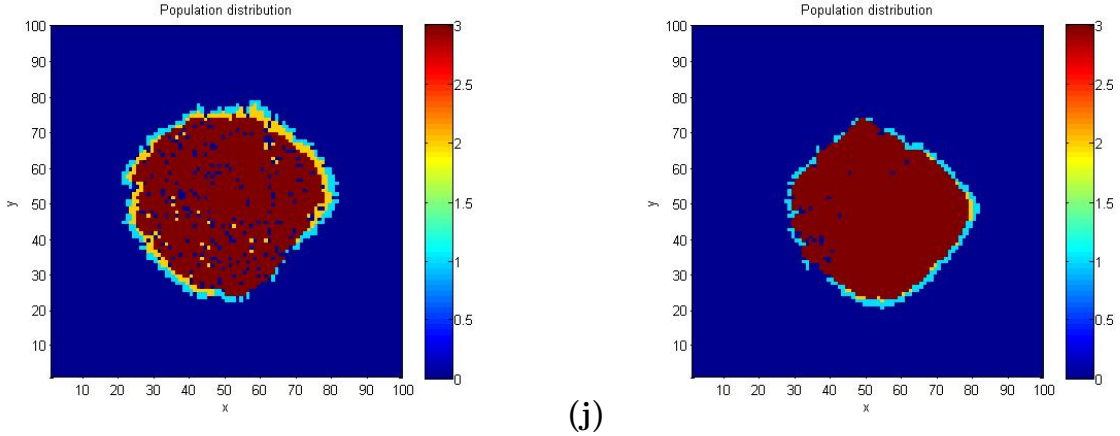

(i) (j)

Figure 2.14: An example of the final configuration of the tumor for thresholds **(a)** $f_t = 0.1$, **(b)** $f_t = 0.2$, **(c)** $f_t = 0.3$, **(d)** $f_t = 0.4$, **(e)** $f_t = 0.5$, **(f)** $f_t = 0.6$, **(g)** $f_t = 0.7$, **(h)** $f_t = 0.8$, **(i)** $f_t = 0.9$, **(j)** $f_t = 1$.

2.3.2 Conclusions

The density of the ECM plays a vital role in the expansion of the tumor. For $f_t \leq 0.3$, the invasion into the surrounding tissue is restricted, and the tumor remains small and compact. When $f_t = 0.4, 0.5$, long branches extrude from the core of the tumor into the tissue. A significant change is seen for larger threshold values (i.e., $f_t \geq 0.6$), with the cells growing around the high density barriers. Although various factors contribute to phenotype selection (i.e., high MDE degradation coefficient, low oxygen consumption rate), cells with a low proliferation age are consistently selected, whenever the ECM poses little to no restriction on the propagation of the cells.

The results we obtained are promising. As future work, we suggest incorporating biological information about variation in the density of the tissue and including obstacles such as organs in the simulation studies. Furthermore, the effects of cellular migration should be examined.

2.4 Analyzing and extending the HDC model

Despite an extensive investigation of related literature, no publication was found which rigorously reviewed and analyzed the stability of the HDC model. However, models that are similar to the continuous system discussed in Section 2.1.1 have undergone both stability and phase plane analysis (see: [50, 55, 62]).

Besides conducting the necessary mathematical analysis, we can expand this model by including more biologically relevant details. For instance, cell preference to moderate levels of stress can be addressed [49]. In general, this is incorporated into a model via an algorithm which respects the well-known transition away from cell-cell adhesion in favor of forming cell-matrix bonds. However, Armstrong [63], Gerisch [64], Chaplain [49] and their colleagues present more intricate methods that can be used.

Armstrong et al. [63] present a continuous model which describes the binding of cell adhesion molecules and cell sorting in response to surface tension. Their descriptions of self-population adhesion and cross-population adhesion are particularly relevant to our study of tumor progression. In the context of our investigation, we can apply their ideas to replicate the development of a rim of proliferating cells which surrounds a ring of quiescent cells and encloses the tumor's necrotic core.

On the other hand, Gerisch and Chaplain [64] compare and contrast the effects of local versus non-local adhesion. By systematically varying the radius of sensitivity of the non-local adhesive pull, the ECM density, and cell-cell and cell-matrix adhesion coefficients, they examine the role these variables play with regards to the speed and intensity of invasion. Their work also takes into account cell crowding and its role in inhibiting haptotaxis and regulating the ECM.

Chaplain et al. [49] take a markedly different approach by formulating a model which explores the idea that the incorrect sensing of its contacts and its compressive state allows a mutated cell line to induce hyperplasia and abnormal cell growth. In this model, biomechanical factors, such as the perception and response to stress, are discussed in the context of porous media. In addition, tumor progression is shown to trigger morphological and chemical changes in the ECM and the concept of normal and abnormal ECM is introduced.

This ties well with a study conducted by by Anderson and colleagues [22] which ex-

plores the concept of micro-environmental independence. Anderson et al. claim that since cancer is a disease marked by deregulation and the disruption of normal controls, it is reasonable to assume that the fitness of cancer cells may be independent of environmental controls, such as the availability of space, growth factors, and nutrients. The results from this model suggest a preference for micro-environment dependent cells in environments with a low cost of reliance, and micro-environment independent cells in a resource-limited scenario.

In keeping with the theme of incorporating new parameters, another topic that can be examined is biased migration in response to gradients of multiple external stimuli, $\underline{r}$. To accomplish this, Anderson [59] suggests using a modified version of the cell density equation

$$\frac{\partial n}{\partial t} = \frac{\partial}{\partial x}\left(d_n \frac{\partial n}{\partial x} - n\sum_{i=1}^{w}\chi_i \frac{\partial r_i}{\partial x}\right) + \frac{\partial}{\partial y}\left(d_n \frac{\partial n}{\partial y} - n\sum_{i=1}^{w}\chi_i \frac{\partial r_i}{\partial y}\right) + f\left(\frac{\partial n}{\partial x}, \frac{\partial r_i}{\partial x}, \frac{\partial n}{\partial y}, \frac{\partial r_i}{\partial y}\right),$$

where $\underline{r} = [r_1 r_2 r_3 ... r_w]^T$ is a vector representing the different external stimuli, and f represents other forms of directed migration (i.e., convection). Here it is assumed that the diffusive stimuli satisfy

$$\frac{\partial \underline{r}}{\partial t} = \mathbf{D}\Delta\underline{r} + \underline{g}(\underline{r}, n).$$

where $\underline{g}$ specifies the reaction kinetics.

When considering migration, it seems reasonable to allow variance in the distance travelled by the cells during each time step, and to explicitly incorporate chemotaxis. To take chemotaxis into account, one can either model cellular motion up gradients of oxygen or couple a forward-pulling haptotactic force with a retarding or restraining chemotactic pull [31]. Before incorporating these changes it is important to keep in mind that there is no experimental evidence that cancer cells respond chemotactically to nutrients [36] and that haptotaxis has only been measured in vitro [8]. Currently, the existence of haptotaxis is a hotly contested and controversial issue. Perumpanani and his colleagues [31] claim that our understanding of the architecture of tissue suggests that haptotaxis is a major component of directed motion. However, Anderson and Quaranta [8] refute this statement, expressing their opinion that it is more likely that proteolytic activity in the tissue results in the rearrangement of the ECM rather than in the generation of smooth haptotactic gradients. This highlights the need to develop new tools which extract biological details and increase our knowledge of the biomechanics of cancer progression.

In addition to these ideas, it seems reasonable to incorporate the effects of cell metabolism. To accomplish this, Ferreira and colleagues [65] model a tumor which is supplied nutrients via a single capillary vessel at the top of the lattice. In this case, two types of nutrients are considered: a generic one that is necessary for cell survival and motility and one specific to cell division. It is in this context that migration, morphological patterns, and nutrient distribution and demand are examined.

In Ferreira's model and in the one presented by Piotrowskia and Angus [10], more than one cancer cell is able to occupy a single lattice site. The significance of this feature is that it allows for the restrictions on division to be eased and for the increased density of the proliferative rim to be taken into account [10]. Piotrowskia and Angus use this framework to describe the induction of glycolysis (i.e., anaerobic respiration) by hypoxia. They then examine the concentration of acid that is produced through glycolysis and its impact on the cell population. Their model suggests that acid alone is not sufficient to generate necrosis in the absence of nutrient deficiency and that the toxicity caused by the decline in pH serves solely to provoke quiescence.

Smallbone et al. [52] explore tumor progression and metabolism in the context of ductal anatomy. Their results indicate that the depletion of the oxygen source allows cells which have acquired hyperplastic, glycolytic, and acid resistant properties to flourish. These traits are acquired and accumulated via random mutations and are reversible albeit with small probability. By examining population dynamics, the benefit of each mutation can be gauged. Based on their analysis, Smallbone and colleagues suggest an overwhelming preference for cells which first acquire hyperplasticity, then switch to glycolysis, and finally become acid-resistant.

In a related study on pre-neoangiogenic tumor development, Patel et al. [66] examine cell metabolism and the relationship between pH and tissue vasculature. The key variables in this model are normal cells, tumor cells, blood vessels, oxygen, glucose, and lactic acid. To take into account the blood flow, a random microvascular network is generated through which metabolic substrates are delivered and metabolites are removed. This model suggests that cancer cells favor environments where the acid level is sufficiently high to eliminate normal cells but the vasculature is still able to prevent self-toxification.

The hybrid discrete-continuum model highlights the evolutionary nature of cancer pro-

gression [8]. In particular, we see how the selective pressures in a harsh environment impact tumor genetics by favoring mutations that drive competitive behavior. Thus, clonal selection oversees that the best adapted phenotypes emerge to dominate the tumor population. A different way to examine the evolution of cellular phenotypes is by using a feed-forward neural network to model the decision-making mechanisms of the cells. This approach will be examined in the next chapter and will be used to analyze tumor growth, motility, and cellular metabolism.

Chapter 3

Evolutionary Hybrid Cellular Automaton

The evolutionary hybrid cellular automaton (EHCA) model builds upon the foundations of the HDC model and employs an artificial neural network to drive the behavior of the cells. The strength of this approach is its ability to provide insight into the dynamics at the subcellular scale and to illustrate how a cell's genotype may drive its response to cues from its microenvironment [21, 23].

To build an artificial network, we can train a system by collecting a set of readings from the tumor environment and then linking each sample with the appropriate response [14,51,67]. Once sufficiently trained, the system can be used to predict the outcome for an unknown sample that has not been previously considered. An error minimizing algorithm, such as back-propagation, is often used to optimize the accuracy of this approach.

3.1 The Response Network

In this chapter, we will describe an EHCA model of tumor development. We will consider a pre-vascular stage of cancer where various phenotypes co-exist and propose that the disruption of the response network is at the root of abnormal tumor growth [51, 67].

To model a 2-dimensional slice of the tumor tissue, Gerlee and colleagues use an NxN grid on which each lattice site contains a cancerous cell or is empty. Initially, the oxygen concentration is evenly distributed over the domain and aggressive subclones[1] that lack growth inhibition are placed at the centre of the grid [17]. There are many different ways the network can be designed to capture the appropriate cellular interactions. Gerlee and colleagues claim that this does not pose a problem since they are interested in studying the evolution of the network, which is largely independent of the initial wiring [51], and aim to produce the appropriate response rather than to mimic particular signaling pathways.

To increase the reliability of their model, Gerlee and Anderson update the tumor cells at random. At each time step, the cells sample their local environment (i.e., the grid point). In the simplest case[2], they retrieve the number of neighbors $n(\mathbf{x}, t)$ and local oxygen concentration $c(\mathbf{x}, t)$, and let $\xi_i = (n(\mathbf{x}, t), c(\mathbf{x}, t))$ denote a cell surface receptor. The emphasis on these two variables stems from the ability of cancer cells to avoid hypoxia induced apoptosis and their tendency to separate from their neighbors [17].

To model the transfer of information from the cell surface receptors through molecular pathways, a deterministic artificial feed-forward neural network is used, with the behavior of the cells predicted and classified based on the network weights and thresholds. Although this is a very abstract approach, Gerlee and Anderson assert that it embodies features of in vivo signaling and regulatory networks [51].

A visual representation of the response network is illustrated in Figure 3.1 [51]. In this diagram, node j in the hidden layer V_j is equipped with a threshold θ_j. Similarly, node i in the output layer O_i has a threshold ϕ_i. Links of varying strength connect the nodes in the different layers. Use of the transform function

$$T(x) = \frac{1}{1 + e^{-\beta x}}. \tag{3.1}$$

ensures that the value of these nodes remains within the range of $[0, 1]$.

To define the connections between the input and hidden layers, Gerlee and colleagues use the matrix w where w_{jk} is the connection strength between the k^{th} node in the input

[1] Two cells are considered to be subclones if they have an identical response network.

[2] In later sections the concentrations of glucose and hydrogen ions will also be considered.

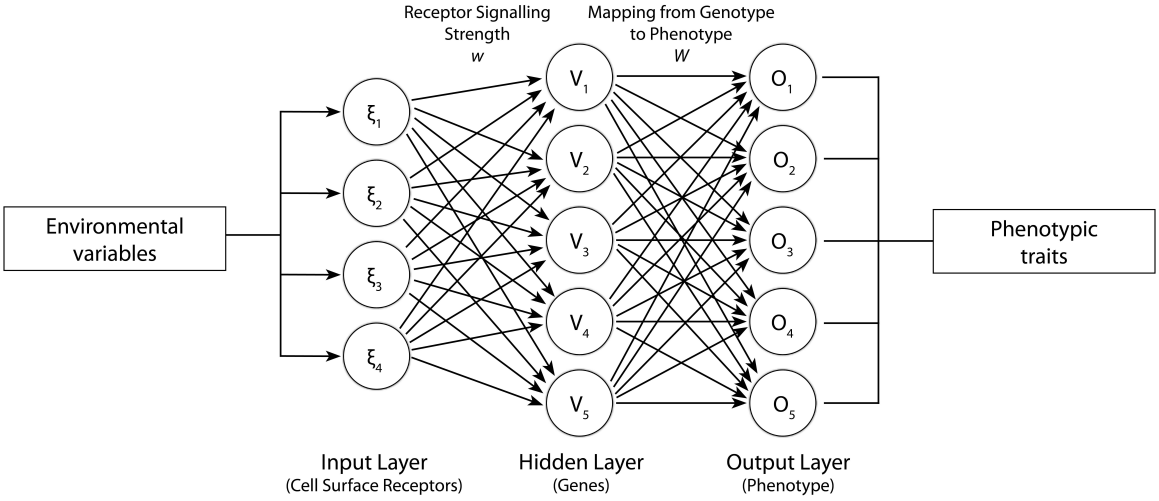

Figure 3.1: The response network
A schematic of the connections linking the input, hidden, and output layers. Adapted from Gerlee and Anderson [67].

layer ξ_k and the j^{th} node in the hidden layer V_j [67]. The value of node V_j is determined using a weighted sum and the transfer function $T(x)$ with

$$V_j = T\left(\sum_k w_{jk}\xi_k - \theta_j\right). \tag{3.2}$$

A similar procedure is applied when examining the connections between the hidden and output layers. Here, the connections are defined by a matrix W where W_{ij} determines the connection strength between node j in the hidden layer V_j and node i in the output layer O_i with

$$O_i = T\left(\sum_j W_{ij}V_j - \phi_i\right) = T\left(\sum_j W_{ij}T\left(\sum_k w_{jk}\xi_k - \theta_j\right) - \phi_i\right). \tag{3.3}$$

To successfully interpret the response network, we must understand the biological assumptions made by the authors. In the next section, we will review the interpretation of the cell cycle presented by Gerlee and colleagues.

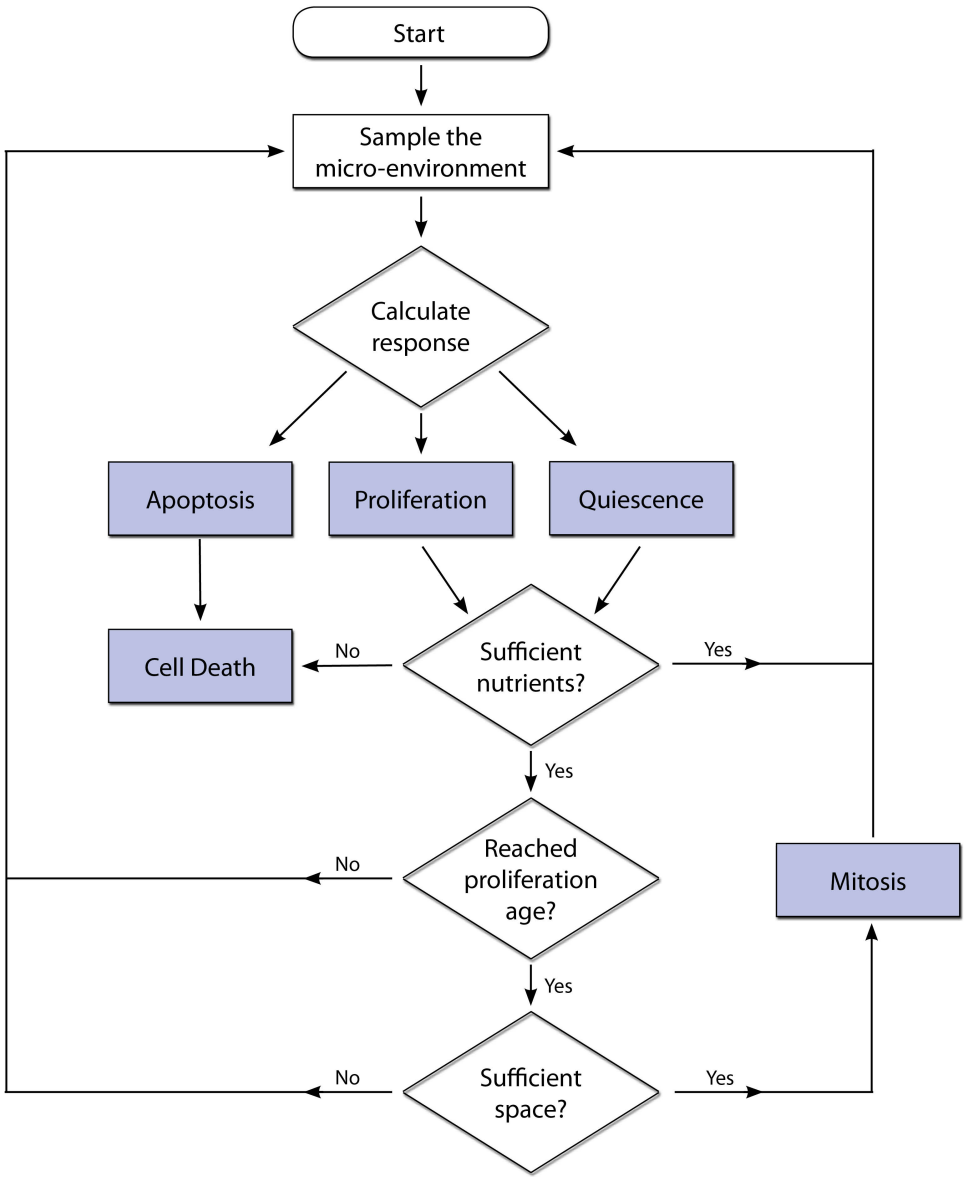

Figure 3.2: The life cycle of a cancer cell
Adapted from Gerlee and Anderson [54].

3.2 The Life Cycle of the Cells

The mitotic age of a cell is a normally distributed variable with $N(A_p, \frac{A_p}{2})$ where A_p is the base proliferation age [51]. A newly formed cell has age 0 and develops according to the life-cycle flow chart presented in Figure 3.2.

When a cell attains its proliferative age and cell division is determined as the network response, the network parameters are copied to the daughter cells and then adjusted to account for mutations. The probability of mutation is $p_{mut} = 0.01$ and the number of mutations is generated using a Poisson distribution. Mutations are assumed not to possess directionality and are randomly dispersed throughout the matrices which specify the threshold levels, the properties of the nodes, and the strength of the connections. To model a mutation, a normally distributed number s is summed with the appropriate matrix entry, where $s \in N(0, \sigma)$ and σ indicates the mutation strength. Hence, if x is an entry selected for mutation, then $x \to x + s$.

Mutations will up-regulate or down-regulate the connections between the nodes [67] and thereby control the fitness of the cell and its response to its micro-environment. In this so called open-ended model, the cell's genotype is not confined to a predefined set. In fact, a mutation can occur at a link that was initially set to zero (i.e., a mutation can create new connections between nodes).

Consider a mutation that decreases the weight between the nodes which correspond to the number of neighbors and the proliferative response. This will cause increased proliferation if the cell has a weak response to contact inhibition. On the other hand, the cell will become more resilient to hypoxia if subject to a mutation that increases the weight connecting the nodes that designate the oxygen concentration and the apoptotic response.

Biologically, the strength of the connections linking the input and the hidden layers represents the signaling strength of the receptors. Hence, a mutation in these connections corresponds to a change in the expression level of the receptors. On the other hand, the hidden layer can be thought of as the processing layer [51, 67]. Mutations here are akin to modifying the expression of the regulatory genes.

The output layer determines the cellular response based on the input vector, the weight matrices, and the threshold vectors. To describe the phenotype of the cell, the response

vector $R = R(\xi, G)$, where G is the genotype, may provide continuous or Boolean information [17, 23]. This vector conveys the "average" response of the cell and should be interpreted as the likelihood of observing the different outcomes. Accordingly, this vector can also be viewed as the steady-state of the gene regulatory network if the intra-cellular dynamics are assumed to occur at a significantly faster rate than the changes in the cell's environment [67].

By examining the magnitude of each component of the output vector, one can determine whether the cell proliferates, becomes/remains quiescent, or dies[3]. Of these three mutually exclusive outcomes, the strongest response is declared to be the cell's state. If proliferation is the determined response, it is necessary to ensure that the maturation age has been attained and that sufficient space is available for the daughter cells to form (i.e., $n(\mathbf{x}, t) \leq 3$). If these conditions are not satisfied, the cell enters quiescence. Cell death occurs when apoptosis is selected as the network response, via necrosis when the oxygen level falls below a predetermined threshold $h(\mathbf{x}, t) < 0.15$, or at a random rate independent of the network response [14]. Regardless of the cause of mortality, dead cells are not updated.

In some studies, the grid point which holds the dead cell is declared empty at the beginning of the next time step, regardless of the cause of death [14,67]. In others, necrotic cells occupy space while the apoptotic cells are discarded at the next time step [51]. To account for the immune system, Gerlee and Anderson [54] also model a scenario where a necrotic cell will occupy space until it is removed after a given timeframe, specifically $t_N = 5$ cell cycles. It should be noted that the value of the apoptotic threshold, h, is difficult to obtain experimentally and is known to depend on the properties of the cell and the vasculature.

Although various chemicals are indispensable for cell maintenance and division, oxygen c is the focus of these simulations. In this model, oxygen production is expressed in a manner consistent with a scenario where the tissue is surrounded by blood vessels that supply nutrients at a constant rate [23]. Specifically,

$$\frac{\partial c(\mathbf{x}, t)}{\partial t} = D_c \Delta c(\mathbf{x}, t) - f_c(\mathbf{x}, t) \tag{3.4}$$

[3]Motility and the metabolic pathways will also be considered in the following sections.

where D_c is the diffusion constant and

$$f_c(\mathbf{x},t) = \begin{cases} 0 & \text{if the automaton element at } \mathbf{x} \text{ is empty} \\ \kappa F(\mathbf{x}) & \text{if the automaton element at } \mathbf{x} \text{ is occupied} \end{cases} \tag{3.5}$$

The variable κ denotes the base consumption rate and $F(\mathbf{x}) = max\{k(R - T_r) + 1, 0.25\}$ is a modulation function with target response[4] T_r, life cycle response R, and strength k. By using this modulation function, it is ascertained that the nutrient consumption rate is proportional to the strength of the network response and cellular metabolism is restricted to at least a quarter of the base-line consumption rate. Proliferating cells are assumed to consume oxygen at a rate k_0 while the consumption rate of the quiescent cells is $k_q < k_0$ [17].

3.3 Oxygen Modulated Growth

Motivated by clinical trials that indicate a strong correlation between hypoxia and poor prognosis, Anderson and colleagues explored the relationship between oxygen availability and tumor growth. As expected, the results from their simulations clearly demonstrate that decreased oxygen levels are conducive to the selection of aggressive phenotypes and the expression of invasive features [23].

Stable growth can be observed when a high concentration of oxygen, $c(x,0) = c_0$, is dispersed throughout the domain. In this environment, a large, compact tumor forms. This tumor has a smooth boundary and is characterized by a wide proliferating rim which encloses a small cluster of quiescent cells [51, 67]. After the tumor attains a critical size, a slowly expanding necrotic core is seen to emerge, as illustrated in Figure 3.3. Meanwhile, Figure 3.4 shows that tumor growth is slowed, both in terms of the invasive distance[5] and the total number of cells, when the initial oxygen level is decreased. In this case, the tumors which form are noted to exhibit finger-like and branched patterns along their gradually disintegrating boundaries. In addition, they are composed almost exclusively of dead cells and only those cells which are at the very tips of the finger-like margins survive in the face of stiff competition [19]. Hence, the only way that a cell can ensure the survival of its progeny is by placing the daughter cells outside of the tumor boundary, where oxygen

[4] T_r is the response of a normal cell.

[5] The invasive distance is the distance from the centre of the grid (e.g., the centre of the tumor) to the most distant cell. To compensate for stochasticity in the system, this value is averaged over 20 simulations.

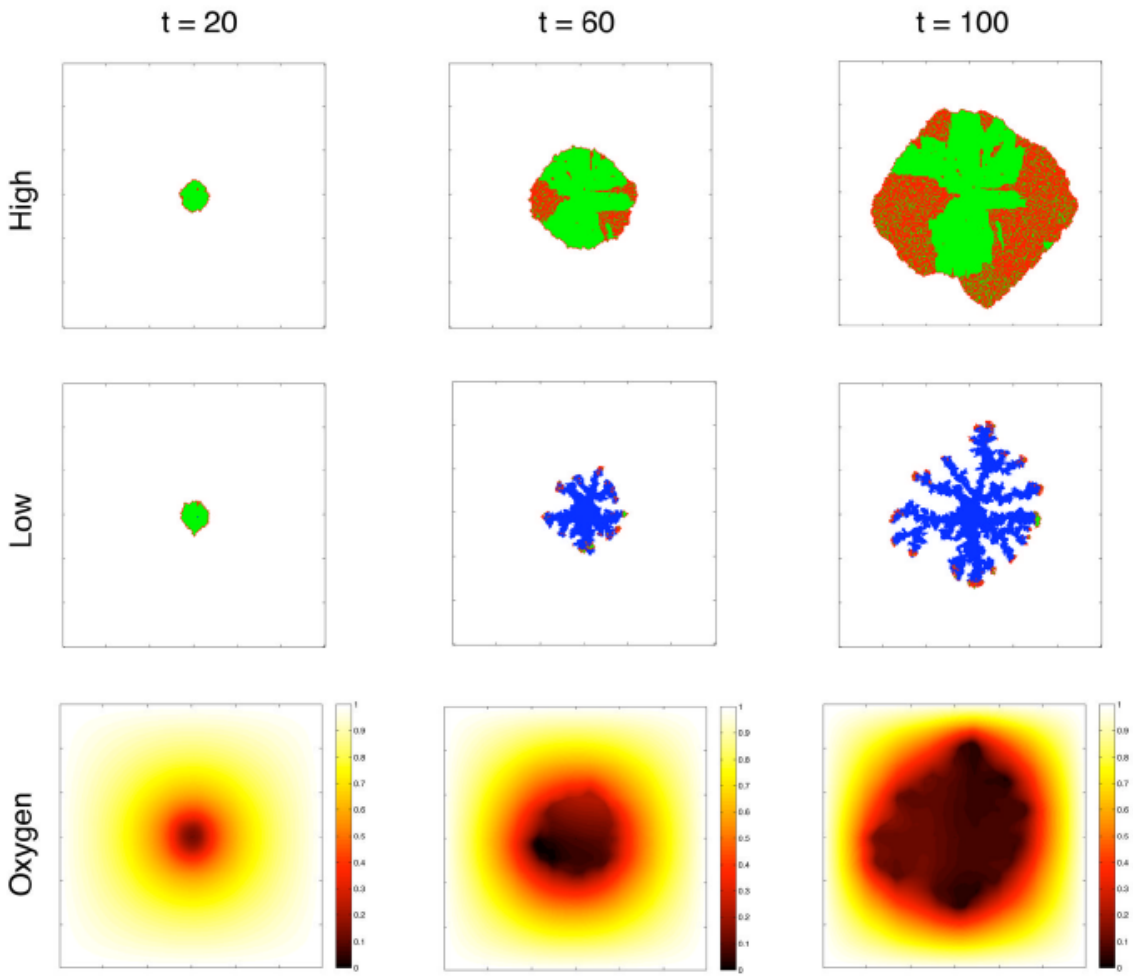

Figure 3.3: The effect of oxygen on tumor growth

*Tumor growth is assessed in environments with high (**top**) and low (**centre**) oxygen availability. The proliferating cells are red, quiescent cells are green, and dead cells are blue. The bottom panel illustrates the oxygen concentration in the low oxygen scenario. Reprinted from Biosystems, 95, P. Gerlee and A.R.A Anderson, Modelling evolutionary cell behaviour using neural networks: Application to tumour growth, 166-174, Copyright (2009), with permission from Elsevier. http://www.sciencedirect.com/science/journal/03032647 [67]*

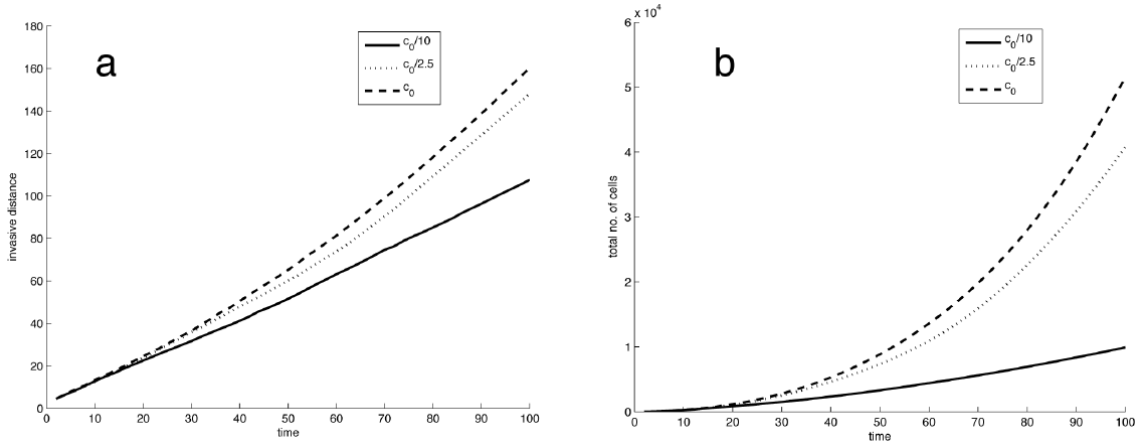

Figure 3.4: Time evolution of the (**a**) invasive distance and (**b**) the total number of the cells for oxygen background concentrations: $\frac{c_0}{10}$, $\frac{c_0}{2.5}$, and c_0.
Reprinted from Journal of Theoretical Biology, 24, P. Gerlee and A.R.A. Anderson, An evolutionary hybrid cellular automaton model of solid tumour growth, 583-603, Copyright (2007), with permission from Elsevier. http://www.sciencedirect.com/science/journal/00225193 [51]

is more readily available.

In Anderson et al. [17], the effects of oxygen switching on tumor growth are assessed. In these simulations, each cell has a unique genotype that is one mutational step away from an ancestral clone. Initially, a high concentration of oxygen is available to the cells. This allows the tumor to develop a thin proliferating rim around its quiescent core. The tumor's area expands at a rate that is proportional to its radius while the number of quiescent cells increases at a rate proportional to the square of the radius. When the oxygen level is lowered, a necrotic core develops. As shown in Figure 3.5, widespread cell death kills all but a few isolated groups of cells that form finger-like structures around the leading edge to maximize their access to space and nutrients. When the oxygen concentration is subsequently increased and then decreased, periods of rapid proliferation and invasive growth are observed, respectively.

From their simulations, Anderson et al. ascertain that the width of the proliferating rim d is

$$d \sim \frac{1-h}{\tau k}, \tag{3.6}$$

where τ is the maturation age, h is the apoptotic threshold, and k is the consumption rate [17]. This means that a large flux in the oxygen concentration will amplify spatial perturbations, contributing to the instability of the system. Likewise, a high consumption also correlates well with unstable growth and the development of a thin proliferating rim [68].

3.3.1 Population Dynamics

In order to study population dynamics, the proportion of proliferating, quiescent and apoptotic cells $S = (|x_P|, |x_Q|, |x_A|)$ is determined using the formula $|x_i| = \frac{1}{B}\int_I \delta_{i,R(x)} dx$ for $i = P, Q, A$ where B is the volume of the input space. Once these calculations have been performed, each entry in the response vector is grouped into one of 10 equal sized bins. In this way, the number of phenotypes is reduced to a manageable size [22].

In Figure 3.6, the effect of oxygen on the phenotype distribution is examined. When oxygen is readily available, there is a steady decline in the initial phenotype and several mutants emerge, albeit in low abundance. There is a slight network bias which favors

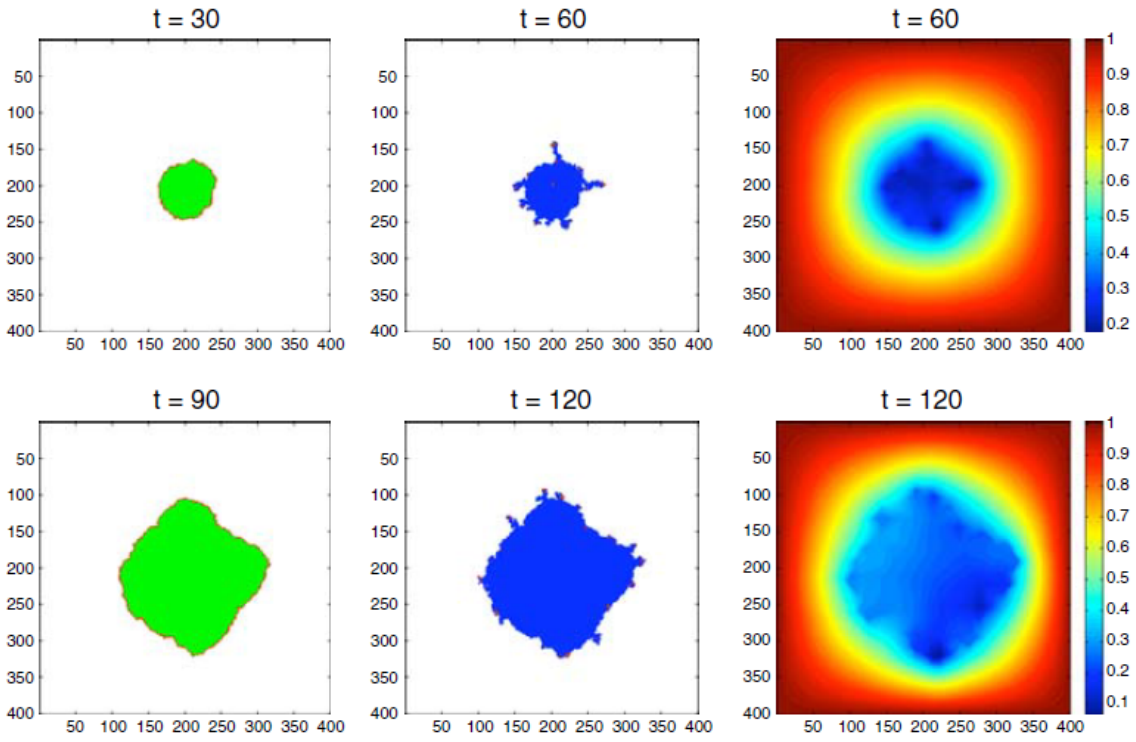

Figure 3.5: The effect of oxygen switching on tumor morphology
*The spatial distribution of the cells (**left**, **centre**) and the oxygen concentration (**right**) for the oxygen switching experiment. The proliferating cells are red, quiescent cells are green, and dead cells are blue. Springer and the Journal of Mathematical Biology, 58, 2009, 579-624, Microenvironment driven invasion: a multiscale multimodel investigation, Alexander R.A. Anderson, Katarzyna A. Rejniak, Philip Gerlee, and Vito Quaranta, Fig. 11; with kind permission from Springer Science and Business Media. [17]*

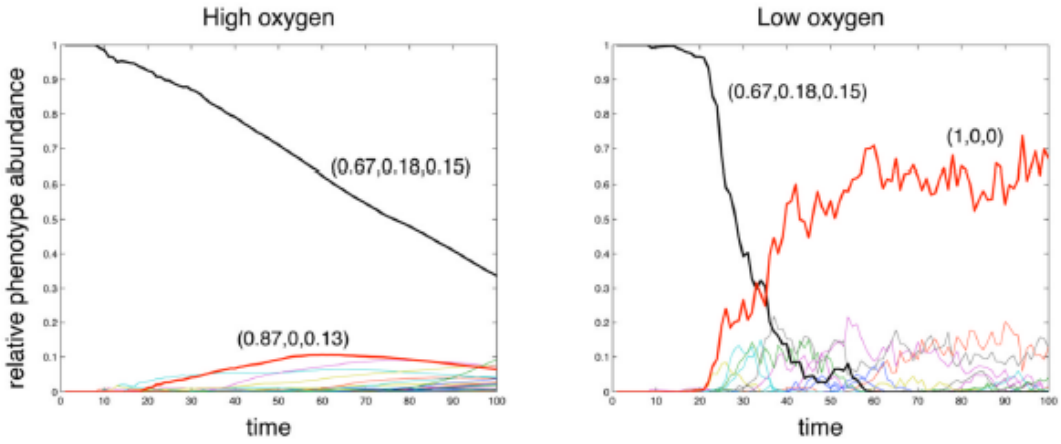

Figure 3.6: The time evolution of the relative phenotype abundance in high (**left**) and low (**right**) oxygen environments. *The response vectors of the most abundant phenotypes are displayed. Reprinted from Biosystems, 95, P. Gerlee and A.R.A Anderson, Modelling evolutionary cell behaviour using neural networks: Application to tumour growth, 166-174, Copyright (2009), with permission from Elsevier. http://www.sciencedirect.com/science/journal/03032647 [67]*

cells with a shorter maturation period, but this effect is weak [22]. In contrast, the initial phenotype becomes extinct in the hypoxic environment. In its place, a single clone is seen to flourish, encompassing approximately 70% of the population within 100 time steps. This clone is characterized by the loss of growth inhibition and will attempt to proliferate regardless of environmental stress.

The Shannon index

$$H = -\frac{1}{ln(N)} \sum_{i=0}^{N} p_i ln(p_i), \tag{3.7}$$

where p_i is the probability of finding genotype i and N is the number of distinct genotypes, is a helpful tool that can be used to accurately measure genotype diversity [17]. The value of H ranges from 0 (i.e., all of the cells have the same genotype) to 1 (i.e., no two cells have the same genotype).

In Gerlee and Anderson [67], the authors set $H(0) = 0$ and examine how differences in the availability of oxygen impact the Shannon index. The results of this study are illustrated in Figure 3.7. In a highly oxygenated environment, a slow increase in the Shannon index can be seen, with this value rising to $H \approx 0.5$. In comparison, a sharp increase is observed when there is only scarce oxygen and the value settles around $H \approx 0.7$. In the latter scenario, a faster convergence toward the aggressive phenotypes is noted, with competition favoring cells with a high proliferative potential and low consumption rate [51]. Directionality in mutation and phenotype selection is strongly implied based on the observation that these highly heterogeneous tumors have low variance in size [51].

In a series of simulations, the results of which can be seen in Figure 3.8, oxygen switching is examined. At the onset of these simulations, the Shannon index is set to $H(0) = 1$ in a highly oxygenated environment. As the tumor grows, genotype diversity decreases and, although different phenotypes continue to peacefully co-exist, rapidly proliferating cells become increasingly abundant. A drop in the background oxygen concentration, and the resulting cell death, generate extreme fluctuations in the phenotype distribution, as the number of distinct phenotypes plummets from 39 to 4 within a few time steps. A simultaneous spike in genotype diversity is observed. Once the cells' behavior has stabilized, the oxygen concentration is raised. This prompts a steep drop in genotype diversity but only minor changes in the phenotype distribution. When the oxygen concentration is lowered one last time, the Shannon index quickly converges to a value of approximately 0.9 and over 80% of the cells are observed to have the response vector $S = (1, 0, 0)$.

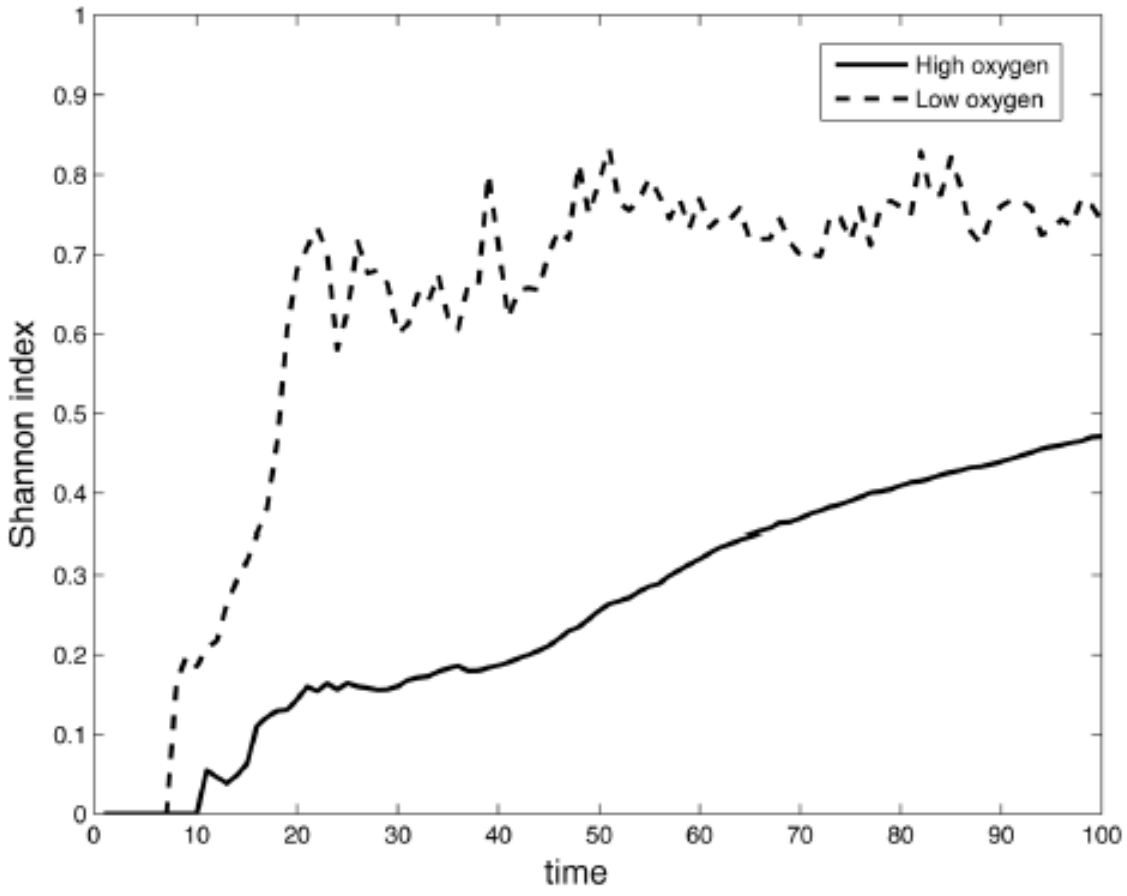

Figure 3.7: The time evolution of the Shannon index in low and high oxygen environments *Reprinted from Biosystems, 95, P. Gerlee and A.R.A Anderson, Modelling evolutionary cell behaviour using neural networks: Application to tumour growth, 166-174, Copyright (2009), with permission from Elsevier.*http://www.sciencedirect.com/science/journal/03032647 *[67]*

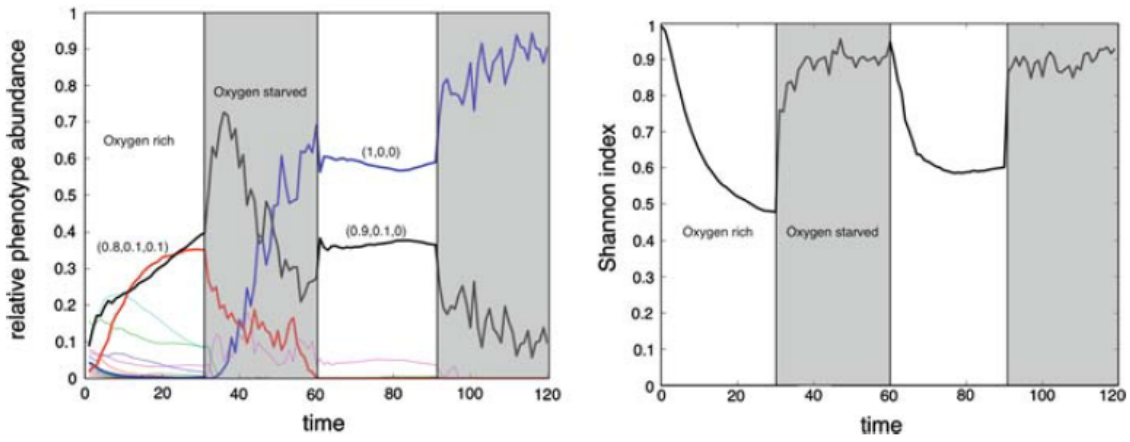

Figure 3.8: The time evolution of the relative phenotype abundance and the Shannon index *The relative abundance of each of the 100 randomly defined phenotypes (**left**) and the Shannon index (**right**) is shown for the oxygen switching experiment. In both diagrams, the grey areas correspond to periods with high oxygen availability. Springer and the Journal of Mathematical Biology, 58, 2009, 579-624, Microenvironment driven invasion: a multiscale multimodel investigation, Alexander R.A. Anderson, Katarzyna A. Rejniak, Philip Gerlee, and Vito Quaranta, Fig. 13; with kind permission from Springer Science and Business Media. [17]*

At first glance, the inverse relationship between phenotype and genotype diversity may seem peculiar. However, it seems reasonable to observe higher genetic variability in an oxygen starved environment by virtue of the increased selective pressures and the high cell turnover rate. Furthermore, it is important to keep in mind that many of the genotypes are redundant and correspond to the same phenotype. Some may be concerned that the number of phenotypes is influenced by the manner in which they are binned. To take this into account, Anderson et al. group the data using a variety of different techniques [17]. Regardless of the method used, their results remained consistent.

These simulations corroborate current views of cancer biologist regarding the influence of oxygen on the evolution of phenotype and genotype diversity and tumor morphology. In particular, aggressive cells with a reduced apoptotic potential are recognized as being the best suited to survive under harsh conditions and are consistently shown to drive tumor progression. Two other characteristics of malignant cells are a reliance on glycolysis and an increase in motility. These topics will be explored in the next section.

3.4 Metabolism and Motility

3.4.1 Metabolism

Under normal conditions, cells produce energy via aerobic respiration (i.e., the Krebs-cycle) with

$$\text{Glucose} \; + \; 6O_2 \; \rightarrow \; 6CO_2 \; + \; n_A\text{ATP} \tag{3.8}$$

where n_A is the number of ATP molecules[6,7] produced during the oxidation of a glucose molecule. However, according to the Warburg effect, cancer cells tend to rely on anaerobic metabolism (i.e., glycolysis) [52] with

$$\text{Glucose} \; \rightarrow \; 2\text{lactic acid} \; + \; 2\text{ATP}. \tag{3.9}$$

Comparing equations 3.8 and 3.9, glycolysis is observed to produce an excess of hydrogen ions and is 18 times less efficient at creating ATP molecules.

[6] Although this value is cell specific, Gerlee et al. consistently assume that $n_A = 36$.

[7] ATP is defined as the energy unit of the cell [51].

Since anaerobic respiration will allow cells to survive in a poorly oxygenated environment, it seems logical that it is upregulated during hypoxia. However, it is somewhat surprising that glycolysis persists even in the abundance of oxygen, especially when considering the fact that it is a less efficient way to produce energy and may limit cell proliferation [52]. In addition, if the production of hydrogen ions overcomes the buffering capacity of the tissue, the vasculature may be unable to transport the ions away from the cells at a sufficiently high rate [19]. Ultimately, this will cause the pH in the tissue to decrease and self-acidification may follow [54].

To incorporate glycolysis, Gerlee and Anderson [51,54,69] expand their model to include the concentrations of glucose and hydrogen ions as input nodes, and establish a connection network which determines whether a cell will undergo anaerobic or aerobic metabolism. The value of this output node specifies both the metabolic pathway and the metabolic rate. Although, anaerobic and aerobic metabolism are considered to be two mutually exclusive biological processes here, a cell may rely on a combination of these two pathways in vivo [54].

The amount of nutrients consumed by a cell depends on its metabolic pathway and life cycle status. If the oxygen concentration dips below the threshold c_m, then there is an automatic switch to anaerobic metabolism [51]. On the other hand, a cell will die from starvation if it tries to consume more glucose than is available or if the concentration drops below the threshold $g_{ap} = 0.5g_0$.

As mentioned above, the production of hydrogen ions is a by-product of anaerobic metabolism. Although cancer cells are able to survive in more acidic environments, a normal cell will undergo apoptosis if the pH drops below 7.1 in its micro-environment. If the pH continues to decline and falls below $h_{ap} = 6.5$, the cell will die from apoptosis regardless of its network response. Gerlee and Anderson [54] propose that chronic acidification degrades the ECM, creating an acellular gap between the normal tissue and the tumor. This grants cancerous cells a clear advantage, allowing them to invade into the tissue without having to compete against normal cells when $6.5 \leq pH \leq 7.1$.

3.4.2 Cell Motility

To describe the motion of the cells, Gerlee and Anderson consider a path-finding mode in which the cells move by pushing through existing gaps and pores in the ECM [69]. Since they are not interested in the degradation of the matrix when they adopt this approach, they ignore specifics regarding the composition and the density of the ECM and the size of the different cells. Initially, they let the ECM density be $f(\mathbf{x}, 0) = 1 + s$ where $s \in [-0.2, 0.2]$ is a uniformly distributed variable that is determined randomly at each grid point. At each time step, $max\{\Delta_x f, \Delta_y f\}$ is input into the response network, where $f_{i,j}$ is the concentration of the ECM at the point (i, j), $\Delta_x f = |f_{i+1,j} - f_{i-1,j}|$, and $\Delta_y f = |f_{i,j-1} - f_{i,j+1}|$.

Suppose that the network's decision is that the cell will migrate. Since migration, proliferation, and chemical diffusion are all on different time scales, a random number $r \in [0, 1]$ is generated and an additional constraint is imposed, namely that the cell will be allowed to move only if $R(\xi, G) \cdot p_m > r$. If this condition is satisfied, the cell will move one grid point up the larger gradient, provided that this lattice site is unoccupied.

Gerlee and Anderson [54] also propose a path generating mode in which the cells degrade the ECM at a constant rate, $e_c = 0.1$. When considering this approach, the density of the matrix at each grid point is closely monitored and a cell is allowed to migrate to a neighboring site only if the density there falls below the threshold $e_t \in [0.65, 0.9]$.

For both the path-finding and path-generating algorithms, the changes in the ECM satisfy:

$$\frac{\partial f(\mathbf{x}, t)}{\partial t} = -e_c I(\mathbf{x}, t) f(\mathbf{x}, t) - e_h (h(\mathbf{x}, t) - h_0) f(\mathbf{x}, t) \tag{3.10}$$

where $e_c = 0.1$ is the rate at which the ECM is degraded by short-range MDEs at sites adjacent to the lattice point being considered and $e_h = 10^{-3}$ is the rate at which the acid degrades the ECM. The latter value is considerably smaller to signify the fact that the effects of acid on the matrix are poorly understood, and to limit the growth advantage of the glycolytic cells [17]. The indicator function $I(\mathbf{x}, t)$ designates the number of cells adjacent to $\mathbf{x}$ and alternates between examining the cells' orthogonal and diagonal neighbors to avoid acid anisotrophy [17]. Finally, h_0 is the acid concentration in normal tissue; hence, the expression $h(\mathbf{x}, t) - h_0$ signifies that the acid-induced degradation of the ECM occurs at a rate proportional to the amount of excess acid.

When modeling the environment around the cells, oxygen, glucose, and hydrogen ions are also considered. In particular, it is the set of equations

$$\frac{\partial c(\mathbf{x},t)}{\partial t} = D_c\nabla^2 c(\mathbf{x},t) - f_c(\mathbf{x},t) \tag{3.11}$$

$$\frac{\partial g(\mathbf{x},t)}{\partial t} = D_g\nabla^2 g(\mathbf{x},t) - f_g(\mathbf{x},t) \tag{3.12}$$

$$\frac{\partial h(\mathbf{x},t)}{\partial t} = D_h\nabla^2 b(\mathbf{x},t) + f_h(\mathbf{x},t) \tag{3.13}$$

where

$$f_i(\mathbf{x},t) = \begin{cases} 0 & \text{if the automaton element at } \mathbf{x} \text{ is empty} \\ \kappa_i F(\mathbf{x}) & \text{if the automaton element at } \mathbf{x} \text{ is occupied} \end{cases} \tag{3.14}$$

which describe tissue dynamics. Here c, g, and h are the concentrations of oxygen, glucose, and hydrogen ions, respectively and D_c, D_g, and D_h are the respective rates of diffusion. $f_c(\mathbf{x},t)$ and $f_g(\mathbf{x},t)$ denote the respective rates at which oxygen and glucose are consumed, while $f_h(\mathbf{x},t)$ is the rate at which hydrogen ions are produced. As mentioned above, κ_i is the base consumption rate and $F(\mathbf{x}) = max\{k(R-T_r)+1, 0.25\}$ is a modulation function where T_r is the target response, R is the life cycle response, and k determines the strength of the modulation.

In equation 3.13, the hydrogen ions are modeled to diffuse through the tissue as they move toward the blood vessels, through which they are then transported away from the tumor. One immediate concern with this assumption is that basic diffusion laws would induce charge separation. In truth, these ions diffuse in association with mobile buffering species, such as bicarbonate, phosphate, or amino acids. Although their movements may be approximated by simple diffusion, Smalbone et al. [52] emphasize that the diffusion coefficient must be properly modified.

To model the blood vessels that surround the tissue, supply nutrients, and remove hydrogen ions, the boundary condition $c(\mathbf{x},t) = g(\mathbf{x},t) = h(\mathbf{x},t) = 1$ for $\mathbf{x} \in \partial\Omega$ are introduced [51]. In addition, the initial conditions are set to $c(\mathbf{x},0) = g(\mathbf{x},0) = h(\mathbf{x},0) = 1$.

3.4.3 Population Dynamics

In Gerlee and Anderson [54], the cells can mutate to become hypoxia adapted, glycolytic, or acid resistant. In an environment with weak selection pressures, only a few mutant cells are visible and they tend to die out. However, if the oxygen source is gradually depleted, a sharp increase in the hypoxia adapted and glycolytic cells will be observed as the necrotic core beings to expand. As seen in Figure 3.9, over 70% of the cells become glycolytic when exposed to a low oxygen environment for a prolonged period of time. This switch to anaerobic respiration gives rise to a surge in the production of hydrogen ions and ultimately alters the fitness landscape to favor the survival of acid-resistant clones.

For a given acid production rate, Gerlee and Anderson [54] note that there is an optimal range of vessel densities that maximize tumor growth. Outside of this range, high vessel densities ensure that the hydrogen ions are removed at a rate which prevents acid induced tissue degradation, while low densities evoke cell death from self-acidification.

The morphochart presented in Figure 3.10 shows that increasing the matrix density stabilizes growth and contributes to the formation of compact tumors with smooth, circular boundaries. In particular, we note that the tumors in the low oxygen environment form progressively wider fingers as the matrix density is increased. In the least dense matrix, a rough tumor boundary is observed, regardless of the availability of oxygen.

It is not surprising that glycolytic phenotypes thrive in dense and poorly oxygenated tissue [54]. As the matrix density is decreased and the selection pressures become weaker, there is a steady decline in the probability that the glycolyic cells will dominate. In fact, there is a near zero probability in a low density matrix with abundant oxygen. Results for acid resistance are similar; however the probability that the acid resistant clones will dominate the cell population is notably higher in oxygen rich, high density regions.

With an "almost universal presence of aerobic glycolysis in . . . a wide range of cancers arising in multiple different sites" [52], the importance of studying cell metabolism cannot be sufficiently stressed. As Smallbone and colleagues [52] point out, there is a direct correlation between the presence of aggressive clones and the rate of glucose consumption. Furthermore, increased glucose uptake and high lactate levels indicate an increased chance of tumor recurrence and an overall poor prognosis [52, 66]. Without a doubt, this is a research area which will continue to offer keen insight into tumor dynamics in the near future.

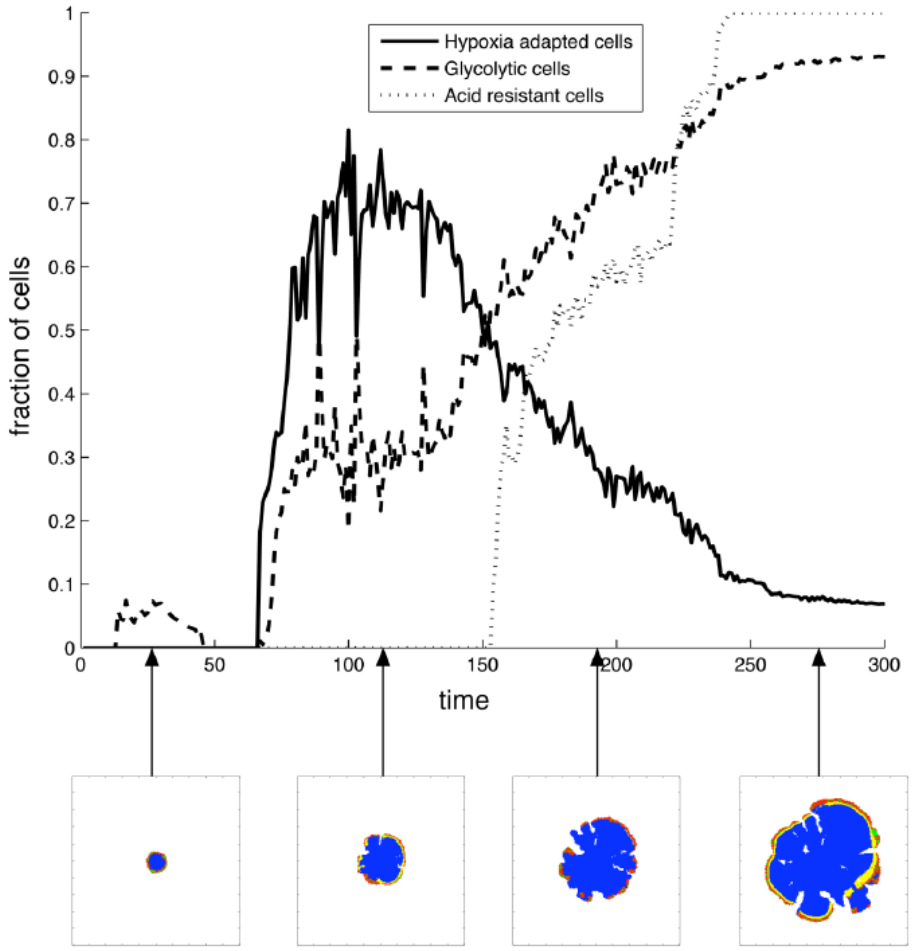

Figure 3.9: The time evolution of the hypoxia adapted, glycolytic, and acid resistant phenotypes

The bottom panel illustrates the evolution of the tumor morphology during the simulation. Reprinted from Journal of Theoretical Biology, 250, P. Gerlee and A.R.A. Anderson, A hybrid cellular automaton model of clonal evolution in cancer: The emergence of the glycolytic phenotype, 705-722, Copyright (2008), with permission from Elsevier. http://www.sciencedirect.com/science/journal/00225193 [54]

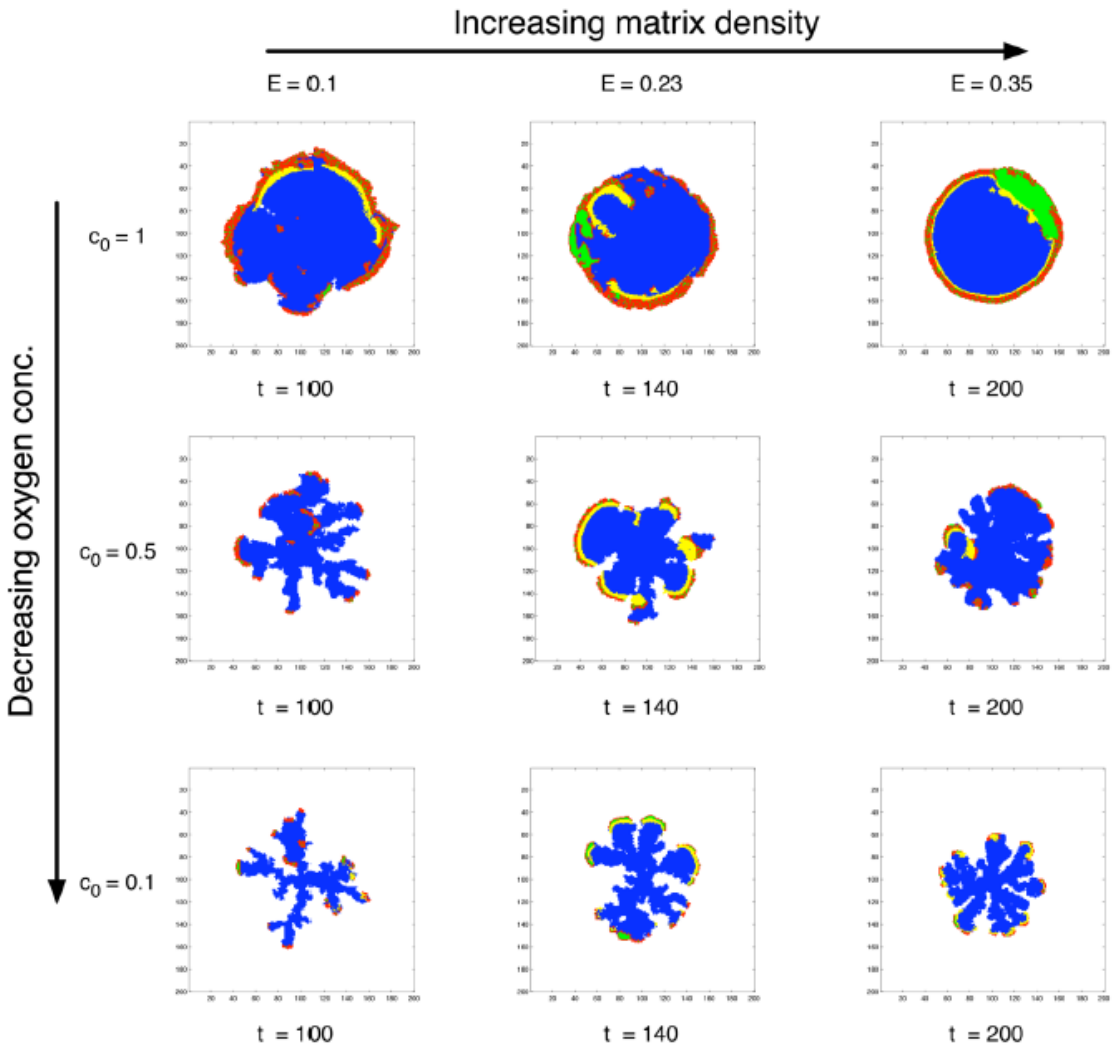

Figure 3.10: Tumor development for various background oxygen concentrations and matrix densities

The proliferating cells are red, quiescent cells are green, necrotic cells are yellow, and apoptotic cells are blue. Reprinted from Journal of Theoretical Biology, 250, P. Gerlee and A.R.A. Anderson, A hybrid cellular automaton model of clonal evolution in cancer: The emergence of the glycolytic phenotype, 705-722, Copyright (2008), with permission from Elsevier. http://www.sciencedirect.com/science/journal/00225193 *[54]*

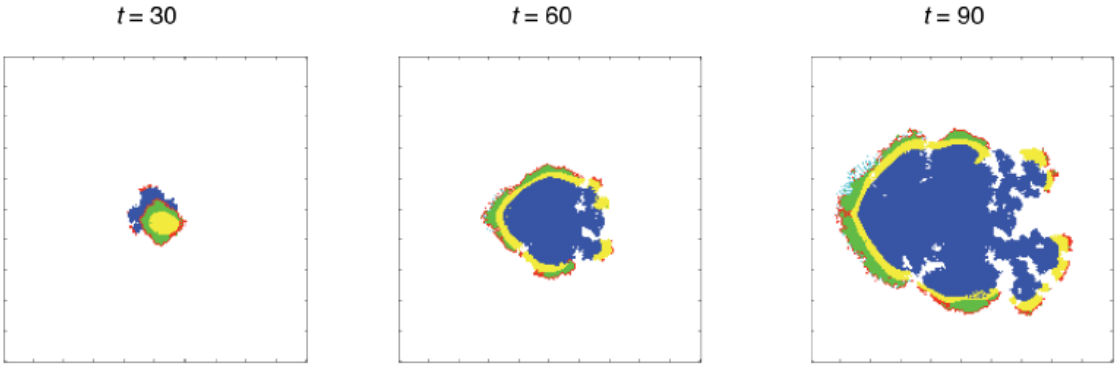

Figure 3.11: The spatial distribution of the cells in a high oxygen environment
In this simulation, the asymmetric morphology on the left side of the tumor is attributed to the emergence of a haptotactic clone. The proliferating cells are red, quiescent cells are green, necrotic cells are yellow, moving cells are cyan, and dead cells are blue. Reprinted from Journal of Theoretical Biology, 259, P. Gerlee and A.R.A. Anderson, Evolution of cell motility in an individual-based model of tumour growth, 67-83, Copyright (2009), with permission from Elsevier. http://www.sciencedirect.com/science/journal/00225193 [69]

3.4.4 Go versus grow

When describing movement through the ECM, Gerlee and Anderson [69] model a system in which proliferation and migration are mutually exclusive and a mutation is required to allow a cell to switch from one mode to the other. However, even if the cell prefers to migrate, it must sense a sufficiently large gradient in the ECM to do so, and will proliferate otherwise. To emphasize hypoxia-driven motility, the magnitude of this gradient is reduced in a low oxygen environment. Likewise, a steeper ECM gradient is required when the cell is surrounded by many neighbors to account for contact inhibition. According to the simulations performed by Gerlee and Anderson, a tumor composed of motile subclones tends to have an asymmetric and fragmented boundary, low cell density, and a sparse distribution [69]. Depending on whether the oxygen concentration is high or low, it will exhibit either a compact or branched morphology, as seen in Figures 3.11 and 3.12.

Gerlee and Anderson [69] also examine the selection of haptotactic clones in various environments. They claim to obtain inconclusive results (i.e., see Figure 3.13) but mention that there is an indication that motile cells are favored in soft tissue and in environments

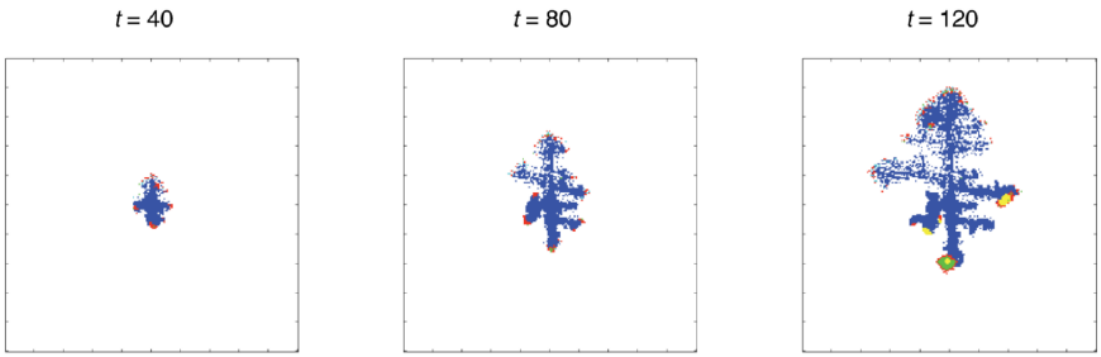

Figure 3.12: The spatial distribution of the cells in a low oxygen environment *Branched morphology is observed, with the motile subclones located in the top part of the tumor. The proliferating cells are red, quiescent cells are green, necrotic cells are yellow, moving cells are cyan, and dead cells are blue. Reprinted from Journal of Theoretical Biology, 259, P. Gerlee and A.R.A. Anderson, Evolution of cell motility in an individual-based model of tumour growth, 67-83, Copyright (2009), with permission from Elsevier. http://www.sciencedirect.com/science/journal/00225193 [69]*

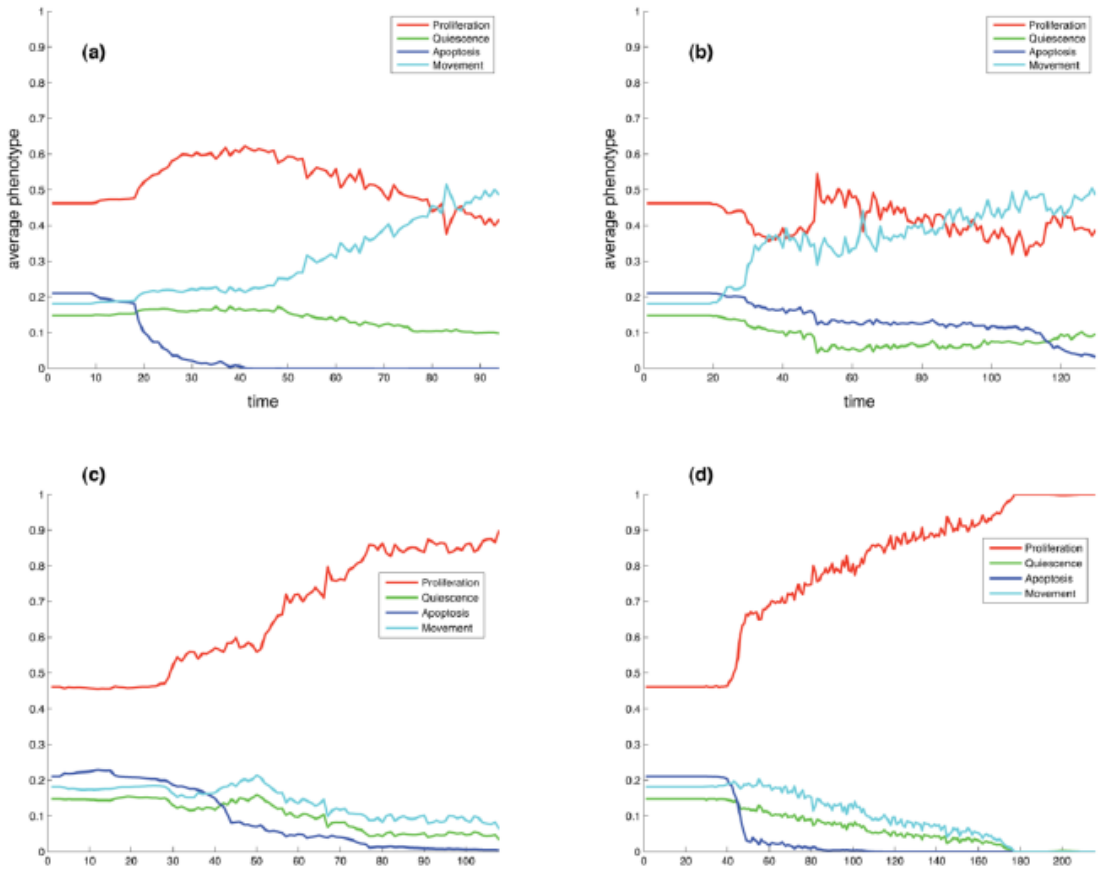

Figure 3.13: The time evolution of the proliferating, quiescent, apoptotic, and migratory cells

*Panels (**a**) and (**b**) map the time evolution of the average response vector of the tumors shown in Figures 3.11 and 3.12, respectively. In panels (**c**) and (**d**), the cells are subject to identical micro-environmental conditions as (**a**) and (**b**), respectively, but evolve to form proliferating clusters (instead of motile clusters). Reprinted from Journal of Theoretical Biology, 259, P. Gerlee and A.R.A. Anderson, Evolution of cell motility in an individual-based model of tumour growth, 67-83, Copyright (2009), with permission from Elsevier. http://www.sciencedirect.com/science/journal/00225193 [69]*

with intermediate oxygen levels. Sensitivity analysis also shows that increasing the probability of mutation corresponds to an increase in the growth rate but, generally, will not alter evolutionary dynamics. As an exception to this rule, the migratory phenotypes will become suppressed when movement and proliferation are on the same time scale and no clear advantage is conferred to these cells (i.e., the cells can invade the tissue faster if they proliferate rather than migrate).

3.5 Conclusion

Using the EHCA model allows researchers to study how the genotype drives the behavior of the cell and how mutations in the signaling network can alter the cellular response to the environment. Hence, a cell's evolution and adaptation can be assessed as well as the relationship between the fitness of a clone and its micro-environment [51, 67]. Initially, a limited supply of oxygen drives evolutionary forces that favor cells that can effectively compete for nutrients [67]. Accordingly, glycolytic and migratory phenotypes will often come to dominate the population [69]. However, a by-product of glycolysis is the production of acid. Although the precise impact of acidification on peritumoral tissue is relatively unknown, Gerlee's model indicates that if it promotes the degradation of the ECM, it will increase the prominence of glycolysis and stimulate tumor invasion [54].

On the contrary, if the cells are exposed to high levels of nutrients and the acid can be effectively removed by the vasculature, the selective pressures favoring aggressive clones disappear and invasive features in the tissue fail to materialize [54]. This suggests that treatments should aim to normalize the tissue since hostile environments serve only to destabilize the morphology and to induce aggressive behavior in the cells. Alternatively, there is no longer a preferred phenotype associated with a given micro-environment when the cells can take on either migratory or proliferative capabilities [69]. In this case it becomes much more difficult to develop and generalize an optimal treatment.

Artificial networks are able to capture important features of clonal evolution and regulatory pathways [51, 67]. Since there is no restriction on the inputs, outputs, and the connections between the nodes, this framework is both versatile and open-ended [67]. However, this simplified approach yields results of questionable accuracy. As future work, this model needs to be properly parameterized, with gene expression levels determined using microarrays [67]. Not only is it time consuming and difficult to obtain this data, it is also

expensive. Another problem is that this method is not capable of memory storage, while many cellular processes, such as the cell cycle and chemotaxis, are memory-dependent [67]. Finally, we must concur that mathematical analysis of this model is, at best, difficult.

One limitation of the HDC and EHCA models is that the cells are represented as gird points, without any regard for variability in their shape or size [22, 70]. In the next section, we will explore the Immersed Boundary model, in which a tumor is conceived as a collection of elastic cells immersed in an incompressible, viscous fluid.

Chapter 4

Immersed Boundary Models

The immersed boundary model attempts to capture the behavior of neutrally buoyant[1], elastic (or viscoelastic) bodies submerged in an incompressible, viscous fluid [71]. In this model, the fluid is described using Cartesian coordinates while the boundary forces and the configuration of the elastic bodies are represented in Lagrangian form. The Lagrangian variables move along a curvilinear mesh that overlaps, but is not constrained by, the Cartesian grid [71]. In terms of physical assumptions, the laws of conservation of energy and momentum are enforced.

4.1 The Model

In this chapter, we will describe the immersed boundary model developed by Rejniak and colleagues [72]. Unlike the HDC and EHCA models, this approach models cells as fully deformable entities [72]. To interact with one another, these viscoelastic bodies [73] use membrane bound receptors that function on a local scale. These receptors, shown in Figure 4.1, sense cues, send signal, and play a major role in determining cellular dynamics.

All of the cells are governed by the same set of laws that regulate their growth, division, polarisation, death, and communication [74,75]. Unlike the HDC and ECHA models,

[1]This property signifies that the elastic links occupy so little volume that their mass can be neglected [71].

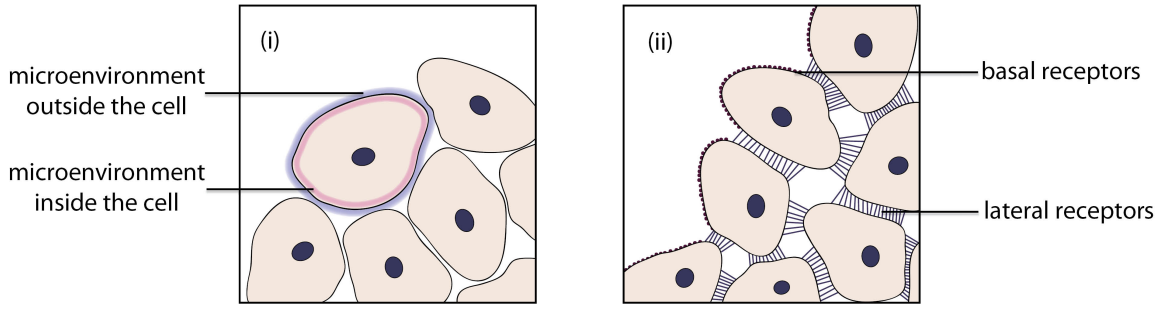

Figure 4.1: The microenvironment of a cell
*The microenvironment inside (light grey) and outside (dark grey) the cell is shown in (**i**). In addition, the membrane bound receptors are illustrated in (**ii**). Adapted from Rejniak and Anderson [75].*

the cell cycle here is not subject to mutation [74]. Rather, it is assumed that it is variation in the distribution of the surface receptors that accounts for cellular heterogeneity [61].

In their model, Rejniak et al. examine the cross-section of the tumor in a two-dimensional domain Ω and map it onto a Cartesian grid with fixed coordinates $\mathbf{x} = (x_1, x_2)$. This grid integrates information about fluid transport and nutrient availability, and provides a physical representation of the elastic tumor cells [72].

The plasma membrane of each cell is composed of a mesh of massless linear springs, which link a set of evenly distributed boundary points $\mathbf{X}_{i,l}(t)$, where l is the position of the point along the cell's membrane[2] and t is time [74]. Besides defining the shape and the size of the tumor, the boundary points also play the role of membrane bound receptors. These receptors act locally and sense information in the cell's microenvironment, $\Theta^{\varepsilon}_{\Gamma} = \bigcup_{\mathbf{X}\in\Gamma}\{\mathbf{x} : ||\mathbf{x} - \mathbf{X}|| < \varepsilon\}$, where Γ denotes the configuration of the membrane.

Although the receptors are structurally identical, they can be differentiated based on their function. In this chapter, we will consider two types of receptors: lateral receptors, which link neighboring cells, and basal receptors, which connect cells to the ECM. Contrary to biological receptors, which are created and relocated in response to extrinsic signals, the simulated receptors preserve their location, and change their status and function to direct

[2]taken modulo the total number of boundary points

the initiation and progression of various cell life processes [56].

Within the plasma membrane, a cell has no internal structure besides the fluid cytoplasm, which provides cell mass, and a single point nucleus that contains the genetic material. To compensate for the fact that the cytoskeleton and organelles are neglected, the fluid is assigned a high viscosity [75]. This homogeneous, incompressible, Newtonian fluid is also used to represent the ECM [72]. It is assumed that its density and viscosity are constant [75] and that cellular expansion and contraction are a result of its flow patterns. The boundary points and the nuclei move along at the local fluid velocity [72, 74], and are influenced by sources and sinks and the forces that act on the elastic boundaries of the cells [72].

One of the fundamental properties that must be enforced at every point in the domain Ω at all times t is the law of conservation of mass,

$$\int_{\Omega} s d\mathbf{x} = \rho \int_{\Omega} \nabla \cdot \mathbf{u} d\mathbf{x} = 0, \tag{4.1}$$

where $s(\mathbf{x}, t)$ is the local fluid expansion based on the distribution of sources and sinks [4] and ρ and $\mathbf{u}(\mathbf{x}, t)$ are the density and the velocity of the fluid, respectively.

In addition, the tumor must satisfy the law of mass balance,

$$\rho \nabla \cdot \mathbf{u} = s(\mathbf{x}, t). \tag{4.2}$$

The fluid inside and around the cells is assumed to be incompressible and to satisfy $\nabla \cdot \mathbf{u} = 0$ at all points, except for a discrete collection of isolated point sources and sinks. To describe the motion of the fluid, Rejniak and colleagues use the Navier-Stokes equation,

$$\rho \left(\frac{\partial \mathbf{u}(\mathbf{x}, t)}{\partial t} + (\mathbf{u}(\mathbf{x}, t) \cdot \nabla)\mathbf{u}(\mathbf{x}, t) \right) = -\nabla p(\mathbf{x}, t) + \mu \Delta \mathbf{u}(\mathbf{x}, t) + \frac{\mu}{3\rho} \nabla s(\mathbf{x}, t) + \mathbf{f}(\mathbf{x}, t) \tag{4.3}$$

where $\mathbf{f}(\mathbf{x}, t)$ is the external force density and μ and $p(\mathbf{x}, t)$ are the viscosity and the pressure of the fluid, respectively.

One concern is that $\nabla \cdot \mathbf{u}$ need not be continuous. This can be problematic when the gradient $\nabla s(\mathbf{x}, t)$ is determined in equation 4.3. Despite a thorough search, no mathemat-

ical justification could be found for the term $\nabla s(\mathbf{x}, t)$ in either Rejniak's papers or in the sources they referenced. This suggests that finding a new method or appropriate justification for incorporating the distribution of the sources and sinks into the Navier-Stokes equation in this manner is an important direction for future research in this area.

Another issue is that $s(\mathbf{x}, t)$ is a discrete field. This calls into question the validity of the formulations for the law of conservation of mass and the law of mass balance in equations 4.1 and 4.2, respectively.

Along the boundary of the cells, Rejniak et al. apply the no-slip condition. The condition

$$\frac{\partial \mathbf{X}_i(l,t)}{\partial t} = \mathbf{u}(\mathbf{X}_i(l,t),t) = \int_\Omega \mathbf{u}(\mathbf{x},t)\delta(\mathbf{x} - \mathbf{X}_i(l,t))d\mathbf{x}. \tag{4.4}$$

implies that the material points on the membrane are carried along with the viscous fluid.

In the following sections, the external force density f (mentioned in equation 4.3) and the mechanics of the point sources and sinks will be described.

4.1.1 The boundary forces

The force density $\mathbf{f}$ is the sum of the local contractive-repulsive forces $\mathbf{F}_i(l,t)$, which determine the boundary configuration of the cells [74, 75]. These forces control the direction of cellular expansion and fluid flow, and are influenced by cell-cell adhesion, mitosis, and the elastic properties of the membrane [4, 76]. They are assumed to follow Hooke's law and are applied directly to a 2-dimensional δ-layer in the fluid, $\delta(\mathbf{x}) = \delta(x_1)\delta(x_2)$, around the boundary Γ_i of the cell being considered. The external force density $\mathbf{f}(\mathbf{x}, t)$ satisfies

$$\begin{aligned} \mathbf{f}(\mathbf{x},t) = \quad & \textstyle\sum_i \mathbf{f}_i(\mathbf{x},t) \text{ where } \mathbf{f}_i(\mathbf{x},t) = \int_{\Gamma_i} \mathbf{F}_i(l,t)\delta(\mathbf{x} - \mathbf{X}_i(l,t))dl, \\ & \text{and } \mathbf{F}_i(l,t) = \textstyle\sum_\alpha \mathbf{F}_{\alpha(i)}(l,t), \\ & \text{and } \mathbf{F}_{\alpha(i)}(l,t) = \mathcal{F}_\alpha \frac{\|\mathbf{X}_{i,k}(t) - \mathbf{X}_{i,l}(t)\| - \mathcal{L}_\alpha}{\|\mathbf{X}_{i,k}(t) - \mathbf{X}_{i,l}(t)\|}(\mathbf{X}_{i,k}(t) - \mathbf{X}_{i,l}(t)), \end{aligned} \tag{4.5}$$

where α is the acting force, and $\mathcal{L}_\alpha$ and $\mathcal{F}_\alpha$ are the resting length and the spring stiffness, respectively.

When studying tumor growth, Rejniak and colleagues discuss adjacent, adhesive, and contractile forces. The adjacent force connects each boundary point $\mathbf{X}(l,t)$ to its two adjacent neighbors $\mathbf{X}(l+1,t)$ and $\mathbf{X}(l-1,t)$ by linear springs that satisfy Hooke's law and have constant resting length $\mathcal{L}_{adj}$ and spring stiffness $\mathcal{F}_{adj}$. This force

$$\mathbf{F}_{adj(i)}(l,t) = \mathcal{F}_{adj}\frac{\parallel \mathbf{X}_{i,l+1}(t) - \mathbf{X}_{i,l}(t) \parallel - \mathcal{L}_{adj}}{\parallel \mathbf{X}_{i,l+1}(t) - \mathbf{X}_{i,l}(t) \parallel}(\mathbf{X}_{i,l+1}(t) - \mathbf{X}_{i,l}(t)) \tag{4.6}$$

determines the cells' structure and geometry.

The adhesive force is the force exerted on the i^{th} cell by a boundary points belonging to the j^{th} cells where $i \neq j$,

$$\mathbf{F}_{adh(i,j)}(l,t) = \mathcal{F}_{adh}\frac{\parallel \mathbf{X}_{j,k}(t) - \mathbf{X}_{i,l}(t) \parallel - \mathcal{L}_{adh}}{\parallel \mathbf{X}_{j,k}(t) - \mathbf{X}_{i,l}(t) \parallel}(\mathbf{X}_{j,k}(t) - \mathbf{X}_{i,l}(t)). \tag{4.7}$$

This force can only be introduced between two receptors that are within a distance[3] $\parallel \mathbf{X}_{j,k} - \mathbf{X}_{i,l} \parallel \leq \mathcal{L}_{adh}^{max}$ and is otherwise set to zero [74] . Typically, this force results in the contraction of the springs and reduces the separation distance between the receptors that link the adjacent cells [75]. However, if the membrane receptors are within the distance of the resting length $\mathcal{L}_{adh}$, then this force $\mathcal{F}_{adj}$ will become repulsive in nature.

Finally, the contractile force

$$\mathbf{F}_{div(i)}(l,t) = \mathcal{F}_{div}\frac{\parallel \mathbf{X}_{i,k}(t) - \mathbf{X}_{i,l}(t) \parallel - \mathcal{L}_{div}}{\parallel \mathbf{X}_{i,k}(t) - \mathbf{X}_{i,l}(t) \parallel}(\mathbf{X}_{i,k}(t) - \mathbf{X}_{i,l}(t)). \tag{4.8}$$

is defined between two opposing boundary points $\mathbf{X}_{i,k}(t)$ and $\mathbf{X}_{i,l}(t)$ of a single cell. This force causes the boundary points to compress together until they are within a distance $\mathcal{L}_{div}^{min}$, at which point, the force nullifies and the parent splits into two daughter cells.

4.1.2 The distribution of sources and sinks

It is assumed that the motion of each cell is governed by the forces discussed above as well as the distribution of local sources $S^{+}(\mathbf{Y}_{i,k}^{+},t)$ and sinks $S^{-}(\mathbf{Y}_{i,k}^{-},t)$. In some cases, a finite

[3] $\mathcal{L}_{adh} \leq \mathcal{L}_{adh}^{max}$

collection of these "water channels" are positioned along the cell's boundary Γ_i, gathered together in small groups Ξ_i^p of isolated points $\mathbf{Y}_{i,k}^p$ (where $p = +$ or $p = -$). Alternatively, another representation clusters these material points around the nuclei of the cell and the outside of its boundary[4].

The fluid flux through each of the water channels is assumed to be the same; hence, the overall fluid transport depends only on the number of active channels [75]. Suppose that the strength of each fluid source $S_0^+(\mathbf{Y}_{i,k}^+, t)$ is

$$|S_0^+(\mathbf{Y}_{i,k}^+, t)| = \begin{cases} S_0^+ & \text{if the cell is growing} \\ 0 & \text{otherwise .} \end{cases} \tag{4.9}$$

Since mass must be conserved globally, the sources and sinks must balance. However, Rejniak et al. enforce the condition that the fluid created on one side of the cell boundary is lost on the other [74]. Given that the number of point sources and sinks need not be the same, the following condition is applied:

$$\sum_{k \in \Xi_i^+} S^+(\mathbf{Y}_{i,k}, t)^+ + \sum_{m \in \Xi_i^-} S^-(\mathbf{Y}_{i,m}^-, t) = 0. \tag{4.10}$$

From equation 4.10, Rejniak and colleagues calculate that, given K point sources and M point sinks, the strength of each sink is

$$|S_0^-(\mathbf{Y}_{i,m}^-, t)| = \begin{cases} S_0^- & \text{if the cell is growing} \\ 0 & \text{otherwise} \end{cases} \tag{4.11}$$

where

$$S_0^- = \frac{1}{M} \sum_{k=1}^{K} S^+(Y_k^+(t), t) \tag{4.12}$$

[4]When distributing the water channels around the outside of the cell, special care must be taken to ensure that the assumption that that sources and sinks act locally is upheld [74].

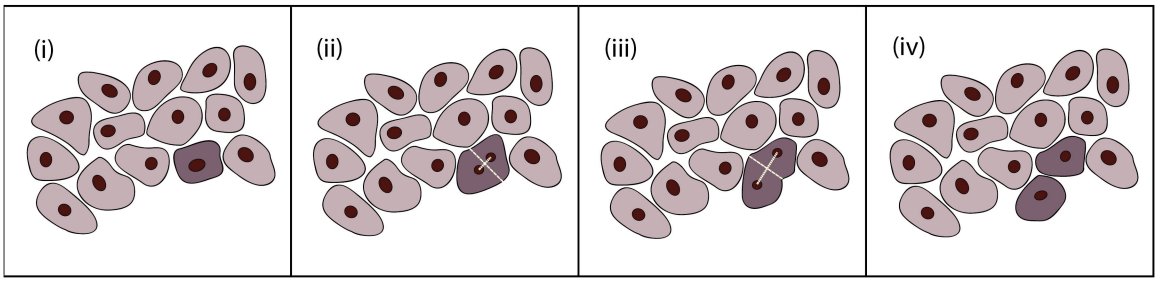

Figure 4.2: The growth and division of a cell
*When a cell is ready to undergo mitosis, (**ii**) the location of the contractile ring is determined. The cell then (**iii**) divides along the contractile connection, (**iv**) forming two daughter cells. Adapted from Rejniak [74].*

In summary, the source distribution, $s(\mathbf{x}, t)$, can be defined as follows:

$$
\begin{aligned}
s(\mathbf{x},t) \quad &= \quad \sum_i s_i(\mathbf{x},t) \\
&\text{where} \quad s_i(\mathbf{x},t) = \sum_{k\in\Xi_i^+} S^+(\mathbf{Y}_{i,k}^+,t)\delta(\mathbf{x}-\mathbf{Y}_{i,k}^+) + \sum_{m\in\Xi_i^-} S^-(\mathbf{Y}_{i,m}^-,t)\delta(\mathbf{x}-\mathbf{Y}_{i,m}^-) \\
&\text{and} \quad \sum_{k\in\Xi_i^+} S^+(\mathbf{Y}_{i,k}^+,t) + \sum_{m\in\Xi_i^-} S^-(\mathbf{Y}_{i,m}^-,t) = 0.
\end{aligned}
$$

From here, we focus more on the inner workings of the cell and the basic assumptions regarding its life cycle.

4.1.3 The life cycle of the cells

If more than 20% of its receptors are free from cell-cell contact, cell growth can be observed as the fluid is transported from the extracellular medium into the cell (i.e., point sources are placed inside the cell, while point sinks are positioned outside its boundary). This condition restricts growth to cells around the leading edge; those in the interior are considered to be too crowded to grow. Visually, cellular expansion is depicted by the continuous deformation of the elastic membrane in response to the accumulation of fluid inside the cell. To account for the increase in area, an addition boundary point is placed halfway between two adjacent ones, whenever the spring connecting them exceeds its prescribed

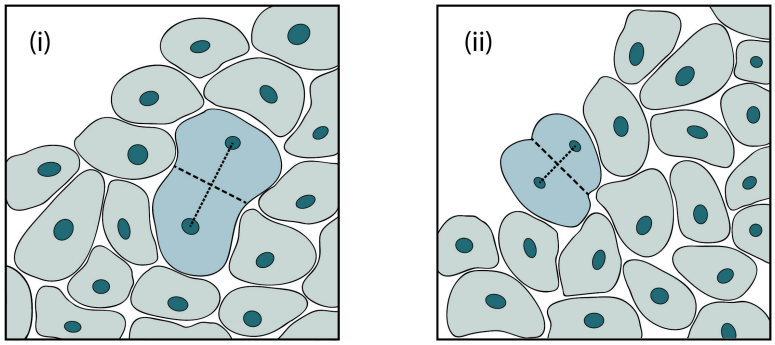

Figure 4.3: The orientation of cell division
*In (**i**) and (**ii**), the axis of cell division (dashed line) is orthogonal to the longest axis and the part of the membrane in contact with the ECM, respectively. Adapted from Rejniak and Anderson [75].*

resting length [56].

To indicate proliferation, two nuclei (corresponding to two sets of sister chromatids) are placed inside the cell[5] [72] and fluid flow is directed to induce cellular growth. As seen in Figure 4.2, the sources and sinks are deactivated and the axis of cell division is determined once the total area of the cell has doubled. The appropriate springs are then introduced and a contractile ring forms between two opposing boundary points. Once these boundary points are within a distance of $\mathcal{L}_{div}^{min}$, the contractile forces are deactivated and the host cell divides into two daughter cells, each of which has its own nucleus [75]. The daughter cells are approximately the same size and are regulated to be within 5% of the area of the parent cell [75].

One factor which will impact the shape and the size of the daughter cells is the orientation of cell division [61]. When it is orthogonal to the longest axis or determined randomly, inhomogeneous and irregularly shaped daughter cells form degenerate tumors [76]. On the other hand, the cluster is more structured when the axis of division is determined to be orthogonal to the portion of the membrane that is in contact with the extracellular space [75]. A diagram depicting cell division is presented in Figure 4.3.

[5]Hence, when fluid flows through sources located around the nuclei, two clusters of sources will be considered, with one at each nucleus.

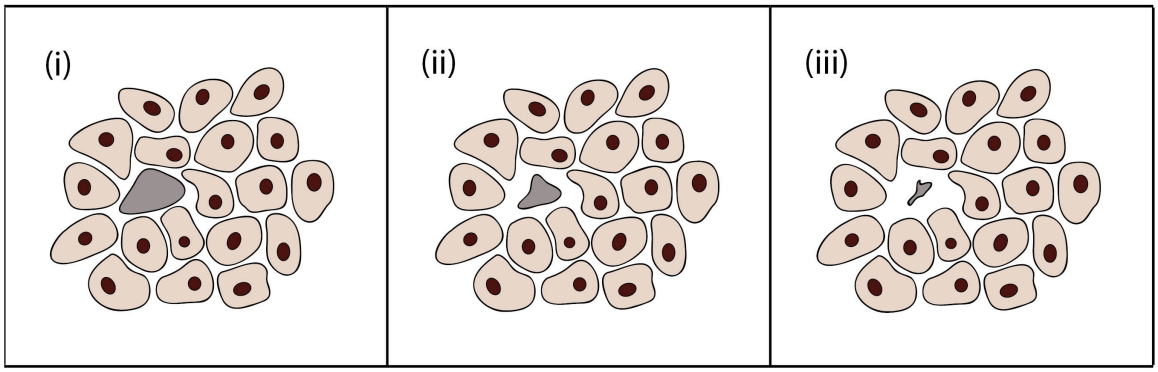

Figure 4.4: Apoptosis
During apoptosis, a cell becomes detached from its neighbours and gradually shrinks in size. Adapted from Rejniak and Anderson [75].

In contrast to cellular growth, apoptosis is a process characterized by the contraction of volume, the collapse of the cytoskeleton, and the detachment of the cell from its neighbors [17]. To model the release of fluid into the extracellular space, Rejniak et al. disassemble the cell's adherent links and re-arrange the sink-source couplets such that the sources are placed outside of the membrane while the sinks are located inside the cell [4,75]. Figure 4.4 shows how the cell's area shrinks as the fluid flows from its interior. This process continues until only 15% of the cell's initial area remains, at which point it is be declared "dead".

4.1.4 Nutrients

For a cell to propagate, it must have access to oxygen, nutrients, and growth factors [74]. In this model, oxygen $c(\mathbf{X}_i(l,t),t)$ is assumed to diffuse uniformly on the whole domain and is locally degraded according to the Michaelis-Menten formulation. Θ_Γ is defined to be $\Theta_\Gamma = \bigcup_i \Theta_{\Gamma_i}$ and

$$\frac{\partial c(\mathbf{x},t)}{\partial t} = \mathcal{D}\nabla^2 c(\mathbf{x},t) - k\frac{c(\mathbf{x},t)}{\kappa + c(\mathbf{x},t)} \cdot \chi_{\Theta_\Gamma}(\mathbf{x})$$

where k is the maximum consumption rate, κ is the Michaelis constant, and χ is a set of characteristic functions defined as

$$\chi_{\Theta_\Gamma}(\mathbf{x}) = \begin{cases} 1 & \text{if } \mathbf{x} \in \Theta_\Gamma \\ 0 & \text{if } \mathbf{x} \notin \Theta_\Gamma. \end{cases} \tag{4.13}$$

Although, its kinetics are defined on the entire domain, the amount of oxygen available to a cell is equal to the concentration in its microenvironment,

$$c(\mathbf{X}_i(l,t),t) = \int_\Omega c(\mathbf{x},t)\delta(\mathbf{x} - \mathbf{X}_i(l,t),t)d\mathbf{x}. \tag{4.14}$$

Typically, the consumption rate is independent of the amount available. However, when only a low concentration is present, consumption will generally decrease.

Rejniak assumes that the concentration of oxygen must exceed some threshold value h for the fluid source of the i^{th} cell to be activated. In the event that the concentration falls below this threshold, hypoxia is observed. The authors note that growth is dependent on the concentration of $c(\mathbf{x},t)$ and label the fluid source $S^+ = S^+(c(\mathbf{Y}^+_{i,k},t),t)$.

According to the initial condition,

$$c(\mathbf{x},0) = c_0 \text{ for } \mathbf{x} \in \Omega, \tag{4.15}$$

the domain Ω is uniformly saturated with an optimal concentration of oxygen, c_0. Throughout the simulations, a constant source of value c_0 is continuously applied at the boundary, with

$$c(\mathbf{x},t) = c_0 \text{ for } \mathbf{x} \in \partial\Omega \text{ and } t \geq t_0.$$

4.2 Numerical implementation

To implement this model numerically, Rejniak and colleagues use the fast Fourier transform method and impose periodic boundary conditions. They assume that the local neighbourhood around each boundary point consists of 16 grid points in the fluid domain (see Figure

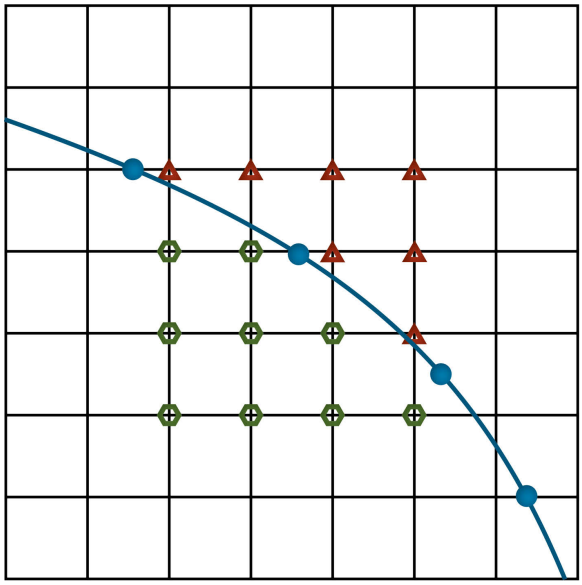

Figure 4.5: Fluid-cell interactions
A schematic diagram of the 16-point local neighborhood around a cell (black curve) is presented. This representation provides insight into the manner in which the sources (∘) and sinks (△) may be distributed during cell growth. Adapted from Rejniak [4].

4.5) and use a bell-shaped continuous function of bounded support,

$$\delta_h(r) = \begin{cases} 0 & \text{if } |r| \geq 2h \\ \frac{1}{4h}\left(1 + cos\left(\frac{\Pi r}{2h}\right)\right) & \text{if } |r| < 2h, \end{cases} \tag{4.16}$$

to model the Dirac delta function, $\delta_h(\mathbf{x}) = \delta_h(x_1) \cdot \delta_h(x)$ [4].

When performing their simulations, Rejniak and colleagues begin by revising the oxygen field to account for cellular consumption. During this process, cells that do not have access to sufficient nutrients are automatically declared to be necrotic. Although necrotic cells maintain their physical structure, they are no longer updated and do not consume any oxygen.

Next, Rejniak et al. examine fluid flow through the sources and sinks, and calculate the local growth rate s^n by "spreading" the fluid to its neighboring grid points. In a similar

manner, they also determine the force $\mathbf{F}^n$ around each boundary point and again spread this value to the neighboring grid points to determine the local force density $\mathbf{f}^n$.

The authors then proceed to solve the Navier-Stokes equation in order to determine the fluid velocity field. They interpolate this field to calculate the fluid velocity at each immersed boundary point and, when applicable, the cell's nucleus[6]. Using this information, they determine the position of the sources and sinks.

4.3 Simulation results

Simulations suggest that exponential growth is observed during the early stages of tumor development [74]. However, as the tumor continues to grow, a signification reduction in the expansion rate is seen, as mitotic events become confined to the leading edge. Concurrently, the cells located at the centre of the tumor begin to acquire an increasingly polygonal shape due to their tendency to develop multiple cell-cell adhesive connections [74]. Although these cells are too crowded to grow freely, pressure from growing neighbors may still cause them to move or deform. In an environment with significant competition for space and high selective pressures, small aggregates with irregular and elongated shapes form [74]. However, when abundant nutrients are available and selection pressures are weak, the tumors generally exhibit a round shape.

The total area[7] increases rapidly when small aggregates are considered, since all of the cells can actively proliferate. However, due to the small population size, this coincides with long intervals of constant cell count. In later stages of tumor development, the increase in the total area slows (due to contact inhibition) [4], but new cells are created more often. As shown in Figure 4.6, this corresponds to infrequent plateaus in the cell count, that last only a short period of time. Some factors that influence cell growth include the maturation age, the fluid flow, and the growth receptor threshold (i.e., the minimum number of basal or unbound receptors required to trigger growth).

In Figure 4.7, the impact of the hypoxic threshold and the oxygen consumption rate on tumor growth is shown [17]. Based on these results, Anderson et al. claim that the condi-

[6]It is only necessary to consider the nucleus when it is assumed that sources or sinks are located there.
[7]The total area refers to the net area of the individual cells.

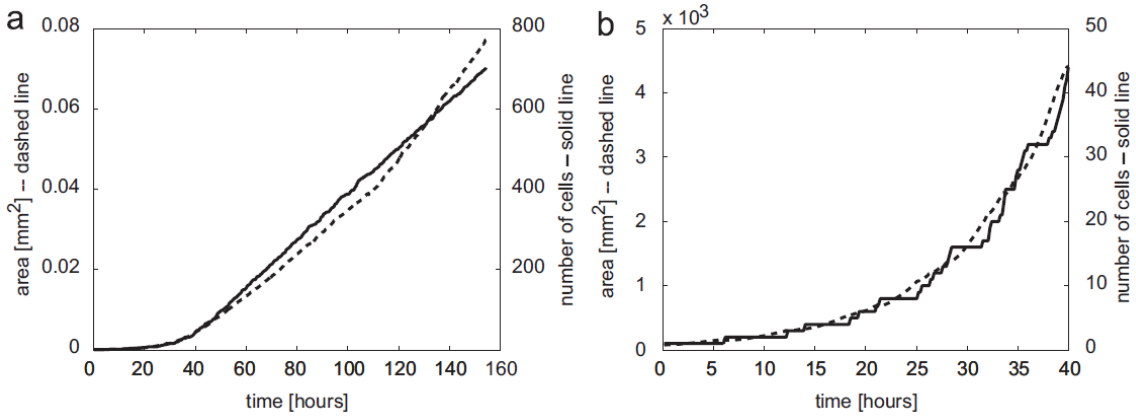

Figure 4.6: The time evolution of the total number of cells and the net area of the tumor *The solid line denotes the total number of cells while the dashed line represents the total area. Panel (**b**) is a magnification of the time interval* $0 - 40h$ *in panel (**a**). Reprinted from Journal of Theoretical Biology, 247, Katarzyna A. Rejniak, An immersed boundary framework for modelling the growth of individual cells: An application to the early tumour development, 186-204, Copyright (2007), with permission from Elsevier. http://www.sciencedirect.com/science/journal/00225193 [74]*

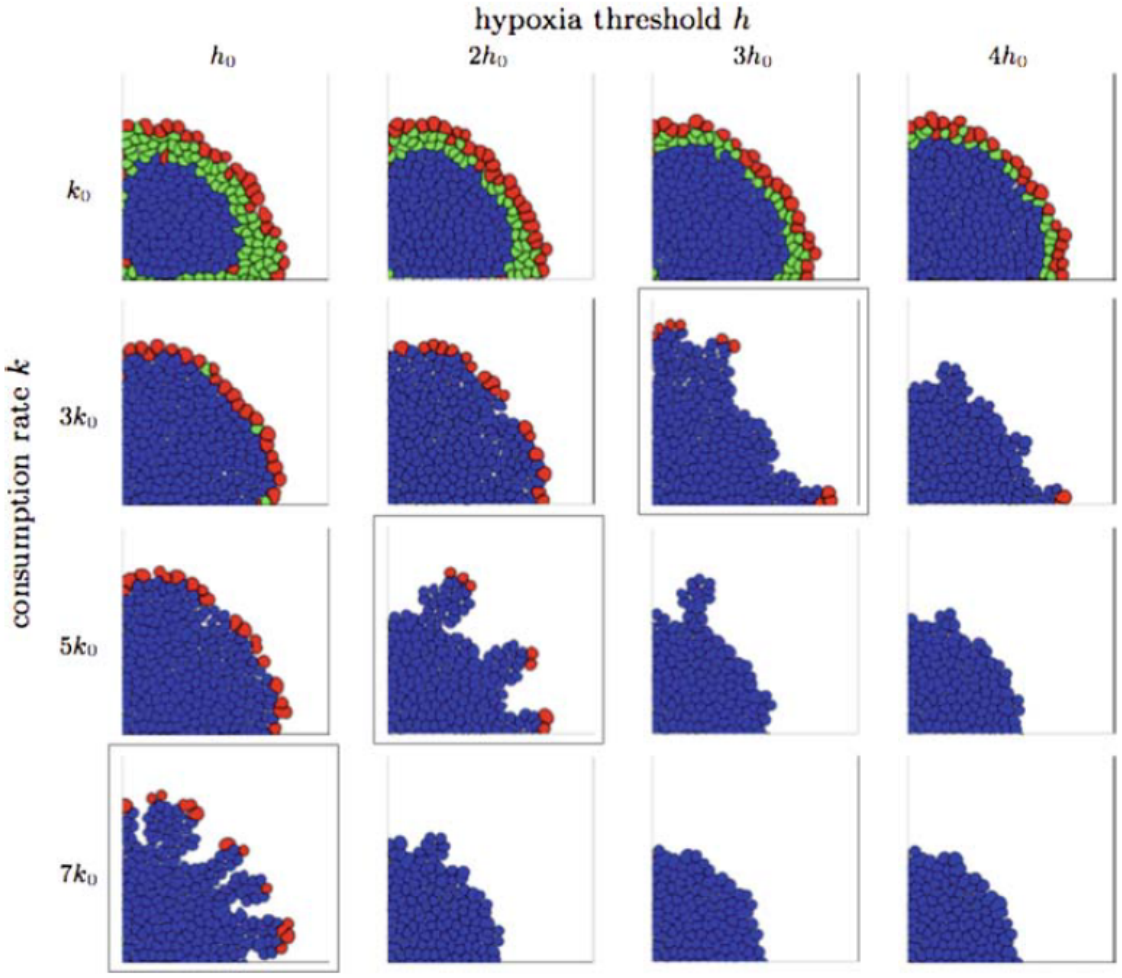

Figure 4.7: The effect of the hypoxic threshold and the consumption rate on tumor growth *The spatial distribution of the cells for various hypoxic thresholds and consumption rates is presented. The growing cells are red, quiescent cells are green, and hypoxic cells are blue. Springer and the Journal of Mathematical Biology, 58, 2009, 579-624, Microenvironment driven invasion: a multiscale multimodel investigation, Alexander R.A. Anderson, Katarzyna A. Rejniak, Philip Gerlee, and Vito Quaranta, Fig. 6; with kind permission from Springer Science and Business Media. [17]*

tions favoring the selection of aggressive clones correspond to the diagonal rising from left to right. Above this line, the tumors have smooth boundaries and grow at a constant rate. In contrast, invasive fingers and growth arrest are observed below the diagonal, regardless of the availability of space. This seems to suggest that the development of finger-like margins is related to growth suppression rather than overcrowding.

Intrigued by its effect on cellular behavior, Anderson and colleagues [17] set about documenting the cellular response to oxygen availability. To accomplish this, they consider an environment with a high concentration of oxygen uniformly distributed over the entire domain, but supply no additional nutrients to the tumor once the simulations begin. Initially, the cells sense the abundance of nutrients and proliferate continuously, forming a rapidly expanding, round cluster of growing cells [4]. However, the tumor eventually attains a size at which the diffusion of oxygen to its core is limited. As the first necrotic cells appear, the growth rate slows and the proportion of quiescent cells declines. At this stage, there is a near zero concentration of nutrients at the center of the tumor and steep gradients around its rim [74]. Although the cells at the boundary are exposed to elevated concentrations of oxygen, they are still subject to high competition. To maximize their proliferative potential and their ability to compete for nutrients, these tumors develop a rim of finger-like sprouts. Regardless of this structural adaptation, which is presented in Figure 4.8, the increasing prevalence of hypoxia triggers the extinction of the quiescent cells and a 95% reduction in the number of proliferating cells within a dozen cell cycles. The cells which survive often display an elliptical shape, with boundary points closer to the nutrients moving at a relatively faster pace [4].

Repeating these simulation using 7 color-coded clones [72], asymmetric growth is observed, even though the cells have identical properties. As illustrated in Figure 4.9, those that have access to high levels of oxygen proliferate readily, while the centrally located cells becomes extinct due to a lack of space. For future work, the authors suggest exploring the effects of mutations that alter properties such as the doubling time and the strength of the cell-cell connections.

4.4 Conclusions

IBCell models describe the behavior of cells that vary in shape and function and generate novel information regarding cell plasticity and fluid flow [4, 77]. The architectural stability

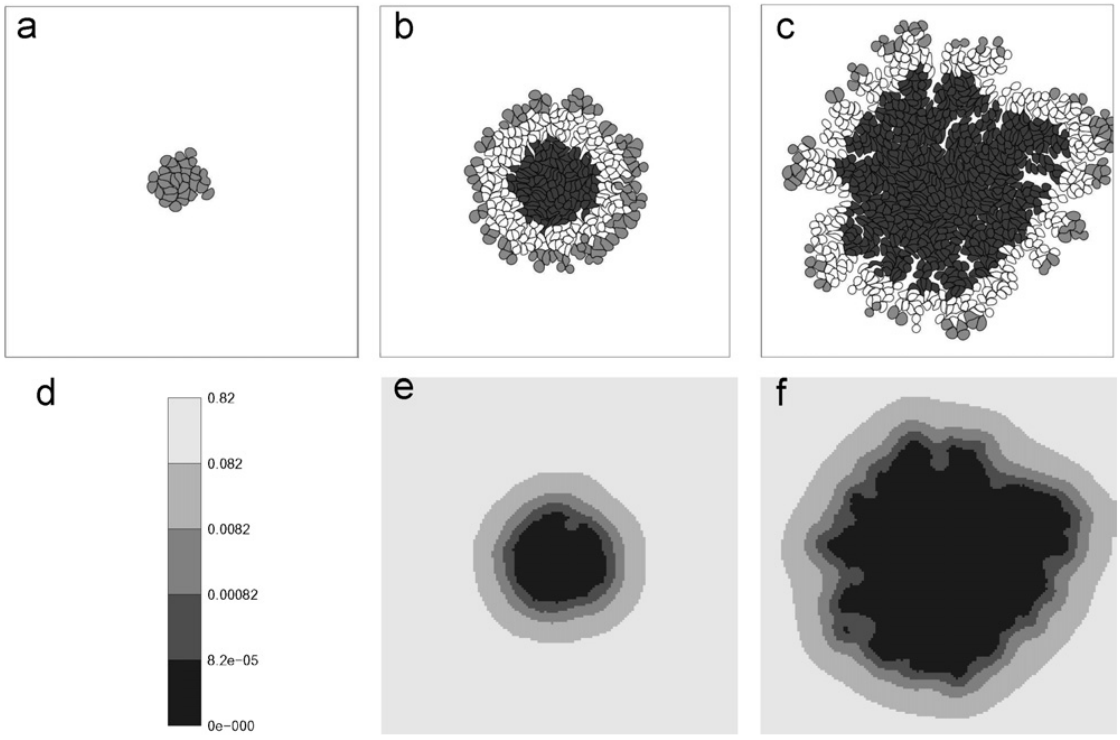

Figure 4.8: Nutrient-driven tumor growth

*The development of a tumor is shown in panels (**a**-**c**). Moreover, the oxygen distribution for the tumor configurations in panels (**b**) and (**c**) is presented in (**e**) and (**f**), respectively. The necrotic cells are black, proliferating cells are grey, and the viable cells are white. The color bar in (**d**) provides a numerical description of the oxygen concentrations in panels (**e**) and (**f**). Reprinted from Journal of Theoretical Biology, 247, Katarzyna A. Rejniak, An immersed boundary framework for modelling the growth of individual cells: An application to the early tumour development, 186-204, Copyright (2007), with permission from Elsevier. http://www.sciencedirect.com/science/journal/00225193 [74]*

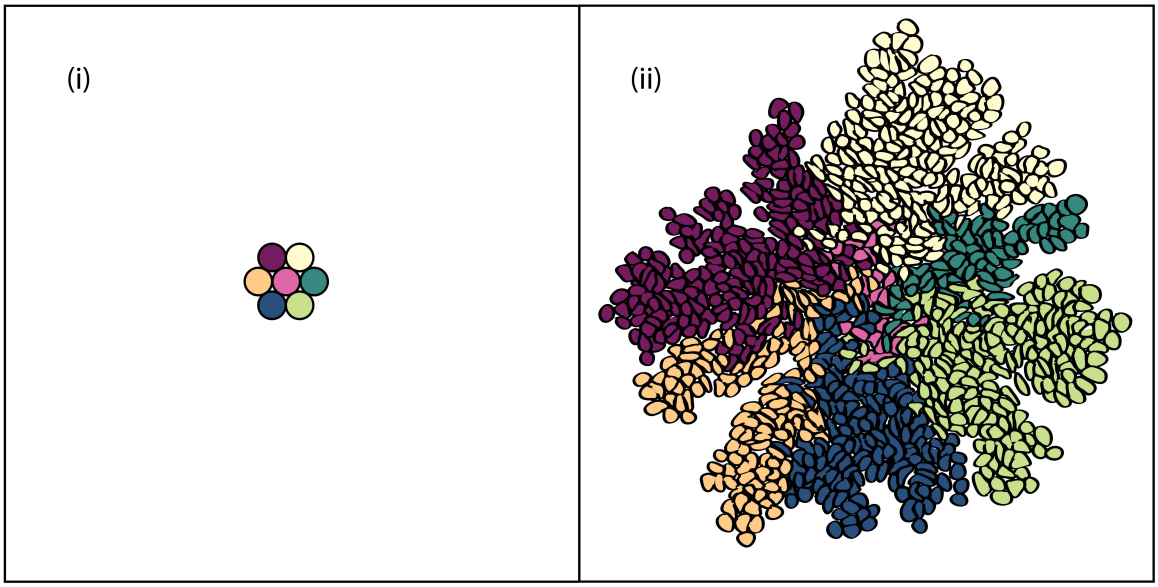

Figure 4.9: Tumor expansion in a nutrient limited environment
*The 7 cells in (**i**) form an asymmetric cluster whose final configuration is shown in (**ii**). Adapted from Rejniak [72].*

these models exhibit over a wide range of parameters [56, 74, 76] attest to their robust nature; however, the increased biological realism, comes with a computational cost. To compensate for the expense of calculating the deformations in the spring network that result from cell growth and division, a population of at most 100 cells can be considered [30] and specific features of the internal cell structure are neglected in favor of choosing a sufficiently high fluid viscosity [75].

Besides tumor growth, Rejniak and colleagues have also used this approach to study the development of acinar structures and the conditions under which degenerate clusters form. In particular, they have examined the impact of the cell cycle, differentiation, and polarization on growth [75,76]. Likewise, Rejniak and Dillon [70] have investigated the degenerate microarchitectural patterns that emerge in response to changes in the orientation of cellular division and the replicative potential of the cells.

4.5 Future work

There are many directions in which this model could be improved. For starters, formulating a 3D representation of the tumor would be ideal, albeit challenging. Rejniak [74] recommends using parallel algorithms to overcome the increased computational costs associated with this modification, but acknowledges the inherent difficultly given that the location of the boundary points will change during the simulation. Rejniak and colleagues [61] also propose fine-tuning the model by obtaining the necessary experimental data. This would allow for a more faithful representation of in vivo dynamics and individual cell processes.

To integrate new components, such as organelles, extracellular fibers, stromal cells or the cytoskeleton, additional immersed bodies can be included. Rejniak has made contradictory claims about the relative ease with which this may be accomplished [4, 74] and how expensive this could be from a computational standpoint. However, an extension that is discussed at length and straightforward to incorporate is the inclusion of the basal membrane. In fact, Rejniak and Dillion [70] describe two different layouts which can be implemented. As shown in Figure 4.10, one consists of a single closed curve while the other is a crossed network of springs that interlink two concentric circles.

To model how the basement membrane maintains the cell as a stiff and immobile structure, the concept of a linear tethered force $\mathbf{F}_{th}$ is introduced. This force,

$$\mathbf{F}_{th}(l,t) = \mathcal{F}_{th}(\mathbf{Z}_{i,l}(t) - \mathbf{Z}^{'}_{i,l}(t)), \tag{4.17}$$

links each point along the basement membrane $\mathbf{Z}_{i,l}$ to its initial location $\mathbf{Z}^{'}_{i,l}(t)$ using springs with stiffness $\mathcal{F}_{th}$.

Rejniak [4] suggests that the cells should be able to sense the direction and the relative steepness of gradients in the oxygen field. These gradients would then guide the motion of the cells, with cellular sensitivity derived based on exposure to the chemoattractant. Given membrane receptor $\mathbf{X}_{i,k}$, Rejniak lets $\mathbf{x}_{i,*}$ denote the point in the receptor's microenvironment $\Theta_{\mathbf{X}_{i,k}}$ with the highest concentration of the stimulus $\gamma(\mathbf{x}_{i,*}, t)$ and defines the drag motility force as

$$\mathbf{F}_{mov}(\mathbf{X}_{i,k}) = \mathcal{F}_{mov}(\gamma(\mathbf{X}_{i,k}, t))||\mathbf{X}_{i,k} - \mathbf{x}_{i,*}||\frac{\nabla\gamma(\mathbf{x}_{i,*}, t)}{||\nabla\gamma(\mathbf{x}_{i,*}, t)||}. \tag{4.18}$$

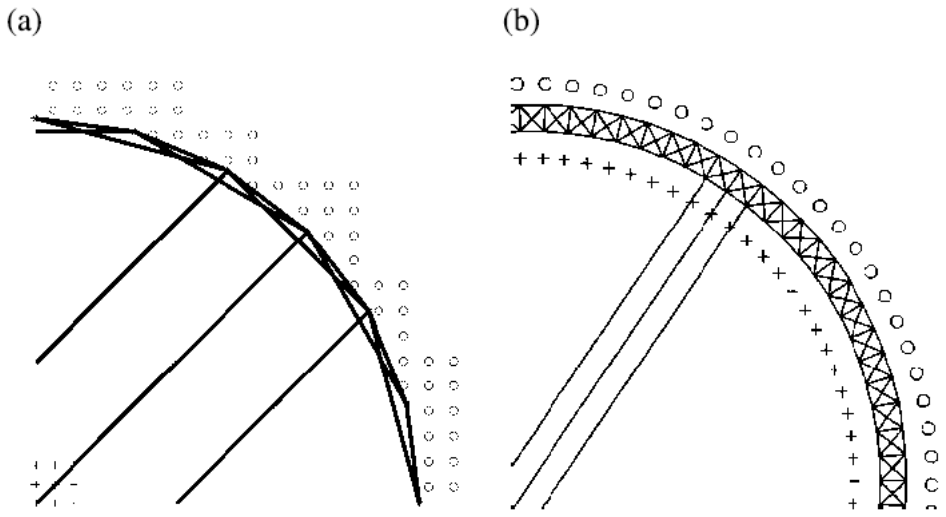

Figure 4.10: Two distinct representations of the basal membrane
*The cell wall is depicted as (**a**) a single closed curve, with each boundary point connected to its four nearest neighbours, and as (**b**) a mesh of linear elastics that interlink two closed curves. The distribution of the sources (+) and sinks (o) is also presented in this diagram. Reprinted from Computational and Mathematical Methods in Medicine, 8, Katarzyna A. Rejniak and Robert H. Dillon, A single cell-based model of the ductal tumour microarchitecture, 51-69, Copyright (2007). http://www.hindawi.com/journals/cmmm/ [70]*

According to the author, the spring stiffness $\mathcal{F}_{mov}$ is dependent on the concentration of γ to account for the fact that a receptor will become dormant if the concentration of oxygen falls below some threshold value γ_{min} in its microenvironment.

The next chapter summarizes the results from our analysis of the HDC, EHCA, and IBCell models, and examines the advantages and disadvantages of using multi-scale mathematical models to study cancer progression. To conclude, we present future areas of research.

Chapter 5

Conclusions

5.1 Overview of Model Outcomes

Current theories postulate that the mutation of critical genes triggers the unchecked proliferation of malignant cells [8]. As these cells multiply, the limited availability of both space and nutrients ultimately drives selection pressures which favor the survival of the most fit clones [54]. However, as a precursor, there must first be variability either within the cell population or the micro-environment [7]. It is this which permits adaptation and competition in response to environmental stressors and hence provokes invasion into healthy tissue [6]. In the context of tumor progression, the best adapted clones are believed to be those which are least likely to become dormant upon crowding and lack sensitivity to apoptotsis [6].

During the early stages of tumor expansion, cell-cell interactions regulate growth. However, tumor progression is associated with a transition into a phase where cellular migration and cell-matrix interactions direct tumor dynamics [46]. In a highly vascularized, nutrient rich environment, the cells form rapidly expanding, spherical clusters with a dense, compact core and a smooth, symmetric boundary [6, 33, 39]. On the other hand, in an environment with limited space, low nutrient availability, or a high hypoxic threshold, small tumors with finger-like margins emerge and growth suppression is often observed [6].

The simulations conducted by various researchers and for the purpose of this thesis suggest that the behavior of a cell affects and is affected by its microenvironment [17]. In

other words, the adaptions that enable a cell to survive unfavorable conditions increase the hostility of its environment [23]. This promotes the selection of invasive phenotypes and the progression toward malignancy. Although these findings suggest that the microenvironment regulates tumor growth, they do not refute the claim that certain phenotypes may have intrinsically invasive properties [6, 7].

5.2 The Advantages and Disadvantages of Mathematical Modeling

Just as there is no single, all-encompassing biological approach to cancer, there is no ideal mathematical or computational model [26]. Each mathematical model described in the previous chapters has its particular strengths and limitations, and each is best suited to address certain types of questions. In terms of cancer, we can examine the expression of genes, proteins, and signalling pathways, or focus on the cell, tissue, or organ scales. Only when activity on each scale is understood, should we attempt to explore how changes in one or more variables may impact the system as a whole.

Adopting a computational approach allows us to systematically manipulate variables that are difficult to control experimentally and to reproduce in vivo conditions that may be impossible to replicate in vitro. [7]. In addition, we are able to perform sensitivity analyses and to examine how the system responds to the simultaneous variation of multiple parameters [7, 53, 63]. This allows researchers to examine various interactions and to differentiate between the crucial and the peripheral factors [31].

Mathematical models complement conventional experimental methods both logistically and financially [7, 31]. They are straightforward to use, and easy to adapt and modify. In addition, they are helpful since they provide an intuitive framework for analyzing a problem and for making predictions [13]. In light of recent developments in biotechnology and continually increasing computational power, it is not surprising that this approach is becoming increasingly prevalent in cancer research [43, 78].

The main drawback of multiscale modeling is that it presents an oversimplification of biological processes [1]. This is expected given our lack of knowledge regarding the underlying mechanisms that give rise to cancer [29, 40], and makes it difficult to define the

properties of the cells and to create algorithms that describe how a cell transitions from one state to the next [34]. For instance, even though they can capture individual cell processes, the HDC and the EHCA models establish only a vague outline of cell-cell and cell-matrix adhesion [1, 23]. In addition, our assumptions of linear dynamics and constant coefficients seem unreasonable in the context of such a complex biological system. Accordingly, we cannot expect our simulations to mirror exact tumor dynamics, although morphological similarities between in vivo and in silico tumors could indicate that our theoretical model is in line with the biomechanics of cancer [9, 68].

5.3 Future Research

The models summarized here are very basic and deal with a limited number of variables. In terms of improvements, a reasonable starting point is to fine-tune our representation of angiogenesis, oxygen production, and cell-cell adhesion. A more accurate representation of the structure of the ECM and how it helps and hinders tumor development is also a promising avenue of research. Furthermore, Rejniak and Anderson [46] suggest modifying the system to alter only one aspect of the cell's phenotype during each mutation and enabling the cells to displace their neighbors (i.e., to create space for proliferation).

When modelling such an intricate system, it is important to guard against creating an overly complicated and poorly parameterized in silico representation which may appear sophisticated but is little more than curve fitting [13]. Having too many interacting variables makes parameter analysis difficult and is unlikely to provide new information [6, 47]. Nevertheless, a model is only as good as the assumptions and the data on which it is based [26, 39]. Thus, it is important to have the correct biochemistry and to represent it faithfully using models that have been properly parameterized [39].

Integrating cutting-edge biological knowledge and experimental data is necessary to validate a model and to spur on the necessary refinements [26]. Biologists may also benefit from this partnership, with models inspiring new hypotheses and guiding experimental design and interpretation [36, 37]. The ultimate goal of this type of cross-disciplinary collaboration is to optimize treatments, build patient-specific models, and guide the design of novel therapeutics [5, 79]. By means of a co-operative approach, we may be able to speed up this process, and better diagnose and treat cancer patients.

Appendices

Appendix A

Appendix A: Continuous Model of Tumor Growth

In this continuous, multi-scale model [80], a tumor is regarded as a heterogeneous agglomeration of invasive cells, and proliferation, quiescence and necrosis are the three cell cycle states. Proliferating cells are motile and consume oxygen at a faster rate than the immobile resting (quiescent) cells. Specifically, $p_i(x, a, s, t)$ is the density of the proliferating tumor cells of type i, size s, and age a, located at x at time t. Similarly, $q_i(x, a, s, t)$ denotes the density of quiescent tumor cells with mutation type i, age a, and size s at grid position x and time t. Here, $i = 0$ corresponds to a mutated $p53$ gene and $i = 1, 2, ..., n$ correspond to a sequence of mutated phenotypes, which exhibit linearly increasing levels of aggressive behavior. In this framework, the aggressiveness of the phenotype positively correlates with its proliferative potential and its capacity for movement.

Cellular age a is defined as the time that has elapsed since the cell last underwent mitosis and is bounded by a_M with $0 \leq a \leq a_M$. Similarly, cell size s varies from s_m to s_M, with $s_m \leq s \leq s_M$. No specific interpretation is provided for the concept of cell size; rather, the authors state that this variable may denote any measurable property, including mass, volume, and diameter.

Initially, the tumor mass is radially symmetric and surrounded by a heterogeneous distribution of macromolecules (MM). When building this model, the authors consider the variables listed below:
$f(x, t)$ is the density of MM at position x and time t. The macromolecules are distributed

heterogeneously and are immobile inside the domain.
$m(x,t)$ is the concentration of the MDEs produced by the tumor cells. These enzymes degrade the surrounding tissue and thus generate gradients of adhesion, which induce haptotactic migration in the cells. Moving toward regions with high oxygen availability, the cells are provided with nutrients which enable them to grow and flourish.
$c(x,t)$ is the oxygen concentration. The extracellular macromolecules produce the oxygen, which diffuses throughout the domain Ω and is consumed by the tumor cells
$P(x,t) = \sum_{i=0}^{n} \int_0^{a_M} \int_{s_m}^{s_M} p_i(x,a,s,t)dsda$ is the population density of proliferating cells at position x and time t.
$Q(x,t) = \sum_{i=0}^{n} \int_0^{a_M} \int_{s_m}^{s_M} q_i(x,a,s,t)dsda$ is the population density of quiescent cells at position x and time t.
$N(x,t) = P(x,t) + Q(x,t)$ is the population density of the cells in the tumor at position x and time t.

The density of the proliferating cells is governed by the equation

$$\begin{aligned}\frac{\partial}{\partial t}p_i(x,a,s,t) = &- \frac{\partial}{\partial a}p_i(x,a,s,t) - \frac{\partial}{\partial s}(\kappa_i(a,s,c)p_i(x,a,s,t)) \\ &+ \nabla\cdot(D_{p_i}(x,a,s,N)\nabla p_i(x,a,s,t)) - \chi_i\nabla\cdot(p_i(x,a,s,t)\nabla f(x,t)) \\ &- \rho_i(x,a,s,c,N)p_i(x,a,s,t) - \theta_i(x,a,s,c,N)p_i(x,a,s,t)) \\ &- \sigma_i(x,a,s,c,N)p_i(x,a,s,t) + \tau_i(x,a,s,c,N)q_i(x,a,s,t).\end{aligned} \tag{A.1}$$

and is subject to the age-boundary condition

$$\begin{aligned}p_i(x,0,s,t) = &\quad 4(1-\psi_i)\int_0^{a_M}\theta_i(x,a,2s,c,N(x,t))p_i(x,a,2s,t)da \\ &+ 4\psi_{i-1}\int_0^{a_M}\theta_{i-1}(x,a,2s,c,N(x,t))p_{i-1}(x,a,2s,t)da\end{aligned} \tag{A.2}$$

where ψ_i is the fraction of the type i cells with a type $i+1$ mutation. κ_i is the rate of cell growth, D_{p_i} is the diffusion coefficient, χ_i is the haptotaxis coefficient, ρ_i is the rate of cell death (from insufficient oxygen), θ_i is the rate of cell division, σ_i is the rate at which proliferating cells become quiescent, and τ_i is the rate at which quiescent cells re-enter a proliferative state.

To study proliferation, Ayati et al. let the probability density function $k(s,u)$ denote the likelihood that a daughter cell of size s results from the division of a mother cell of size

u. Assuming that the two daughter cells are equal in size, they let $k(s,u) = k(u-s,u)$ and $k(s,u) = \delta(s - \frac{u}{2})$ where δ is the Dirac delta function. In their work, they claim that a mother cell of size $2s$ will produce two daughter cells of size s at a rate equivalent to

$$\begin{aligned} & 2\int_{s_m}^{s_M}\int_0^{a_M} k(s,u)\theta_i(x,a,u,c,N(x,t))p_i(x,a,u,t)dadu \\ = \;& 2(2\int_{s_m}^{s_M}\int_0^{a_M} \delta(s-\hat{u})\theta_i(x,a,2\hat{u},c,N(x,t))p_i(x,a,2\hat{u},t)dad\hat{u}) \\ = \;& 4\int_0^{a_M} \theta_i(x,a,2s,c,N(x,t))p_i(x,a,2s,t)da \end{aligned} \tag{A.3}$$

The equation

$$\begin{aligned} \frac{\partial}{\partial t}q_i(x,a,s,t) &= -\frac{\partial}{\partial a}q_i(x,a,s,t) - \nu_i(x,a,s,c,N(x,t))q_i(x,a,s,t) \\ &+ \sigma_i(x,a,s,c,N(x,t))p_i(x,a,s,t) - \tau_i(x,a,s,c,N(x,t))q_i(x,a,s,t) \end{aligned} \tag{A.4}$$

describes the change in the density of the quiescent cells. Specifically, ν_i is the rate at which the quiescent cells die from insufficient oxygen, σ_i is the rate at which proliferating cells become quiescent, and τ_i is the rate at which quiescent cells re-enter a proliferative state.

Changes in the density of the MM, the MDEs, and the oxygen are represented by the equations

$$\frac{\partial}{\partial t}f(x,t) = -\delta m(x,t)f(x,t), \tag{A.5}$$

$$\frac{\partial}{\partial t}m(x,t) = D_m\nabla^2 m(x,t) + \mu P(x,t) + \omega Q(x,t) - \lambda m(x,t), \tag{A.6}$$

and

$$\frac{\partial}{\partial t}c(x,t) = D_c\nabla^2 c(x,t) + \beta f(x,t) - \gamma P(x,t) - \eta Q(x,t) - \alpha c(x,t), \tag{A.7}$$

respectively. Equation A.5 denotes the degradation of the tissue at a rate δ, while equation A.6 describes the diffusion (D_m), production (μ and ω), and decay (λ) of MDEs. Lastly, equation A.7 represents the diffusion (D_c), production(β), uptake (γ and η), and decay (α) of oxygen.

Ayati et al [80] also consider this system in two spatial dimensions $(x, y) \in \Omega$, under the assumption of no size structure, and propose that the equations

$$\begin{aligned} \frac{\partial}{\partial t}p(x,y,a,t) = & - \frac{\partial}{\partial a}p(x,y,a,t) \\ & + D_p\nabla^2 p(x,y,a,t) - \chi\nabla\cdot(p(x,y,a,t)\nabla f(x,y,t)) \\ & - \rho(x,y,a,c)p(x,y,a,t) - \theta(x,y,a,c)p(x,y,a,t) \\ & - \sigma(x,y,a,c,N(x,t))p(x,a,s,t) + \tau(x,y,a,c)q(x,y,a,t) \end{aligned} \tag{A.8}$$

and

$$\begin{aligned} \frac{\partial}{\partial t}q(x,y,a,t) = & - \frac{\partial}{\partial a}q(x,y,a,t) - \nu(x,y,a,c)q(x,y,a,t) \\ & + \sigma(x,y,a,c,N(x,t))p(x,a,s,t) - \tau(x,y,a,c)q(x,y,a,t) \end{aligned} \tag{A.9}$$

describe the density of the tumor cells and are subject to the age-boundary condition

$$p(x,y,0,t) = 2\int_0^{a_M} \theta(x,y,a,c)p(x,y,a,t)da. \tag{A.10}$$

In equations A.8 and A.9, D_p is the diffusion coefficient, χ is the haptotaxis coefficient, ρ and ν are the rates at which proliferating and quiescent cells die from insufficient oxygen, respectively, θ is the rate of cell division, σ is the rate at which proliferating cells become quiescent, and τ is the rate at which quiescent cells become proliferative..

In both the one dimensional and two dimensional models, zero flux boundary conditions are imposed on the domain.

A.1 Results

To implement this approach numerically, Ayati et al. use the Galerkin finite element method on a moving grid. Their results reconfirm many of the standard outcomes of the HDC model. As before, the tumor consists of a band of proliferating cells surrounding a large necrotic core. Nestled in between these two layers are the quiescent cells which thrive in environments with high cell densities and limited oxygen availability. The abundance of oxygen and a sparse distribution of cells favor the 'recruitment [of proliferating cells] from

quiescence,' while low oxygen levels are associated with necrosis.

There are two major concerns that stem from the use of a moving grid. One is determining how to establish size nodes along the boundary in a way that respects the fact that growth may slow once a cell has reached a certain size. The second issue is determining the size of the discretizations. Although the convergence of size-time characteristic curves suggests that the interval size should strictly decrease in length, the nonlinearities of cellular activity make this assumption questionable [80].

References

[1] A. R. A. Anderson, A. M. Weaver, P. T. Cummings, and V. Quaranta, "Tumor morphology and phenotypic evolution driven by selective pressure from the microenvironment," *Cell*, vol. 127, pp. 905–915, 2006.

[2] M. Baum, M. Chaplain, A. R. A. Anderson, M. Doue, and J. Vaidya, "Does breast cancer exist in a state of chaos?," *European Journal of Cancer*, vol. 35, pp. 886–891, 1999.

[3] P. Hinow, P. Gerlee, L. McCawley, V. Quaranta, M. Ciobanu, S. Wang, J. Graham, B. Ayati, J. Claridge, K. Swanson, M. Loveless, and A. R. A. Anderson, "A spatial model of tumor-host interactions: application of chemotherapy," *Mathematical Biosciences and Engineering*, vol. 6, pp. 521–546, 2009.

[4] K. Rejniak, "Modelling the development of complex tissues using individual viscoelastic cells," in *Single-Cell-Based Models in Biology and Medicine (Mathematics and Biosciences in Interaction)* (A. R. A. Anderson, M. Chaplain, and K. Rejniak, eds.), pp. 301–323, Basel, Switzerland: Birkhauser Verlag, 2007.

[5] V. Quaranta, A. Weaver, P. Cummings, and A. R. A. Anderson, "Mathematical modeling of cancer: The future of prognosis and treatment," *Clinica Chimica Acta*, vol. 357, pp. 173–179, 2005.

[6] V. Quaranta, K. Rejniak, P. Gerlee, and A. R. A. Anderson, "Invasion emerges from cancer cell adaptation to competitive microenvironment : Quantitative predictions from multiscale mathematical models," *Seminars in Cancer Biology*, vol. 18, pp. 338–348, 2008.

[7] K. Rejniak and L. McCawley, "Current trend in mathematical modeling of tumor-microenviornment interactions: A survey of tolls and applications," *Experimental Biology and Medicine*, vol. 235, pp. 411–423, 2010.

[8] A. R. A. Anderson and V. Quaranta, "Integrative mathematical oncology," *Nature Reviews Cancer*, vol. 8, pp. 227–234, 2008.

[9] J. Smolle and H. Stettner, "Computer simulation of tumor cell invasion by a stochastic growth model," *Journal of Theoretical Biology*, vol. 160, pp. 63–72, 1993.

[10] M. Piotrowskia and S. Angus, "A quantitative cellular automaton model of in vitro multicellular spheroid tumour growth," *Journal of Theoretical Biology*, vol. 258, pp. 165–178, 2009.

[11] P. Schofield, M. Chaplain, and S. Hubbard, "Evolution of searching and life history characteristics in individual-based models of host-parasitoid-microbe associations," *Journal of Theoretical Biology*, vol. 237, pp. 1–16, 2005.

[12] H. Othmer and A. Stevens, "Aggregation, blowup, and collapse: The abc's to taxis in reinforced random walks," *SIAM Journal on Applied Mathematics*, vol. 57, pp. 1044–1081, 1997.

[13] T. Roose, S. Chapman, and P. Maini, "Mathematical models of avascular tumor growth," *SIAM Review*, vol. 49, pp. 179–208, 2007.

[14] P. Gerlee, D. Basanta, and A. R. A. Anderson, "Evolving homeostatic tissue using genetic algorithms," *Progress in Biophysics and Molecular Biology*, vol. 106, pp. 414–425, 2011.

[15] A. R. A. Anderson and A. Pitcairn, "Application of the hybrid discrete-continuum technique," in *Polymer and Cell Dynamics - Multiscale Modeling and Numerical Simulations* (M. G. M. Alt, W. Chaplain and J. Lenz, eds.), pp. 261–279, Basel, Switzerland: Birkhauser Verlag, 2003.

[16] R. Weinberg, "Using maths to tackle cancer," *Nature*, vol. 449, pp. 978–981, 2007.

[17] A. R. A. Anderson, K. Rejniak, P. Gerlee, and V. Quaranta, "Microenvironment driven invasion: A multiscale multimodel investigation," *Journal of Mathematical Biology*, vol. 58, pp. 579–624, 2009.

[18] D. Hanahan and R. A. Weinberg, "The Hallmarks of Cancer," *Cell*, vol. 100, pp. 57–70, Jan. 2000.

[19] A. R. A. Anderson, "A hybrid multiscale model of solid tumour growth and invasion: Evolution and the microenvironment," in *Single-Cell-Based Models in Biology and*

Medicine (A. R. A. Anderson, M. Chaplain, and K. Rejniak, eds.), pp. 3–28, Basel, Switzerland: Birkhauser Verlag, 2007.

[20] A. R. A. Anderson, "The effects of cell adhesion on solid tumour geometry," in *Morphogenesis and Pattern Formation in Biological Systems: Experiments and Models* (T. Sekimura, S. Noji, N. Ueno, and P. Maini, eds.), pp. 315–325, Tokyo, Japan: Springer-Verlag, 2003.

[21] A. R. A. Anderson, "A hybrid mathematical model of solid tumour invasion: The importance of cell adhesion," *Mathematical Medicine and Biology*, vol. 22, pp. 163–186, 2005.

[22] A. R. A. Anderson, M. Hassanein, K. Branch, J. Lu, N. Lobdell, J. Maier, D. Basanta, B. Weidow, A. Narasanna, C. Arteaga, A. Reynolds, V. Quaranta, L. Estrada, and A. Weaver, "Microenvironmental independence associated with tumor progression," *Cancer Research*, vol. 69, pp. 8797–8806, 2009.

[23] A. R. A. Anderson, K. A. Rejniak, P. Gerlee, and V. Quaranta, "Modelling of cancer growth, evolution and invasion: Bridging scales and models," *Mathematical Modelling of Natural Phenomena*, vol. 2, pp. 1–29, 2007.

[24] H. Enderling, A. R. A. Anderson, M. Chaplain, A. Munro, and J. Vaidya, "Mathematical modelling of radiotherapy strategies for early breast cancer," *Journal of Theoretical Biology*, vol. 241, pp. 158–171, 2006.

[25] D. Hanahan and R. Weinberg, "The hallmarks of cancer: The next generation," *Cell*, vol. 144, pp. 646–674, 2011.

[26] D. Strand, O. Franco, D. Basanta, A. R. A. Anderson, and S. Hayward, "Perspectives on tissue interactions in development and disease," *Current Molecular Medicine*, vol. 10, pp. 95–112, 2010.

[27] J. Sherratt, A. Perumpanani, and M. Owen, "Pattern formation in cancer," in *On Growth and Form: Spatio-temporal Pattern Formation in Biology* (M. Chaplain, G. Singh, and J. McLachlan, eds.), pp. 47–73, Chichester, UK: John Wiley & Sons Ltd., 1999.

[28] M. Chaplain and A. R. A. Anderson, "Mathematical modelling of tissue invasion," in *Cancer Modelling and Simulation* (L. Preziosi, ed.), pp. 269–297, Boca Raton, FL, USA: Chapman & Hall/CRC Press, 2003.

[29] M. Chaplain and A. R. A. Anderson, "Modelling the growth and form of capillary networks," in *On Growth and Form: Spatio-temporal Pattern Formation in Biology* (G. Chaplain, M.A.J Singh and J. McLachlan, eds.), pp. 225–249, Chichester, UK: John Wiley & Sons Ltd., 1999.

[30] J. Lowengrub, H. Frieboes, F. Jin, Y.-L. Chuang, X. Li, P. Macklin, S. Wise, and V. Cristini, "Nonlinear modelling of cancer: Bridging the gap between cells and tumours," *Nonlinearity*, vol. 23, pp. R1–R91, 2010.

[31] A. Perumpanani, J. Sherratt, J. Norbury, and H. Byrne, "Biological inferences from a mathematical model for malignant invasion," *Invasion Metastasis*, vol. 16, pp. 209–221, 1996.

[32] I. Ramis-Conde, M. Chaplain, and A. R. A. Anderson, "Mathematical modelling of cancer cell invasion of tissue," *Mathematical and Computer Modelling*, vol. 47, pp. 533–545, 2008.

[33] N. Poplawski, U. Agero, J. Gens, M. Swat, J. Glazier, and A. R. A. Anderson, "Front instabilities and invasiveness of simulated avascular tumors," *Bulletin of Mathematical Biology*, vol. 71, pp. 1189–1227, 2009.

[34] A. R. A. Anderson and M. A. J. Chaplain, "Continuous and discrete mathematical models of tumor-induced angiogenesis," *Bulletin of Mathematical Biology*, vol. 60, pp. '857–900, 1998.

[35] A. R. A. Anderson, "Solid tumour invasion: The importance of cell adhesion," in *Function and Regulation of Cellular Systems: Experiments and Models* (A. Deutsch, M. Falcke, J. Howard, and W. Zimmermann, eds.), pp. 379–389, Basel, Switzerland: Birkhauser Verlag, 2004.

[36] R. Araujo and L. McElwain, "A history of the study of solid tumour growth: The contribution of mathematical modelling," *Bulletin of Mathematical Biology*, vol. 66, pp. 1039–1091, 2004.

[37] Y. Kam, K. Rejniak, and A. R. A. Anderson, "Cellular modeling of cancer invasion: Integration of in silico and in vitro approaches," *Journal of Cellular Physiology*, vol. 227, pp. 431–438, 2012.

[38] D. Drasdo, S. Dormann, S. Hoehme, and A. Deutsch, "Cell-based models of avascular tumor growth," in *Function and Regulation of Cellular Systems: Experiments and*

Models (A. Deutsch, M. Falcke, J. Howard, and W. Zimmermann, eds.), pp. 367–378, Basel, Switzerland: Birkhauser Verlag, 2004.

[39] H. Byrne, "Dissecting cancer through mathematics: From the cell to the animal model," *Nature Reviews Cancer*, vol. 10, pp. 221–230, 2010.

[40] L. Preziosi, ed., *Cancer Modelling and Simulation*. Boca Raton, FL, USA: Chapman & Hall/CRC Press, 2003.

[41] J. Moreira and A. Deutsch, "Cellular automaton models of tumor development: A critical review," *Advances in Complex Systems*, vol. 5, pp. 247–267, 2002.

[42] S. Dormann, A. Deutsch, and A. Lawniczak, "Fourier analysis of turing-like pattern formation in cellular automaton models," *Future Generation Computer Systems*, vol. 17, pp. 901–909, 2001.

[43] G. Ermentrout and L. Edelstein-Keshet, "Cellular automata approaches to biological modeling," *Journal of Theoretical Biology*, vol. 160, pp. 97–133, 1993.

[44] H. Enderling, A. R. A. Anderson, and M. Chaplain, "Visualisation of the numerical solution of the partial differential equation system in three space dimensions and its importance for mathematical models in biology," *Mathematical Biosciences and Engineering*, vol. 3, pp. 571–582, 2006.

[45] A. R. A. Anderson, M. Chaplain, E. Newman, R. Steele, and A. Thompson, "Mathematical modelling of tumour invasion and metastasis," *Journal of Theoretical Medicine*, vol. 2, pp. 129–154, 2000.

[46] K. Rejniak and A. R. A. Anderson, "Hybrid models of tumor growth," *Wiley Interdisciplinary Reviews: Systems Biology and Medicine*, vol. 3, pp. 115–125, 2010.

[47] R. Gillies, A. R. A. Anderson, R. Gatenby, and D. Morse, "The biology underlying molecular imaging in oncology: From genome to anatome and back again," *Clinical Radiology*, vol. 65, pp. 517–521, 2010.

[48] H. Enderling, A. R. A. Anderson, M. Chaplain, A. Beheshti, L. Hlatky, and P. Hahnfeldt, "Paradoxical dependencies of tumor dormancy and progression on basic cell kinetics," *Cancer Research*, vol. 69, pp. 8814–8821, 2009.

[49] M. Chaplain, L. Graziano, and L. Preziosi, "Mathematical modelling of the loss of tissue compression responsiveness and its role in solid tumor development," *Mathematical Medicine and Biology*, vol. 23, pp. 197–229, 2006.

[50] B. Marchant, J. Norbury, and A. Perumpanani, "Traveling shock waves arising in a model of malignant invasion," *SIAM Journal on Applied Mathematics*, vol. 60, pp. 463–476, 2000.

[51] P. Gerlee and A. R. A. Anderson, "An evolutionary hybrid cellular automaton model of solid tumor growth," *Journal of Theoretical Biology*, vol. 246, pp. 583–603, 2007.

[52] K. Smallbone, R. A. Gatenby, R. J. Gillies, P. K. Maini, and D. J. Gavaghan, "Metabolic changes during carcinogenesis: potential impact on invasiveness.," *Journal of Theoretical Biology*, vol. 244, no. 4, pp. 703–713, 2007.

[53] A. Sottoriva, J. Verhoeff, T. Borovski, S. McWeeney, L. Naumov, J. Medema, P. Sloot, and L. Vermeulen, "Cancer stem cell tumor model reveals invasive morphology and increased phenotypical heterogeneity," *Cancer Research*, vol. 70, pp. 46–56, 2010.

[54] P. Gerlee and A. R. A. Anderson, "A hybrid cellular automaton model of clonal evolution in cancer: The emergence of the glycolytic phenotype," *Journal of Theoretical Biology*, vol. 250, pp. 705–722, 2008.

[55] A. Perumpanani, J. Sherratt, J. Norbury, and H. Byrne, "A two parameter family of travelling waves with a singular barrier arising from the modelling of extracellular matrix mediated cellular invasion," *Physica D*, vol. 126, pp. 145–159, 1999.

[56] K. Rejniak, V. Quaranta, and A. R. A. Anderson, "Computational investigation of intrinsic and extrinsic mechanisms underlying the formation of carcinoma," *Mathematical Medicine and Biology*, vol. 29, pp. 67–84, 2012.

[57] B. Marchant, J. Norbury, and H. Byrne, "Biphasic behaviour in malignant invasion," *Mathematical Medicine and Biology*, vol. 23, pp. 173–196, 2006.

[58] L. Segel, "Simplification and scaling," *SIAM Review*, vol. 4, pp. 547–571, 1972.

[59] A. R. A. Anderson, "A hybrid discrete-continuum technique for individual based migration models," in *Polymer and Cell Dynamics - Multiscale Modeling and Numerical Simulations* (M. G. M. Alt, W. Chaplain and J. Lenz, eds.), pp. 251–259, Basel, Switzerland: Birkhauser Verlag, 2003.

[60] J. Dale and M. v. Schantz, *From Genes to Genomes: Concepts and Applications of DNA Technology (2^{nd} Edition)*. Hoboken, NJ, USA: John Wiley & Sons, Ltd., 2008.

[61] K. Rejniak, S. Wang, N. Bryce, H. Chang, B. Parvin, J. Jourquin, L. Estrada, J. Gray, C. Arteaga, A. Weaver, V. Quaranta, , and A. R. A. Anderson, "Linking changes in epithelial morphogenesis to cancer mutations using computational modeling," *PLoS Computational Biology*, vol. 6, p. e1000900, 2010.

[62] A. Perumpanani and H. Byrne, "Extracellular matrix concentration exerts selection pressure on invasive cells," *European Journal of Cancer*, vol. 35, pp. 1274–1280, 1999.

[63] N. Armstrong, K. Painter, and J. Sherratt, "A continuum approach to modelling cell-cell adhesion," *Journal of Theoretical Biology*, vol. 243, pp. 98–113, 2006.

[64] A. Gerisch and M. Chaplain, "Mathematical modelling of cancer cell invasion of tissue: Local and non-local models and the effect of adhesion," *Journal of Theoretical Biology*, vol. 250, pp. 684–704, 2008.

[65] S. Ferreira, M. Martins, and M. Vilela, "Reaction-diffusion model for the growth of avascular tumor," *Physical Review E*, vol. 65, p. 021907, 2002.

[66] A. Patel, E. Gawlinski, S. Lemieux, and R. Gatenby, "A cellular automaton model of early tumor growth and invasion: The effects of native tissue vascularity and increased anaerobic tumor metabolism," *Journal of Theoretical Biology*, vol. 213, pp. 315–331, =2001.

[67] P. Gerlee and A. R. A. Anderson, "Modelling evolutionary cell behaviour using neural networks: Application to tumour growth," *Biosystems*, vol. 95, pp. 166–174, 2009.

[68] P. Gerlee and A. R. A. Anderson, "Stability analysis of a hybrid cellular automaton model of cell colony growth," *Physical Review E*, vol. 75, p. 051911, 2007.

[69] P. Gerlee and A. R. A. Anderson, "Evolution of cell motility in an individual-based model of tumour growth," *Journal of Theoretical Biology*, vol. 259, pp. 67–83, 2009.

[70] K. Rejniak and R. Dillon, "A single cell-based model of the ductal tumour microarchitecture," *Computational and Mathematical Methods in Medicine*, vol. 8, pp. 51–69, 2007.

[71] C. Peskin, "The immersed boundary method," *Acta Numerica*, vol. 11, pp. 479–517, 2002.

[72] K. Rejniak, "A single cell approach in modeling the dynamics of tumor microregions," *Mathematical Biosciences and Engineering*, vol. 2, pp. 643–655, 2005.

[73] A. R. A. Anderson, M. Chaplain, and K. Rejniak, eds., *Single-Cell-Based Models in Biology and Medicine*. Basel, Switzerland: Birkhauser Verlag, 2007.

[74] K. Rejniak, "An immersed boundary framework for modelling the growth of individual cells: An application to the early tumour development," *Journal of Theoretical Biology*, vol. 247, pp. 186–204, 2007.

[75] K. Rejniak and A. R. A. Anderson, "A computational study of the development of epithelial acini: I. Sufficient conditions for the formation of a hollow structure," *Bulletin of Mathematical Biology*, vol. 70, pp. 677–712, 2008.

[76] K. Rejniak and A. R. A. Anderson, "A computational study of the development of epithelial acini: II. Necessary conditions for structure and lumen stability," *Bulletin of Mathematical Biology*, vol. 70, pp. 1450–1479, 2008.

[77] C. Peskin, "Numerical analysis of blood flow in the heart," *Journal of Computational Physics*, vol. 25, pp. 220–252, 1977.

[78] P. Maini, "Some mathematical models for biological pattern formation," in *On Growth and Form: Spatio-temporal Pattern Formation in Biology* (G. Chaplain, M.A.J Singh and J. McLachlan, eds.), pp. 111–128, Chichester, UK: John Wiley & Sons Ltd., 1999.

[79] H. Enderling, M. Chaplain, A. R. A. Anderson, and J. Vaidya, "A mathematical model of breast cancer development, local treatment and recurrence," *Journal of Theoretical Biology*, vol. 246, pp. 245–259, 2007.

[80] B. Ayati, G. Webb, and A. R. A. Anderson, "Computational methods and results for structured multiscale model of tumor invasion," *Multiscale Modeling and Simulation*, vol. 5, pp. 1–20, 2006.